«ФИЗИКА ЭЛЕМЕНТАРНЫХ ЧАСТИЦ И АТОМНОГО ЯДРА»
1999, ТОМ 30, ВЫП. 3

УДК 539.12.01

NONPERTURBATIVE EFFECTS IN QCD AT FINITE TEMPERATURE AND DENSITY

C.D.Roberts

Physics Division 203, Argonne National Laboratory,
Argonne IL 60439-4843, USA

«ФИЗИКА ЭЛЕМЕНТАРНЫХ ЧАСТИЦ И АТОМНОГО ЯДРА»
1999, ТОМ 30, ВЫП. 3

УДК 539.12.01

NONPERTURBATIVE EFFECTS IN QCD AT FINITE TEMPERATURE AND DENSITY

C.D.Roberts

Physics Division 203, Argonne National Laboratory,
Argonne IL 60439-4843, USA

These lecture notes illustrate the application of Dyson — Schwinger equations in QCD. The extensive body of work at zero temperature and chemical potential is represented by a selection of contemporary studies that focus on solving the Bethe — Salpeter equation, deriving an exact mass formula in QCD that describes light and heavy pseudoscalar mesons simultaneously, and the calculation of the electromagnetic pion form factor and the vector meson electroproduction cross sections. These applications emphasise the qualitative importance of the momentum-dependent dressing of elementary Schwinger functions in QCD, which provides a unifying connection between disparate phenomena. They provide a solid foundation for an extension of the approach to nonzero temperature and chemical potential. The essential, formal elements of this application are described and four contemporary studies employed to exemplify the method and its efficacy. They study the demarcation of the phase boundary for deconfinement and chiral symmetry restoration, the calculation of bulk thermodynamic properties of the quark-gluon plasma and the response of π- and ρ-meson observables to T and μ. Along the way a continuum order parameter for deconfinement is introduced, an anticorrelation between the response of masses and decay constants to T and their response to μ elucidated, and a (T,μ)-mirroring of the slow approach of bulk thermodynamic quantities to their ultrarelativistic limit highlighted. These effects too are tied to the momentum-dependent dressing of the elementary Schwinger functions.

В работе показано применение уравнений Дайсона — Швингера в КХД. Большая часть обзора посвящена изложению современного подхода, основанного на решении уравнения Бете — Солпитера, воспроизводящего точные массовые формулы КХД, описывающие одновременно как легкие, так и тяжелые псевдоскалярные мезоны и вычисления электромагнитного формфактора пиона и сечения электророждения векторных мезонов при нулевой температуре и химическом потенциале. Эти исследования, которые объединяют такие разные явления, качественно указывают на важность импульсной зависимости одетых элементарных функций Швингера в КХД. Они обеспечивают прочную основу для обобщения рассматриваемого подхода на случай ненулевой температуры и химического потенциала. Существенно, что описаны формальные элементы используемого подхода и приведены четыре примера в качестве иллюстрации метода и его эффективности. С их помощью изучается граница фазового перехода для деконфайнмента и восстановления киральной симметрии, вычисляется набор термодинамических свойств кварк-глюонной плазмы и зависимость π- и ρ-мезонных наблюдаемых от T и μ. Аналогичным образом введены непрерывный параметр порядка для деконфайнмента, антикорреляция между зависимостью масс и констант распада от T и их же зависимостью от μ и (T,μ)-зависимость для малых и ультрарелятивистских значений термодинамических величин. Рассмотренные эффекты также ограничиваются импульсной зависимостью одетых элементарных функций Швингера.

1. INTRODUCTION

In this article I describe the application of Dyson — Schwinger equations (DSEs) to QCD at finite temperature, T, and quark chemical potential, μ. It is not a pedagogical introduction, as this can be found in recent reviews [1,2]. The goal instead is to illustrate how contemporary studies at $(T = 0, \mu = 0)$ can be used as a foundation and springboard for the application of DSEs at finite T and μ, and to describe some of these applications and their results.

The DSEs provide a nonperturbative, Poincaré invariant, continuum approach to solving quantum field theories. They are an infinite tower of coupled integral equations, with the equation for a particular n-point function involving at least one $m > n$-point function. A tractable problem is only obtained if one truncates the system, and historically this has provided an impediment to the application of DSEs: *a priori* it can be difficult to judge whether a particular truncation scheme will yield qualitatively or quantitatively reliable results for the quantity sought. As integral equations, the analysis of observables using DSEs rapidly becomes a numerical problem and hence a critical evaluation of truncation schemes often requires, or is at least simplified, by easy access to high-speed computers.* With such tools now commonplace, this evaluation can be pursued fruitfully.

The development of efficacious truncation schemes is not a purely numerical task, and neither is it always obviously systematic. For some, this last point diminishes the appeal of the approach. However, with growing community involvement and interest, the qualitatively robust results and intuitive understanding that the DSEs can provide is becoming clear. Indeed, someone familiar with the application of DSEs in the late-70s and early-80s might be surprised with the progress that has been made. It is now clear [3,4] that truncations which preserve the global symmetries of a theory; for example, chiral symmetry in QCD, are relatively easy to define and implement and, while it is more difficult to preserve local gauge symmetries, much progress has been made with Abelian theories [5] and more is being learnt about non-Abelian ones.

The simplest truncation scheme for the DSEs is the weak-coupling expansion. Using this systematic procedure it is readily established that the DSEs *contain* perturbation theory, in the sense that for any given theory the weak-coupling expansion of the equations generates all the diagrams of perturbation theory. Hence, at the very least, the DSEs can be used as a generating tool for perturbation theory, and in this application they are an essential element in the proof of the renormalisability of a quantum field theory. This feature also places a constraint on other truncation schemes; i.e., the scheme must ensure that perturbative results

*The human and computational resources required are still modest compared with those consumed in contemporary numerical simulations of lattice-QCD.

are recovered in that domain on which a weak-coupling expansion is known to be valid.

The most important feature of the DSEs is the antithesis of this weak-coupling expansion: the DSEs are intrinsically nonperturbative. They can be derived directly from the generating functional of a quantum field theory and at no stage in this derivation is a DSE represented as a sum of diagrams in perturbation theory. Hence their solution contains information that is *not* present in perturbation theory. They are ideal for the study of dynamical chiral symmetry breaking* (DCSB) and confinement in QCD, and of hadronic bound state structure and properties. In this application they provide a means of elucidating identifiable signatures of the quark-gluon substructure of hadrons.

Their intrinsically nonperturbative nature also makes them well suited to studying QCD at finite-T and μ, where the characteristics of the phase transition to a quark-gluon plasma are a primary subject. The order of the transition, the critical exponents, and the response of bound states to changes in these intensive variables: all must be elucidated. The latter is of particular importance because there lies the signals that will identify the formation of the plasma and hence guide the current and future experimental searches.

There is a significant overlap between contemporary DSE studies and numerical simulations of lattice-QCD. Of particular importance is that both admit the simultaneous study of DCSB and confinement, the absence of which *defines* the plasma. The DSEs provide an adjunct to lattice simulations. They are a means of checking them, and the simulations can provide input into the development and constraint of DSE truncations. A truncation that is accurate on the common domain can be used to extrapolate into that domain presently inaccessible to lattice-simulations, such as finite chemical potential and the T- and μ-dependence of hadron properties.

2. ESSENTIAL ELEMENTS OF THE DSEs

In this section I summarise some of the results upon which much of the successful DSE phenomenology is founded. Before doing so it is important to specify that I employ an Euclidean metric throughout. For real 4-vectors, a, b:

$$a \cdot b := a_\mu \, b_\nu \delta_{\mu\nu} := \sum_{i=1}^{4} a_i \, b_i \,, \tag{1}$$

*Historically, the DSE for a fermion propagator has found widespread use in the study of dynamical symmetry breaking; for example, it is the "gap equation" that describes Cooper-pairing in an ordinary superconductor.

and hence a spacelike vector, Q_μ, has $Q^2 > 0$. The Dirac matrices satisfy

$$\gamma_\mu^\dagger = \gamma_\mu \,, \; \{\gamma_\mu, \gamma_\nu\} = 2\,\delta_{\mu\nu} \tag{2}$$

and $\gamma_5 := -\gamma_1\gamma_2\gamma_3\gamma_4$.

My point of view is that the Euclidean formulation is *primary*; i.e., a field theory should be *defined* in Euclidean space, where the propagators and vertices are properly called "n-point Schwinger functions". This is the perspective adopted in constructive field theory and, at least as a pragmatic artifice, by practitioners of lattice-QCD. If the field theory is well-defined, it is completely specified once all its Schwinger functions are known. Analytic continuation in the Euclidean-time variable yields the Wightman functions and, following appropriate time-ordering, the Minkowski space propagators. Additional details and discussion can be found in Sec. 2.3 of Ref.1.

It is important because the analytic structure of nonperturbatively dressed Schwinger functions need not be the same as that of their free-particle seeds. Hence, *a priori* one cannot know the analytic properties of the integrand in a DSE and any rotation of the integration contours, as in a "Wick rotation", is plagued by uncertainty: there may be poles or branch cuts, etc., that cannot be anticipated from the free-particle form of the Schwinger functions involved. This is manifest in the fact that the *transcription rules*:

Configuration Space	Momentum Space
1. $\int^M d^4x^M \to -i \int^E d^4x^E$	1. $\int^M d^4k^M \to i \int^E d^4k^E$
2. $\not\partial \to i\gamma^E \cdot \partial^E$	2. $\not k \to -i\gamma^E \cdot k^E$
3. $\not A \to -i\gamma^E \cdot A^E$	3. $k_\mu q^\mu \to -k^E \cdot q^E$
4. $A_\mu B^\mu \to -A^E \cdot B^E$	4. $k_\mu x^\mu \to -k^E \cdot x^E$,

are valid at every order in perturbation theory; i.e., the correct Minkowski space integral for a given diagram in perturbation theory is obtained by applying these transcription rules to the Euclidean integral. However, for skeleton diagrams; i.e., those in which each line and vertex represents a fully dressed n-point function, this cannot be guaranteed.

2.1. Gluon Propagator. In Landau gauge the two-point, dressed-gluon Schwinger function, or dressed-gluon propagator, has the form

$$g^2 D_{\mu\nu}(k) \;=\; \left(\delta_{\mu\nu} - \frac{k_\mu k_\nu}{k^2}\right) \frac{\mathcal{G}(k^2)}{k^2} \,, \; \mathcal{G}(k^2) := \frac{g^2}{1 + \Pi(k^2)} \,, \tag{3}$$

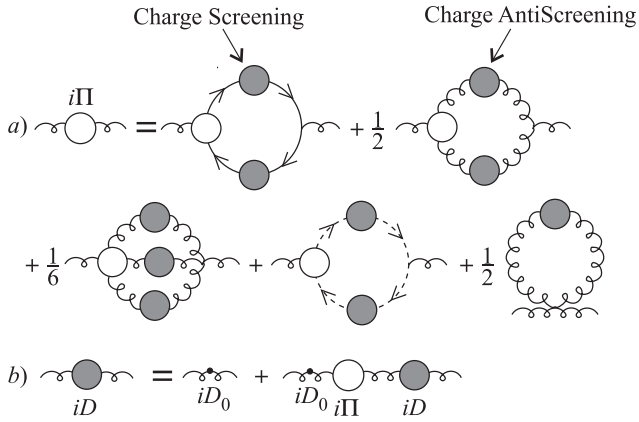

Fig. 1. DSE for the gluon vacuum polarisation and propagator: solid line — quark; spring — gluon; dotted-line — ghost. The open circles are irreducible vertices. As indicated, the quark loop acts to screen the charge, as in QED, while the gluon loop opposes this, antiscreening the charge and enhancing the interaction

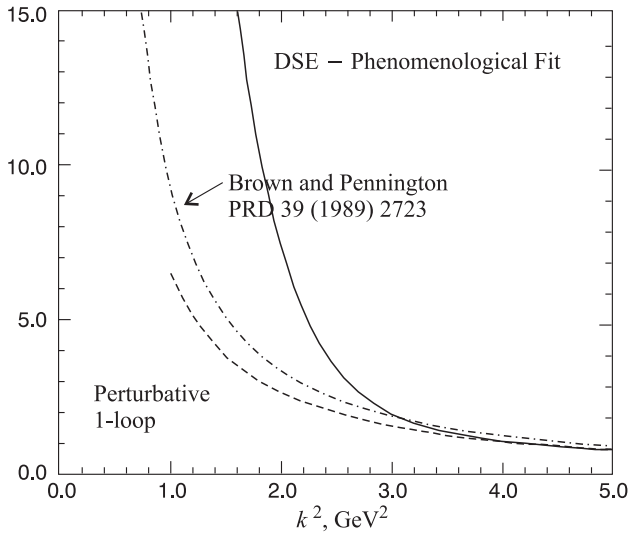

Fig. 2. $\mathcal{G}(k^2)/k^2$ from a solution [6] of the gluon DSE (dash-dot line) compared with the one-loop perturbative result (dashed line) and a fit (solid line) obtained following the method of Ref.7; i.e., by requiring that the gluon propagator lead, via the quark DSE, to a good description of a range of hadron observables

where $\Pi(k^2)$ is the gluon vacuum polarisation, which contains all the dynamical information about gluon propagation. This propagator satisfies the DSE illustrated in Fig. 1 (a nonlinear integral equation). As already stated, a weak-coupling expansion of this DSE reproduces perturbation theory. Using this one sees directly that in the one-loop expression for the running coupling constant:

$$\alpha_S(q^2) = \frac{12\pi}{(11N_c - 2N_f)\ln\left(q^2/\Lambda^2_{\rm QCD}\right)}\,, \tag{4}$$

the "$11N_c$" comes from the charge-antiscreening gluon loop and the "$2N_f$" from the charge-screening fermion loop, which illustrates how the non-Abelian structure of QCD is responsible for asymptotic freedom and suggests that confinement is related to the importance of gluon self-interactions.

Studies of the gluon DSE have been reported by many authors [1] with the conclusion that, if the ghost-loop is unimportant, then the charge-antiscreening 3-gluon vertex dominates and, relative to the free gauge boson propagator, the dressed gluon propagator is significantly enhanced in the vicinity of $k^2 = 0$. The enhancement persists to $k^2 \sim 1 - 2$ GeV^2, where a perturbative analysis becomes quantitatively reliable. In the neighbourhood of $k^2 = 0$ the enhancement can be represented [6] as a regularisation of $1/k^4$ as a distribution, which is illustrated in Fig. 2. As I will elucidate, a dressed-gluon propagator with the illustrated enhancement at $k^2 \simeq 0$ generates confinement and DCSB *without* fine-tuning.

2.2. Quark Propagator. In a covariant gauge the two-point, dressed-quark Schwinger function, or dressed-quark propagator, can be written in a number of equivalent forms

$$S(p) \;:=\; \frac{1}{i\gamma\cdot p + \Sigma(p)} \tag{5}$$

$$:=\; \frac{1}{i\gamma\cdot p\, A(p^2) + B(p^2)} \equiv -i\gamma\cdot p\,\sigma_V(p^2) + \sigma_S(p^2)\,. \tag{6}$$

$\Sigma(p)$ is the dressed-quark self-energy, which satisfies a nonlinear integral equation: the quark DSE (depicted in Fig. 3)

$$\Sigma(p) = (Z_2 - 1)\, i\gamma\cdot p + Z_4\, m_{\rm bm} +$$

$$+ Z_1 \int_q^\Lambda g^2 D_{\mu\nu}(p-q)\frac{\lambda^a}{2}\gamma_\mu S(q)\Gamma^a_\nu(q,p)\,, \tag{7}$$

where $\Gamma^a_\nu(q;p)$ is the renormalised dressed-quark-gluon vertex, $m_{\rm bm}$ is the Λ-dependent current-quark bare mass that appears in the Lagrangian and

$\int_q^\Lambda := \int^\Lambda d^4q/(2\pi)^4$ represents mnemonically a *translationally-invariant* regularisation of the integral, with Λ the regularisation mass-scale. The final stage of any calculation is to remove the regularisation by taking the limit $\Lambda \to \infty$. The quark-gluon-vertex and quark wave function renormalisation constants, $Z_1(\mu^2, \Lambda^2)$ and $Z_2(\mu^2, \Lambda^2)$, depend on the renormalisation point, μ, and the regularisation mass-scale, as does the mass renormalisation constant $Z_m(\mu^2, \Lambda^2) := Z_2(\mu^2, \Lambda^2)^{-1} Z_4(\mu^2, \Lambda^2)$.

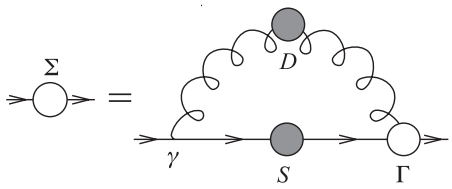

Fig. 3. DSE for the dressed-quark self-energy. The kernel of this equation is constructed from the dressed-gluon propagator (D — spring) and the dressed-quark-gluon vertex (Γ — open circle). One of the vertices is bare (labelled by γ) as required to avoid overcounting

One can define a quark mass-function:

$$M(p^2) := \frac{B(p^2)}{A(p^2)} \tag{8}$$

and, as depicted in Fig. 4, solving the quark DSE using a dressed-gluon propagator that behaves as illustrated in Fig. 2 and a dressed-quark-gluon vertex, $\Gamma_\mu(p, q)$, that does not exhibit particle-like singularities at $(p-q)^2 = 0$,* yields a quark mass-function that mirrors the infrared enhancement of the dressed-gluon propagator. The results in Fig. 4 were obtained [7] with the current-quark masses:

$$m^\mu_{u/d} = 3.7\,\mathrm{MeV}, \quad m^\mu_s = 82\,\mathrm{MeV}, \quad m^\mu_c = 0.59\,\mathrm{GeV}, \quad m^\mu_b = 2.0\,\mathrm{GeV}, \tag{9}$$

at a renormalisation point of $\mu \simeq 20\,\mathrm{GeV}$. Applying the one-loop evolution formula, Eq. (39), these masses correspond to:

$$\begin{aligned} m^{1\,\mathrm{GeV}}_{u/d} &= 5.5\,\mathrm{MeV}, \quad m^{1\,\mathrm{GeV}}_s = 130\,\mathrm{MeV}, \\ m^{1\,\mathrm{GeV}}_c &= 1.0\,\mathrm{GeV}, \quad m^{1\,\mathrm{GeV}}_b = 3.4\,\mathrm{GeV} \end{aligned} \tag{10}$$

and although it is obvious from Fig. 4 that the one-loop formula does not describe correctly the momentum evolution of the mass-function down to $p^2 = 1\,\mathrm{GeV}^2$, the values in Eq. (10) provide a useful and meaningful comparison with the values quoted conventionally.

*A particle-like singularity is one of the form $(P^2)^{-\alpha}$, $\alpha \in (0, 1]$. In this case one can write a spectral decomposition for the vertex in which the spectral densities are non-negative. This is impossible if $\alpha > 1$. $\alpha = 1$ is the ideal case of an isolated, δ-function singularity in the spectral densities and hence an isolated, free-particle pole. $\alpha \in (0, 1)$ corresponds to an accumulation, at the particle pole, of branch points associated with multiparticle production.

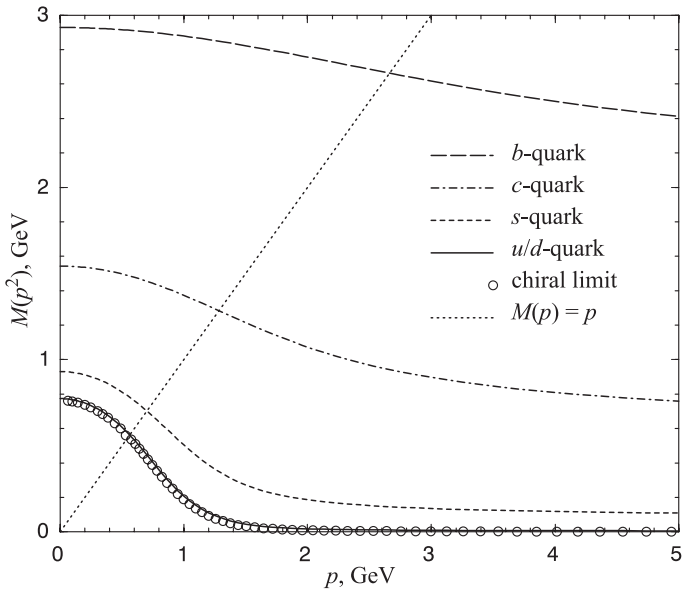

Fig. 4. Dressed-quark mass-function obtained in solving the quark DSE using the dressed-gluon propagator of Ref.7

The quark DSE was also solved in the chiral limit, which in QCD is obtained by setting the Lagrangian current-quark bare mass to zero [7]. From the figure one observes immediately that the mass-function is nonzero even in this case. That *is* DCSB: a momentum-dependent quark mass generated dynamically in the absence of any term in the action that breaks chiral symmetry explicitly. This entails a nonzero value for the quark condensate in the chiral limit. The fact that $M(p^2) \neq 0$ in the chiral limit is independent of the details of the dressed-gluon propagator in Fig. 2; they only affect the magnitude of $M(p^2)$.

Figure 4 illustrates that for light quarks (u, d and s) there are two distinct domains: perturbative and nonperturbative. In the perturbative domain the magnitude of the quark mass-function is governed by the explicit chiral symmetry breaking mass-scale; i.e., the current-quark mass. For $p^2 < 1\,\mathrm{GeV}^2$ the mass-function rises sharply. This is the nonperturbative domain where the magnitude of $M(p^2)$ is determined by the DCSB mechanism; i.e., the enhancement in the dressed-gluon propagator. This emphasises again that DCSB is more than just a nonzero value of the quark condensate in the chiral limit! The boundary, at $p^2 \sim 1\,\mathrm{GeV}^2$, is that point where the enhancement in the dressed-gluon propagator becomes significant.

The solution of $p^2 = M^2(p^2)$ defines an Euclidean constituent-quark mass, M^E.* For a given quark flavour, the ratio M_f^E/m_f^μ is a single, quantitative measure of the importance of the DCSB mechanism in modifying the quark's propagation characteristics. As illustrated in Eq. (11), obtained using the dressed-gluon propagator in Ref.7,

flavour	u/d	s	c	b	t
$\frac{M^E}{m_{\mu\sim 20\,\mathrm{GeV}}}$	150	10	2.3	1.4	$\to 1$

(11)

this ratio provides for a natural classification of quarks as either light or heavy. For light quarks the ratio is characteristically 10-100 while for heavy quarks it is only 1—2 [8]. The values of this ratio signal the existence of a characteristic mass-scale associated with DCSB, which I will denote by M_χ. For $p^2 > 0$ the propagation characteristics of a flavour with $m_f^\mu < M_\chi$ are altered significantly by the DCSB mechanism, while for flavours with $m_f^\mu \gg M_\chi$ it is irrelevant, and explicit chiral symmetry breaking dominates. It is apparent from the figure that $M_\chi \sim 0.2\,\mathrm{GeV} \sim \Lambda_{\mathrm{QCD}}$.

The effect that the enhancement of the dressed-gluon propagator has on the light-quark mass-function is fundamental in QCD and can be identified as the source of many observable phenomena. Further, that this enhancement little affects heavy-quark propagation characteristics at spacelike-p^2 provides for many simplifications in the study of heavy-meson observables [9].

2.3. Confinement. One aspect of confinement is the absence of quark and gluon production thresholds in colour-singlet-to-singlet $\mathcal{S}$-matrix amplitudes. This is manifest if, for example, the quark-loop illustrated in Fig. 5, which describes [10] the diffractive, Pomeron-induced $\gamma \to \rho$ transition, does not have pinch singularities associated with poles at real-p^2 in the quark propagators. This is ensured if the dressed-quark and -gluon propagators do not have a Lehmann representation.

What is a Lehmann representation?

Consider the 2-point free-scalar Schwinger function:

$$\Delta(k^2) = \frac{1}{k^2 + m^2}\,. \tag{12}$$

One can write

$$\Delta(z) = \int_0^\infty d\sigma\, \frac{\rho(\sigma)}{z + \sigma}\,, \tag{13}$$

*In my Euclidean metric a true quark mass-pole exhibits itself as a real-p^2 solution of $p^2 + M^2(p^2) = 0$. This is absent in the solutions of the quark DSE illustrated in Fig. 4, which is a manifestation of confinement, as discussed in Sec. 2.3.

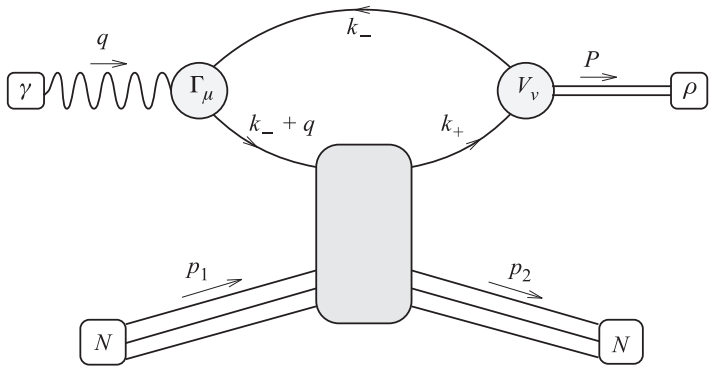

Fig. 5. Illustration of the diffractive electroproduction of a vector meson: $e^- N \to e^{-\prime} N \rho$ with the transition from photon to vector meson proceeding via a quark loop. The shaded region represents [10] a Pomeron-exchange mechanism

where in this case the spectral density is

$$\rho(x) := \frac{1}{2\pi i} \lim_{\epsilon \to 0} [\Delta(-x - i\epsilon) - \Delta(-x + i\epsilon)] = \delta(m^2 - x)\,, \qquad (14)$$

which is non-negative. This is a Lehmann representation: each scalar function necessary to completely specify the Schwinger function has a spectral decomposition in which the spectral densities are non-negative. Only those functions whose poles or branch points lie at timelike, real-k^2 have a Lehmann representation.

The existence of a Lehmann representation for a dressed-particle propagator is necessary if the construction of asymptotic "in" and "out" states for the associated quanta is to proceed; i.e., it is necessary if these quanta are to propagate to a "detector". In its absence there are no asymptotic states with the quantum numbers of the field whose propagation characteristics are described by the Schwinger function. Structurally, the nonexistence of a Lehmann representation for the dressed-propagators of elementary fields ensures the absence of pinch singularities in loops, such as that illustrated in Fig. 5, and hence the absence of quark and gluon production thresholds.

This mechanism can be generalised and applied to coloured bound states, such as colour-antitriplet quark-quark composites (diquarks). In this case a study [3] of the 4-point quark-quark scattering matrix shows that it does not have a spectral decomposition with non-negative spectral densities and hence there are no diquark bound states. The same argument that demonstrates this absence of diquarks in the spectrum of $SU(N_c = 3)$ also proves [4] that in $SU(N_c = 2)$ the "baryons", which are necessarily diquarks in this theory, are degenerate with the mesons.

The infrared-enhanced dressed-gluon propagators illustrated in Fig. 2 do not have a Lehmann representation. Using forms like this in the kernel of the quark

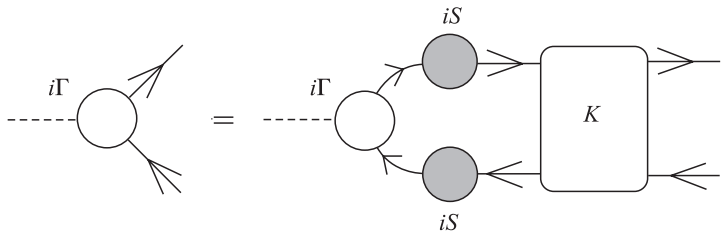

Fig. 6. Homogeneous Bethe — Salpeter equation for a quark-antiquark bound state: Γ is the solution, the Bethe — Salpeter amplitude, S is the dressed-quark propagator and K is the dressed-quark-antiquark scattering kernel

DSE yields automatically a dressed-quark 2-point function that does not have a Lehmann representation. In this sense confinement *breeds* confinement, without fine-tuning.

2.4. Hadrons: Bound States. In QCD the observed hadrons are composites of the elementary quanta: mesons of a quark and antiquark, and baryons of three quarks. Their masses, electromagnetic charge radii and other properties can be understood in terms of their substructure by studying covariant bound state equations: the Bethe — Salpeter equation (BSE) for mesons and the covariant Fadde'ev equation for baryons.

As a two-body problem, the mesons have been studied most extensively. Their internal structure is described by the Bethe — Salpeter amplitude, which is obtained as a solution of the homogeneous BSE, illustrated in Fig. 6. For a pseudoscalar bound state the amplitude has the form

$$\Gamma_H(k;P) = T^H\gamma_5 \Big[iE_H(k;P) + \gamma\cdot P F_H(k;P) + \\ + \gamma\cdot k\, k\cdot P\, G_H(k;P) + \sigma_{\mu\nu}\, k_\mu P_\nu\, H_H(k;P) \Big] , \tag{15}$$

where, if the constituents have equal current-quark masses, the scalar functions E, F, G, and H are even under $k\cdot P \to -k\cdot P$. In Eq. (15), T^H is a flavour matrix that determines the mesonic channel under consideration; e.g., $T^{K^+} := (1/2)\left(\lambda^4 + i\lambda^5\right)$, with $\{\lambda^j, j = 1\ldots 8\}$ the Gell-Mann matrices. The important new element in the BSE is K, the fully-amputated, quark-antiquark scattering kernel: by definition it does not contain quark-antiquark to single gauge-boson annihilation diagrams, such as would describe the leptonic decay of the pion, nor diagrams that become disconnected by cutting one quark and one antiquark line.

K has a skeleton expansion in terms of the elementary, dressed-particle Schwinger functions; e.g., the dressed-quark and -gluon propagators. The first

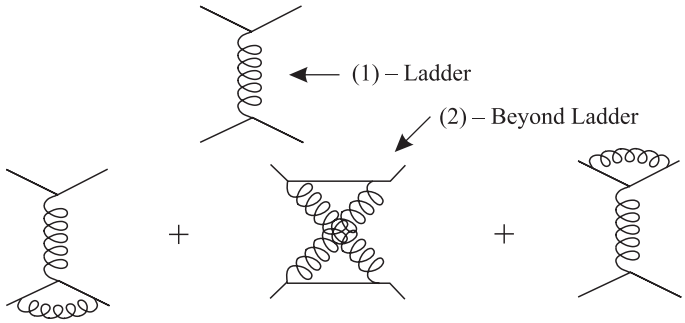

Fig. 7. First two sets of contributions to a systematic expansion of the quark-antiquark scattering kernel. In this expansion, the propagators are dressed but the vertices are bare

two orders in one systematic expansion are depicted in Fig. 7. This particular expansion [3], in concert with its analogue for the kernel in the quark DSE, provides a means of constructing a kernel that, order-by-order in the number of vertices, ensures the preservation of vector and axial-vector Ward — Takahashi identities. This is particularly important in QCD where the Goldstone boson nature of the pion must be understood as a *consequence* of its internal structure.

To proceed with a study of meson properties, one chooses a truncation for K. The homogeneous BSE is then fully specified as a linear integral equation, which is straightforward to solve, yielding the bound state mass and amplitude. The "ladder" truncation of K combined with the "rainbow" truncation of the quark DSE ($\Gamma_\mu \to \gamma_\mu$ in Fig. 3) is the simplest and most often used. The expansion of Fig. 7 allows one to understand why this Ward — Takahashi identity preserving truncation is accurate for flavour-nonsinglet pseudoscalar and vector mesons: there are cancellations between the higher-order diagrams. And also why it provides a poor approximation in the study of scalar mesons, where the higher-order terms do not cancel, and for flavour-singlet mesons where it omits timelike gluon exchange diagrams.

3. A QCD MASS FORMULA

The chiral-limit axial-vector Ward — Takahashi identity (AV-WTI)

$$-iP_\mu \Gamma^H_{5\mu}(k;P) = \mathcal{S}^{-1}(k_+)\gamma_5 \frac{T^H}{2} + \gamma_5 \frac{T^H}{2}\mathcal{S}^{-1}(k_-)\,, \tag{16}$$

where $\mathcal{S} := \mathrm{diag}(S_u, S_d, \ldots)$, is the statement of chiral-current conservation in massless QCD. It relates the divergence of the inhomogeneous axial-vector vertex, $\Gamma^H_{5\mu}(k;P)$, to a sum of dressed-quark propagators. The vertex is the solution of

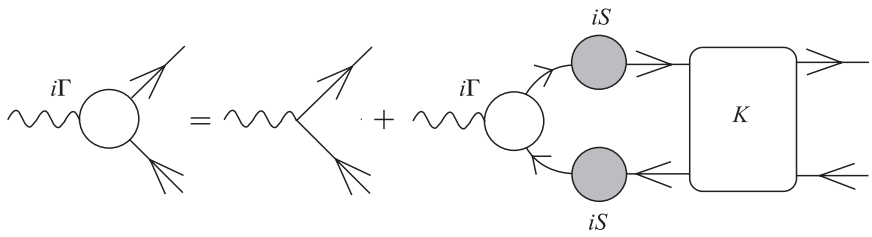

Fig. 8. DSE for the axial-vector vertex. The driving term is the bare vertex: $i\gamma_5\gamma_\mu$

the DSE depicted in Fig. 8, which involves the quark-antiquark scattering kernel, K. It is therefore not surprising that in order to preserve this identity when truncating the DSEs the choice of K and the vertex, Γ_μ, in the quark DSE, are tied together. The divergence $P_\mu\Gamma^H_{5\mu}(k;P)$ is a pseudoscalar and hence contains information about pseudoscalar mesons; i.e., Goldstone modes.

3.1. Dynamical Chiral Symmetry Breaking and Goldstone's Theorem. In the chiral-limit, the axial-vector vertex has the form [7]

$$\Gamma^H_{5\mu}(k;P) = \frac{T^H}{2}\,\gamma_5\left[\gamma_\mu F_R(k;P) + \gamma\cdot k k_\mu G_R(k;P) - \sigma_{\mu\nu}\,k_\nu\,H_R(k;P)\right] + \\ + \tilde{\Gamma}^H_{5\mu}(k;P) + \, f_H\,\frac{P_\mu}{P^2}\,\Gamma_H(k;P)\,, \tag{17}$$

where: F_R, G_R, H_R, and $\tilde{\Gamma}^H_{5\mu}$ are regular as $P^2 \to 0$; $P_\mu\tilde{\Gamma}^H_{5\mu}(k;P) \sim \mathrm{O}(P^2)$; $\Gamma_H(k;P)$ is the pseudoscalar Bethe — Salpeter amplitude in Eq. (15); and the residue of the pseudoscalar pole in the axial-vector vertex is f_H, the leptonic decay constant:

$$f_H P_\mu = Z_2\int_q^\Lambda \frac{1}{2}\mathrm{tr}\left[\left(T^H\right)^{\mathrm{t}}\gamma_5\gamma_\mu\mathcal{S}(q_+)\Gamma_H(q;P)\mathcal{S}(q_-)\right]\,, \tag{18}$$

with the trace over colour, Dirac and flavour indices. This expression is exact: the dependence of Z_2 on the renormalisation point, regularisation mass-scale and gauge parameter is just that necessary to ensure that the left-hand-side, f_H, is independent of all these things.

It now follows from the chiral-limit AV-WTI that

$$f_H E_H(k;0) = B(k^2)\,, \tag{19}$$
$$F_R(k;0) + 2\,f_H F_H(k;0) = A(k^2)\,, \tag{20}$$
$$G_R(k;0) + 2\,f_H G_H(k;0) = 2A'(k^2)\,, \tag{21}$$
$$H_R(k;0) + 2\,f_H H_H(k;0) = 0\,, \tag{22}$$

where $A(k^2)$ and $B(k^2)$ are the solutions of the quark DSE in the chiral limit. As emphasised in Sec. 2.2, the appearance of a $B(k^2) \neq 0$ solution of the quark DSE in the chiral limit signals DCSB. It is an intrinsically nonperturbative effect: in perturbation theory $B(k^2) \propto \hat{m}$, the renormalisation-point independent current-quark mass, and hence vanishes in the chiral limit. Equations (17) and (19)-(22) show that when chiral symmetry is dynamically broken: 1) the homogeneous, flavour-nonsinglet, pseudoscalar BSE has a massless, $P^2 = 0$, solution; 2) the Bethe — Salpeter amplitude for the massless bound state has a term proportional to γ_5 alone, with the momentum-dependence of $E_H(k;0)$ completely determined by that of the scalar part of the quark self energy, in addition to terms proportional to other pseudoscalar Dirac structures, F_H, G_H, and H_H, that are nonzero in general; and 3) the axial-vector vertex, $\Gamma^H_{5\mu}(k;P)$, is dominated by the pseudoscalar bound state pole for $P^2 \simeq 0$. The converse is also true.

Hence, in the chiral limit, the pion is a massless composite of a quark and an antiquark, each of which has an effective mass $M^E \sim 450\,\mathrm{MeV}$. With a dressed-gluon propagator of the type depicted in Fig. 2, this occurs without fine-tuning.

3.2. Nonzero Quark Masses: A Mass Formula. When the current-quark masses are nonzero, the AV-WTI is modified:

$$-iP_\mu \Gamma^H_{5\mu}(k;P) = \mathcal{S}^{-1}(k_+)\gamma_5 \frac{T^H}{2} + \gamma_5 \frac{T^H}{2}\mathcal{S}^{-1}(k_-) - \\ - M_{(\mu)}\,\Gamma^H_5(k;P) - \Gamma^H_5(k;P)\,M_{(\mu)}\,, \tag{23}$$

where: $M_{(\mu)} = \mathrm{diag}(m^\mu_u, m^\mu_d, m^\mu_s, \ldots)$ is the current-quark mass matrix. In this case both the axial-vector and the pseudoscalar vertices have a pseudoscalar pole: i.e.,

$$\Gamma^H_{5\mu}(k;P) = \frac{T^H}{2}\gamma_5 \left[\gamma_\mu F^H_R(k;P) + \gamma\cdot k k_\mu G^H_R(k;P) - \sigma_{\mu\nu}\,k_\nu\,H^H_R(k;P)\right] + \\ + \tilde{\Gamma}^H_{5\mu}(k;P) + \, f_H\,\frac{P_\mu}{P^2+m_H^2}\,\Gamma_H(k;P)\,, \tag{24}$$

and

$$\Gamma^H_5(k;P) = \frac{T^H}{2}\gamma_5 \left[i\mathcal{E}^H_R(k;P) + \gamma\cdot P\,\mathcal{F}^H_R(k;P) + \gamma\cdot k\,k\cdot P\,\mathcal{G}^H_R(k;P) + \right. \\ \left. + \sigma_{\mu\nu}\,k_\mu P_\nu\,\mathcal{H}^H_R(k;P)\right] + \, r_H\,\frac{1}{P^2+m_H^2}\,\Gamma_H(k;P)\,, \tag{25}$$

with: $\mathcal{E}^H_R$, F^H_R, $\mathcal{F}^H_R$, G^H_R, $\mathcal{G}^H_R$, H^H_R, $\mathcal{H}^H_R$, and $\tilde{\Gamma}^H_{5\mu}$ regular as $P^2 \to -m_H^2$ and $P_\mu\tilde{\Gamma}^H_{5\mu}(k;P) \sim \mathrm{O}(P^2)$. The AV-WTI entails [7] that

$$f_H\,m_H^2 = r_H\,\mathcal{M}_H\,, \;\; \mathcal{M}_H := \mathrm{tr}_{\mathrm{flavour}}\left[M_{(\mu)}\,\left\{T^H, \left(T^H\right)^{\mathrm{t}}\right\}\right]\,, \tag{26}$$

where f_H is given by Eq. (18), with massive quark propagators in this case, and the residue of the pole in the pseudoscalar vertex is

$$ir_H = Z_4 \int_q^\Lambda \frac{1}{2}\mathrm{tr}\left[\left(T^H\right)^{\mathrm{t}} \gamma_5 \mathcal{S}(q_+)\Gamma_H(q;P)\mathcal{S}(q_-)\right] . \tag{27}$$

The renormalisation constant Z_4 on the right-hand side depends on the gauge parameter, the regularisation mass-scale and the renormalisation point. This dependence is exactly that required to ensure that: 1) r_H is finite in the limit $\Lambda \to \infty$; 2) r_H is gauge-parameter independent; and 3) the right-hand side of Eq. (26) is renormalisation point *independent*. This is obvious at one-loop order, especially in Landau-gauge where $Z_2 \equiv 1$ and hence $Z_4 = Z_m$.

Equation (26) is a mass formula for flavour-octet pseudoscalar mesons that is valid *independent* of the magnitude of the current-quark masses of meson's constituents. For small current-quark masses, using Eqs. (15) and (19)—(22), Eq. (27) yields

$$r_H^0 = -\frac{1}{f_H^0}\,\langle\bar{q}q\rangle_\mu^0 , \quad -\langle\bar{q}q\rangle_\mu^0 := Z_4(\mu^2,\Lambda^2)\,N_c \int_q^\Lambda \mathrm{tr}_{\mathrm{Dirac}}\left[S_{\hat{m}=0}(q)\right] , \tag{28}$$

where the superscript "0" denotes that the quantity is evaluated in the chiral limit and $\langle\bar{q}q\rangle_\mu^0$, as defined here, is the chiral limit *vacuum quark condensate*, which is renormalisation-point dependent but independent of the gauge parameter and the regularisation mass-scale. Hence Eq. (25) is the statement that *in the chiral limit the residue of the bound state pole in the flavour-nonsinglet pseudoscalar vertex is* $(-\langle\bar{q}q\rangle_\mu^0)/f_H^0$.

Now one obtains immediately from Eqs. (26) and (28)

$$f_\pi^2 m_\pi^2 = -\left[m_u^\mu + m_d^\mu\right]\langle\bar{q}q\rangle_\mu^0 + \mathrm{O}\left(\hat{m}_q^2\right), \tag{29}$$

$$f_{K^+}^2 m_{K^+}^2 = -\left[m_u^\mu + m_s^\mu\right]\langle\bar{q}q\rangle_\mu^0 + \mathrm{O}\left(\hat{m}_q^2\right), \tag{30}$$

which exemplify what is commonly known as the Gell-Mann–Oakes–Renner relation. The primary result, Eq. (26), is valid *independent* of the magnitude of $\hat{m}_q$, and can be rewritten in the form

$$f_H^2\, m_H^2 = -\langle\bar{q}q\rangle_\mu^H\, \mathcal{M}_H, \tag{31}$$

where I have introduced the *notation*

$$-\langle\bar{q}q\rangle_\mu^H := f_H\, r_H = f_H Z_4 \int_q^\Lambda \frac{1}{2}\mathrm{tr}\left[\left(T^H\right)^{\mathrm{t}} \gamma_5 \mathcal{S}(q_+)\Gamma_H(q;P)\mathcal{S}(q_-)\right] , \tag{32}$$

which defines an *in-meson* condensate. This emphasises that, for nonzero current-quark masses, Eq. (26) *does not* involve a difference of vacuum massive-quark condensates; a phenomenological assumption often employed.

As elucidated elsewhere [11], Eq. (26) has another important corollary: it predicts that the mass of a heavy pseudoscalar meson rises linearly with the current-quark mass of its heavy constituent(s). Model calculations [8] show that this linear evolution is dominant at $\approx 2\hat{m}_s$, in agreement with experiment where the mass of the K, D, and B mesons lie precisely on the same straight line.

In Eq. (26) one therefore has a single mass formula, exact in QCD, that provides a unified understanding of light- and heavy-meson masses.

4. AN ILLUSTRATIVE MODEL

I have already made use of a model [7] in illustrating some of the robust results of DSE studies. To further elucidate the method I will describe that model in more detail. For the kernel of the quark DSE it employs the analogue of the lowest-order BSE kernel in Fig. 7:

$$Z_1 \int_q^\Lambda g^2 D_{\mu\nu}(p-q)\frac{\lambda^a}{2}\gamma_\mu S(q)\Gamma^a_\nu(q,p) \to$$

$$\to \int_q^\Lambda \mathcal{G}((p-q)^2)\, D^{\rm free}_{\mu\nu}(p-q)\frac{\lambda^a}{2}\gamma_\mu S(q)\frac{\lambda^a}{2}\gamma_\nu\,. \qquad (33)$$

This is the "rainbow" approximation, in which the specification of the model is complete once a form is chosen for the "effective coupling" $\mathcal{G}(k^2)$.

A choice for $\mathcal{G}(k^2)$ can be motivated by observing that at large-$Q^2 := (p-q)^2$ in an asymptotically free theory the quark-antiquark scattering kernel satisfies

$$g^2(\mu^2)\, D_{\mu\nu}(p-q)\, \left[\Gamma^a_\mu(p_+,q_+) S\,(q_+)\right] \times \left[S(q_-)\,\Gamma^a_\nu(q_-,p_-)\right] =$$

$$= 4\pi\,\alpha(Q^2)\, D^{\rm free}_{\mu\nu}(p-q)\, \left[\frac{\lambda^a}{2}\gamma_\mu\, S^{\rm free}(q_+)\right] \times \left[S^{\rm free}(q_-)\,\frac{\lambda^a}{2}\gamma_\nu\right], \qquad (34)$$

where P is the total momentum of the quark-antiquark pair, $p_+ := p + \eta_P P$ and $p_- := p - (1-\eta_P)P$ with $0 \le \eta \le 1$. Choosing a truncation of K in which this right-hand side is identified with the lowest order contribution in Fig. 7 then consistency with the AV-WTI requires

$$\mathcal{G}(Q^2) := 4\pi\,\alpha(Q^2)\,. \qquad (35)$$

Thus the form of $\mathcal{G}(Q^2)$ at large-Q^2 is fixed by that of the running coupling constant. This *Ansatz* is often described as the "Abelian approximation" because the left- and right-hand sides are *equal* in QED. In QCD, equality between the two sides of Eq. (35) cannot be obtained easily by a selective resummation of

diagrams. As reviewed in Ref.1, Eqs. (5.1) to (5.8), it can only be achieved by enforcing equality between the renormalisation constants for the ghost-gluon vertex and ghost wave function: $\tilde{Z}_1 = \tilde{Z}_3$.

The explicit form of the *Ansatz* employed in Ref.7 is

$$\frac{\mathcal{G}(k^2)}{k^2} = 8\pi^4 D\delta^4(k) + \frac{4\pi^2}{\omega^6} D k^2 \mathrm{e}^{-k^2/\omega^2} +$$

$$+4\pi \frac{\gamma_m \pi}{\frac{1}{2}\ln\left[\tau + \left(1 + k^2/\Lambda_{\mathrm{QCD}}^2\right)^2\right]} \mathcal{F}(k^2)\,, \tag{36}$$

with $\mathcal{F}(k^2) = [1 - \exp(-k^2/[4m_t^2])]/k^2$ and $\tau = \mathrm{e}^2 - 1$,$N_f = 4$ and $\Lambda_{\mathrm{QCD}}^{N_f=4} = 0.234\,\mathrm{GeV}$.

The qualitative features of Eq. (36) are clear. The first term is an integrable infrared singularity [12] and the second is a finite-width approximation to $\delta^4(k)$, normalised such that it has the same $\int d^4k$ as the first term. In this way the infrared singularity is split into the sum of a zero-width and a finite-width piece. The last term in Eq. (36) is proportional to $\alpha(k^2)/k^2$ at large spacelike-k^2 and has no singularity on the real-k^2 axis. Gluon confinement is manifest since $\mathcal{G}(k^2)/k^2$ doesn't have a Lehmann representation.

4.1. Solving the Quark DSE. There are ostensibly three parameters in Eq. (36): D, ω and m_t. However, in the numerical studies the values $\omega = = 0.3\,\mathrm{GeV}(= 1/[.66\,\mathrm{fm}])$ and $m_t = 0.5\,\mathrm{GeV}(= 1/[.39\,\mathrm{fm}])$ were fixed, and only D and the renormalised u/d- and s-current-quark masses varied in order to satisfy the goal of a good description of low-energy π- and K-meson properties. This was achieved with

$$D = 0.781\,\mathrm{GeV}^2\,, \quad m_{u/d}^{\mu} = 3.74\,\mathrm{MeV}\,, \quad m_s^{\mu} = 82.5\,\mathrm{MeV}\ , \tag{37}$$

at $\mu \approx 20\,\mathrm{GeV}$, which is large enough to be in the perturbative domain. The effective coupling obtained is depicted in Fig. 9.

Using Eqs. (33), (36), (37), and the renormalisation boundary condition

$$S(p)^{-1}\big|_{p^2=\mu^2} = i\gamma\cdot p + m^{\mu}\,, \tag{38}$$

the quark DSE, Eq. (7), is completely specified and can be solved by iteration.

The chiral limit in QCD is unambiguously defined by $\hat{m} = 0$. In this case there is no perturbative contribution to the scalar piece of the quark self energy, $B(p^2,\mu^2)$: in fact, there is no scalar, mass-like divergence in the perturbative calculation of the self energy. It follows that $Z_2(\mu^2,\Lambda^2)\, m_{\mathrm{bm}}(\Lambda^2) = 0\,, \forall\Lambda$ and, from Eq. (38), that there is no subtraction in the equation for $B(p^2,\mu^2)$. In terms

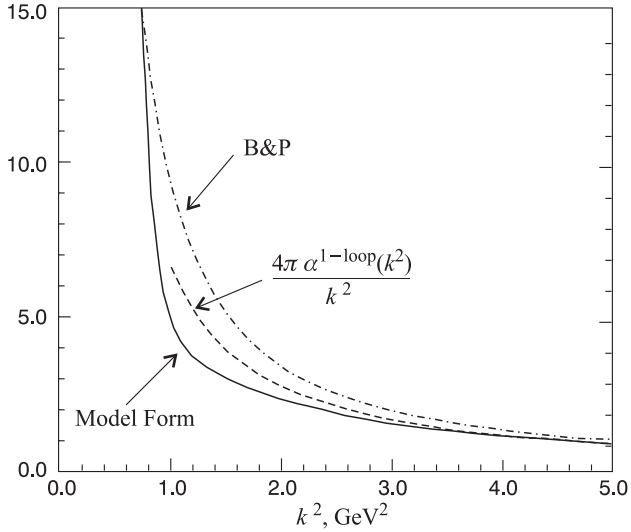

Fig. 9. *Ansatz* for $\mathcal{G}(k^2)/k^2$ employed in Ref.7. "B&P" labels a solution [6] of the gluon DSE, which is presented for comparison, as is the one-loop running coupling in QCD

of the renormalised current-quark mass the existence of DCSB means that, in the chiral limit, $M(\mu^2) \sim \mathrm{O}(1/\mu^2)$, up to $\ln \mu^2$-corrections.*

Figure 10 depicts the renormalised dressed-quark mass function, $M(p^2)$, obtained by solving the quark DSE using the parameters in Eq. (37), and in the chiral limit. It is a complement to Fig. 4 because it highlights the qualitative difference between the behaviour of $M(p^2)$ in the chiral limit and in the presence of explicit chiral symmetry breaking. In the latter case

$$M(p^2) \stackrel{\mathrm{large}-p^2}{=} \frac{\hat{m}}{\left(\frac{1}{2}\ln\left[\frac{p^2}{\Lambda^2_{\mathrm{QCD}}}\right]\right)^{\gamma_m}} \{1 + \mathit{two\ loop}\}\ ,\ \gamma_m = \frac{12}{33 - 2N_f}\,. \quad (39)$$

However, in the chiral limit the ultraviolet behaviour is given by

$$M(p^2) \stackrel{\mathrm{large}-p^2}{=} \frac{2\pi^2\gamma_m}{3}\,\frac{\left(-\langle\bar{q}q\rangle^0\right)}{p^2\left(\frac{1}{2}\ln\left[\frac{p^2}{\Lambda^2_{\mathrm{QCD}}}\right]\right)^{1-\gamma_m}}\,, \quad (40)$$

where $\langle\bar{q}q\rangle^0$ is the renormalisation-point-independent vacuum quark condensate.

*This is a model-independent statement; i.e., it is true in any study that preserves the one-loop renormalisation group behaviour of QCD.

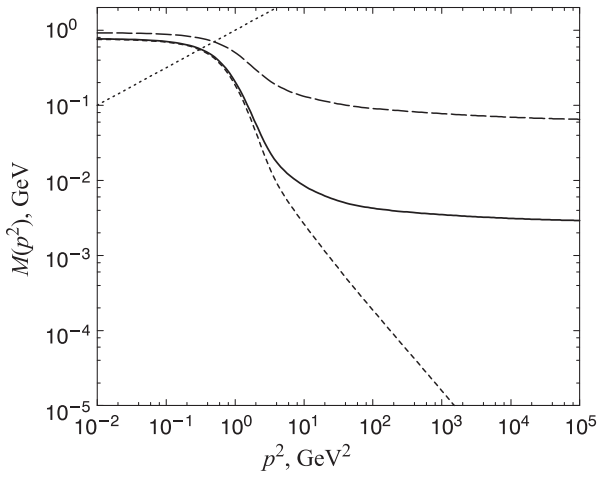

Fig. 10. The renormalised dressed-quark mass function, $M(p^2)$, obtained in solving the quark DSE using the parameters in Eq. (37): u/d-quark (solid line); s-quark (long-dashed line); and chiral limit (dashed line). The renormalisation point is $\mu \approx 20\,\mathrm{GeV}$. The intersection of the line $M^2(p^2) = p^2$ (dotted line) with each curve defines the Euclidean constituent-quark mass, M^E

Analysing the chiral limit solution yields

$$-\langle\bar{q}q\rangle^0 = (0.227\,\mathrm{GeV})^3\,, \tag{41}$$

which is a reliable means of determining $\langle\bar{q}q\rangle^0$ because corrections to Eq. (40) are suppressed by powers of $\Lambda^2_{\mathrm{QCD}}/\mu^2$.

Equation (28) defines the renormalisation-point-dependent vacuum quark condensate

$$-\langle\bar{q}q\rangle^0_\mu\big|_{\mu=19\,\mathrm{GeV}} :=$$
$$= \left(\lim_{\Lambda\to\infty} Z_4(\mu,\Lambda)\,N_c\int_q^\Lambda \mathrm{tr}_{\mathrm{Dirac}}\left[S_{\hat{m}=0}(q)\right]\right)\Bigg|_{\mu=19\,\mathrm{GeV}} = (0.275\,\mathrm{GeV})^3\,, \tag{42}$$

the calculated result. It is straightforward to establish explicitly that $m^\mu\,\langle\bar{q}q\rangle^0_\mu =$ constant, independent of μ, and hence

$$m^\mu\,\langle\bar{q}q\rangle^0_\mu := \hat{m}\,\langle\bar{q}q\rangle^0\,, \tag{43}$$

which unambiguously defines the renormalisation-point-independent current-quark masses. From this and Eqs. (37), (41) and (42) one obtains the values of these masses appropriate to this model

$$\hat{m}_{u/d} = 6.60\,\mathrm{MeV}\,,\ \hat{m}_s = 147\,\mathrm{MeV}\,. \tag{44}$$

Using the one-loop evolution in Eq. (39) these values yield $m^{\mu}_{u/d} = 3.2\,\mathrm{MeV}$ and $m^{\mu}_{s} = 72\,\mathrm{MeV}$, which are within $\sim 10\%$ of the actual values in Eq. (37). This indicates that higher-loop corrections to the one-loop formulae, which are present in the solution of the integral equation as made evident by $A(p^2,\mu^2) \not\equiv 1$ in Landau gauge, provide contributions of $< 10\%$ at $p^2 = \mu^2$. The higher-loop contributions decrease with increasing p^2.

From the renormalisation-point-invariant product in Eq. (43) one obtains

$$-\left.\langle\bar{q}q\rangle^0_\mu\right|_{\mu=1\,\mathrm{GeV}} := (\ln[1/\Lambda_{\mathrm{QCD}}])^{\gamma_m}\ \langle\bar{q}q\rangle^0 = (0.241\,\mathrm{GeV})^3\,. \tag{45}$$

This result can be compared directly with the value of the quark condensate employed in contemporary phenomenological studies: [13] $(0.236 \pm 0.008\,\mathrm{GeV})^3$. Increasing $\omega \to 1.5\,\omega$ in $\mathcal{G}(k^2)$ raises the calculated value in Eq. (45) by $\sim 10\%$, a weak sensitivity.

After this discussion of the vacuum quark condensate it is straightforward to determine the accuracy of Eqs. (29) and (30). Using experimental values on the left-hand side, one finds:

$$(0.0924\times 0.1385)^2 = (0.113\,\mathrm{GeV})^4 \ \mathrm{cf.}\ (0.111\,\mathrm{GeV})^4 = 2\times 0.0055\times 0.24^3 \tag{46}$$

$$(0.113\times 0.495)^2 = (0.237\,\mathrm{GeV})^4 \ \mathrm{cf.}\ (0.206\,\mathrm{GeV})^4 = (0.0055+0.13)\times 0.24^3\,, \tag{47}$$

which indicates that $\mathrm{O}(\hat{m}^2)$-corrections begin to become important at current-quark masses near that of the s-quark, as demonstrated further in Ref.8.

4.2. Solving the Pseudoscalar Meson BSE. The model quark DSE described above employs the rainbow truncation. Following Fig. 7 the consistent Ward — Takahashi identity preserving truncation of the quark-antiquark scattering kernel is the ladder approximation:

$$K^{rs}_{tu}(q,k;P) = -\,\mathcal{G}((k-q)^2)\,D^{\mathrm{free}}_{\mu\nu}(k-q)\,\left(\gamma_\mu\frac{\lambda^a}{2}\right)_{tr}\left(\gamma_\nu\frac{\lambda^a}{2}\right)_{su}\,, \tag{48}$$

in which case the explicit form of Fig. 6 is

$$\Gamma_H(k;P) + \int_q^\Lambda \mathcal{G}((k-q)^2)\,D^{\mathrm{free}}_{\mu\nu}(k-q)\frac{\lambda^a}{2}\gamma_\mu\mathcal{S}(q_+)\Gamma_H(q;P)\mathcal{S}(q_-)\frac{\lambda^a}{2}\gamma_\nu = 0\,. \tag{49}$$

Having an *Ansatz* for $\mathcal{G}(k^2)$, $S(q)$ in Eq. (49) follows by solving the quark DSE. The kernel of the BSE is then completely specified and solving the equation for $\Gamma_H(k;P)$ and the bound state mass is a straightforward numerical problem. Then, with $D_{\mu\nu}(k)$, $S(p)$ and $\Gamma_H(k;P)$, the calculation of other observables such as: the leptonic decay constant, f_H; meson charge radius, r_H; and electromagnetic form factor, $F_H(Q^2)$; etc., is possible.

The general form of the solution of Eq. (49) is given in Eq. (15), where the scalar functions depend on the variables k^2 and $k \cdot P$ and are labelled by the eigenvalue P^2. From this it is clear that the integrand in Eq. (49) depends on the scalars: k^2, $k \cdot q$, q^2, $q \cdot P$, and P^2, which takes a fixed-value at the solution; i.e., at each value of P^2 the kernel is a function of four, independent variables. Solving Eq. (49) can therefore require large-scale computing resources, especially since there are four, independent scalar functions in the general form of the solution.

Two different solution techniques can be employed. In one procedure, which I will label: (A), the scalar functions are treated directly as dependent on two, independent variables: $E(k^2, k \cdot P; P^2)$, etc. This requires straightforward, multidimensional integration at every iteration. Storing the multidimensional kernel requires a large amount of computer memory but the iteration proceeds quickly.

An adjunct, which I will label: (B), employs a Chebyshev decomposition procedure. It is implemented by writing

$$E(k^2, k \cdot P; P^2) \approx \sum_{i=0}^{N_{\max}} {}^iE(k^2; P^2)\, U_i(\cos\beta)\,, \tag{50}$$

with similar expansions for F, $\underline{\hat{G} := k \cdot P\, G}$ and H, where $k \cdot P := \cos\beta\sqrt{k^2 P^2}$ and $\{U_i(x); i = 0, \ldots, \infty\}$ are Chebyshev polynomials of the second kind, orthonormalised according to:

$$\frac{2}{\pi}\int_{-1}^{1} dx\, \sqrt{1-x^2}\, U_i(x) U_j(x) = \delta_{ij}\,. \tag{51}$$

This procedure requires a large amount of time to set up the kernel but does not require large amounts of computer memory.

In Tables 1 and 2 I list values of the dimensionless ratio

$$\mathcal{R}_H := -\frac{\langle\bar{q}q\rangle_\mu^H \mathcal{M}_H}{f_H^2 m_H^2}\,. \tag{52}$$

A value of $\mathcal{R}_H = 1$ means that Eq. (26) is satisfied and hence so is the AV-WTI.* Looking at the tabulated values of $\mathcal{R}_H$ it is clear that the scalar function H is not quantitatively important, with the AV-WTI being satisfied numerically with the retention of E, F and G in the pseudoscalar meson Bethe — Salpeter amplitude. The values of $\mathcal{R}_H$, and the other tabulated quantities, highlight the importance

*It illustrates that the pseudoscalar-meson pole in the axial-vector vertex is related to the pseudoscalar-meson pole in the pseudoscalar vertex in the manner elucidated above. A finite value in the chiral limit emphasises that $m_H^2 \propto \mathcal{M}_H$ as $\mathcal{M}_H \to 0$.

Table 1. Calculated values of the properties of light, pseudoscalar mesons composed of a quark and antiquark of equal-mass. The mass ($m_\pi^{\rm exp} = 0.1385$) and decay constant ($f_\pi^{\rm exp} = 0.0924$) are in GeV, $\mathcal{R}_H$ is dimensionless. With the exception of the calculations that retain only the zeroth Chebyshev moment, labelled by "U_0 only", the results are independent of the momentum partitioning parameter, η_P, in Eq. (34).

All amplitudes	π			chiral limit			$s\bar{s}$		
	m_π	f_π	$\mathcal{R}_H$	m_0	f^0	$\mathcal{R}_H$	$m_{s\bar{s}}$	$f_{s\bar{s}}$	$\mathcal{R}_H$
Method (A)	0.1385	0.0924	1.01	0.0	0.0898	1.00	0.685	0.129	1.00
U_0 only	0.136	0.0999	0.95	0.0	0.0972	0.94	0.675	0.137	0.95
U_0 and U_1	0.1385	0.0925	1.00	0.0	0.0898	1.00	0.685	0.129	1.00
E only									
Method (A)	0.105	0.0667	1.82	0.0	0.0649	1.81	0.512	0.092	1.68
U_0 only	0.105	0.0667	1.82	0.0	0.0649	1.81	0.513	0.092	1.69
E, F									
Method (A)	0.136	0.0992	0.95	0.0	0.0965	0.95	0.677	0.137	0.95
U_0 only	0.136	0.0992	0.95	0.0	0.0965	0.95	0.678	0.138	0.95
E, F, $\hat{G}$									
Method (A)	0.140	0.0917	1.01	0.0	0.0891	1.00	0.688	0.128	1.01
U_0 only	0.136	0.0992	0.95	0.0	0.0965	0.95	0.678	0.138	0.95
U_0 and U_1	0.140	0.0917	1.01	0.0	0.0891	1.00	0.689	0.128	1.01

of F and $\hat{G}$: F is the most important of these functions but $\hat{G}$ nevertheless provides a significant contribution, particularly for bound states of unequal-mass constituents.

From Tables 1 and 2, and Eqs. (31), (32), (37), and (45), one calculates

$$\begin{array}{ccc} -\langle\bar{q}q\rangle^{\pi}_{\mu=1\,\rm GeV} & -\langle\bar{q}q\rangle^{K}_{\mu=1\,\rm GeV} & -\langle\bar{q}q\rangle^{s\bar{s}}_{\mu=1\,\rm GeV} \\ (0.245\,{\rm GeV})^3 & (0.284\,{\rm GeV})^3 & (0.317\,{\rm GeV})^3 \end{array} \tag{53}$$

showing that, for light pseudoscalars, the "in-meson condensate" I have defined increases with increasing bound state mass; as does the leptonic decay constant, f_H.* Both of these trends are modified as one moves into the heavy-quark domain: $-\langle\bar{q}q\rangle^H_\mu \to$ const. and $f_H \to 0$ as $\mathcal{M}_H \to \infty$.

Figure 11 depicts the scalar functions in the Bethe — Salpeter amplitude obtained as solutions of Eq. (49), focusing on the zeroth Chebyshev moment of each function, which is obtained via

$$^0E_H(k^2) := \frac{2}{\pi}\int_0^\pi d\beta\, \sin^2\beta\, U_0(\cos\beta)\, E_H(k^2, k\cdot P; P^2)\,, \tag{54}$$

*$(-\langle\bar{q}q\rangle^H_\mu)/f_H$ is the residue of the bound state pole in the pseudoscalar vertex, just as f_H is the residue of the bound state pole in the axial-vector vertex. As expected, $\langle\bar{q}q\rangle^\pi_{\mu=1\,\rm GeV} \approx \langle\bar{q}q\rangle^0_\mu\big|_{\mu=1\,\rm GeV}$.

Table 2. Calculated properties of the K meson for various values of the momentum partitioning parameter, η_P; "$-$" means that no bound state solution exists in this case. The mass ($m_K^{\rm exp} = 0.496$) and decay constant ($f_K^{\rm exp} = 0.113$) are in GeV, $\mathcal{R}_K$ is dimensionless

All amplitudes	$\eta_P = 0.50$			$\eta_P = 0.25$			$\eta_P = 0.00$		
	m_K	f_K	$\mathcal{R}_K$	m_K	f_K	$\mathcal{R}_K$	m_K	f_K	$\mathcal{R}_K$
Method (A)	0.497	0.109	1.01	0.497	0.109	1.01	0.497	0.109	1.01
U_0 only	0.469	0.117	0.96	0.482	0.117	0.95	0.475	0.113	1.02
U_0 and U_1	0.500	0.111	1.00	0.497	0.109	1.01	0.498	0.110	1.00
U_0, U_1 and U_2	0.497	0.109	1.01	0.497	0.109	1.01	0.496	0.109	1.01
E only									
Method (A)	0.430	0.079	1.55	0.430	0.079	1.55	0.429	0.076	1.55
U_0 only	0.380	0.077	1.54	0.401	0.076	1.51	0.415	0.073	1.55
U_0 and U_1	0.439	0.089	1.52	0.430	0.078	1.55	0.431	0.076	1.57
U_0, U_1 and U_2	0.430	0.078	1.55	0.430	0.078	1.55	0.427	0.076	1.55
E, F									
Method (A)	0.587	0.17	0.79	0.557	0.14	0.86	0.533	0.11	0.94
U_0 only	0.505	0.12	0.82	0.518	0.11	0.86	0.512	0.11	0.96
U_0 and U_1	-	-	-	0.556	0.14	0.86	0.537	0.12	0.94
U_0, U_1 and U_2	0.583	0.16	0.79	0.557	0.14	0.86	0.532	0.12	0.93
E, F, $\hat{G}$									
Method (A)	0.500	0.108	1.01	0.500	0.108	1.01	0.500	0.108	1.01
U_0 only	0.471	0.116	0.96	0.484	0.116	0.95	0.477	0.112	1.02
U_0 and U_1	0.504	0.110	1.00	0.500	0.108	1.01	0.502	0.109	1.00
U_0, U_1 and U_2	0.500	0.108	1.01	0.500	0.108	1.01	0.499	0.108	1.01

and similarly for F, G [$\hat{G}$ for the K meson] and H. I note that: the momentum-space width of ${}^0E_H(k^2)$ increases as the current-quark mass of the bound state constituents increases; ${}^0F_H(k^2=0)$ decreases with increasing current-quark mass but that ${}^0F_H(k^2)$ is still larger at $k^2 > 0.5\,{\rm GeV}^2$ for bound states of higher mass; ${}^0G_H(k^2)$ [${}^0\hat{G}_K(k^2)$] behaves similarly; and the same is true for $H_H(k;P)$ but it is uniformly small in magnitude thereby explaining its quantitative insignificance.

Figure 12 depicts the large-k^2 behaviour of the scalar functions in the pseudoscalar Bethe — Salpeter amplitude. The momentum dependence of ${}^0E_H(k^2)$ at large-k^2 is identical to that of the chiral-limit quark mass function, $M(p^2)$ in Eq. (40), [14] and characterises the form of the quark-quark interaction in the ultraviolet. Figure 12 elucidates that this is also true of ${}^0F_H(k^2)$, $k^2\,{}^0G_H(k^2)$ [$k^2\,{}^0\hat{G}_K(k^2)$ for the K meson] and $k^2\,{}^0H_H(k^2)$. Each of these functions reaches its ultraviolet limit by $k^2 \simeq 10\,{\rm GeV}^2$, which is very-much-less-than the renormalisation point, $\mu^2 = 361\,{\rm GeV}^2$. As I will illustrate below, this result has important implications for the behaviour of pseudoscalar meson form factors.

A direct verification of Eqs. (19)—(22) is possible in this concrete model. Consider the inhomogeneous axial-vector vertex equation, Fig. 8, in the ladder

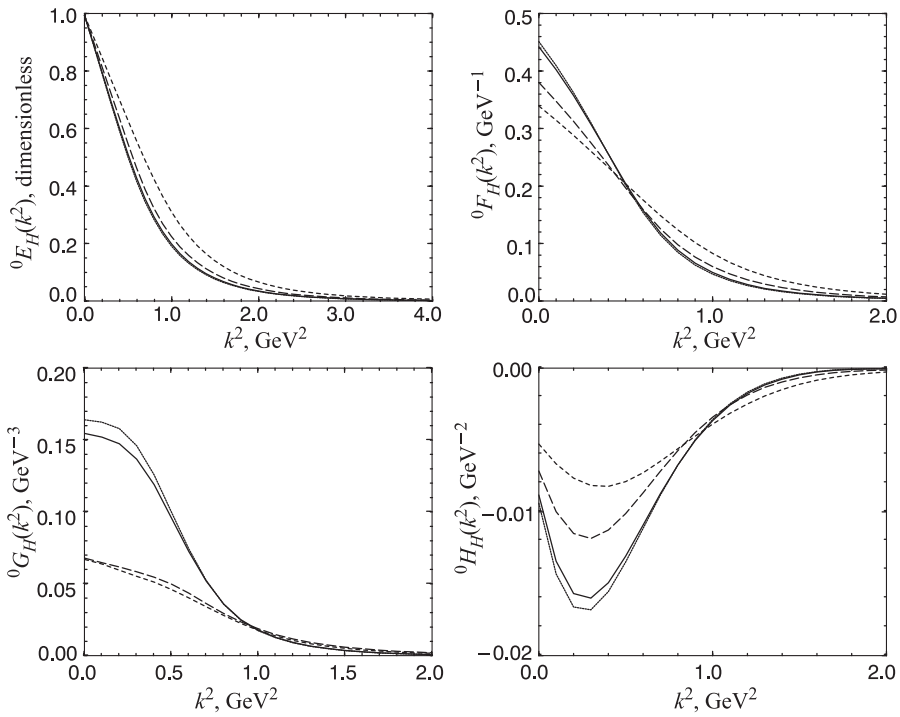

Fig. 11. The zeroth Chebyshev moment of the scalar functions in the mesons' Bethe — Salpeter amplitude: chiral limit (dotted line); π meson (solid line); K meson (long-dashed line); and fictitious, $s\bar{s}$ bound state (dashed line). For ease of comparison the amplitudes are all rescaled so that $^0E_H(k^2=0)=1$

truncation:

$$\Gamma^H_{5\mu}(k;P) = Z_2\gamma_5\gamma_\mu\frac{T^H}{2} -$$

$$-\int_q^\Lambda \mathcal{G}((k-q)^2)\, D^{\rm free}_{\mu\nu}(k-q)\frac{\lambda^a}{2}\gamma_\mu\mathcal{S}(q_+)\Gamma^H_{5\mu}(q;P)\mathcal{S}(q_-)\frac{\lambda^a}{2}\gamma_\nu\,. \qquad (55)$$

From the homogeneous BSE one already has the equations satisfied by $E_H(k;0)$, $F_H(k;0)$, $G_H(k;0)$, and $H_H(k;0)$. To proceed, one substitutes Eq. (17) for $\Gamma^H_{5\mu}(k;P)$ in Eq. (55). Using the coupled equations for $E_H(k;0)$, etc., one can identify and eliminate each of the pole terms associated with the pseudoscalar bound state. [That the homogeneous BSE is linear in the Bethe — Salpeter amplitude allows this.] That yields a system of coupled equations for $F_R(k;0)$, $G_R(k;0)$, and $H_R(k;0)$, which can be solved without complication. [The factor of Z_2 automatically ensures that $F_R(k^2=\mu^2;P=0)=1$.] The realisation of

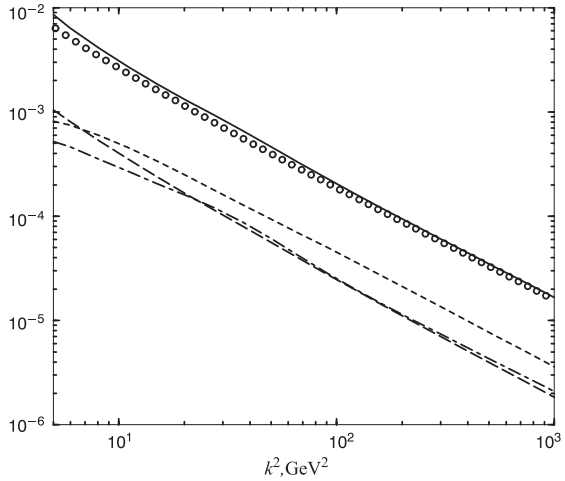

Fig. 12. Asymptotic behaviour of the 0th Chebyshev moments of the functions in the π-meson Bethe — Salpeter amplitude: $f_\pi\ {}^0E_\pi(k^2)$ (GeV, solid line); $f_\pi\ {}^0F_\pi(k^2)$ (dimensionless, long-dashed line); $k^2\ f_\pi\ {}^0G_\pi(k^2)$ (dimensionless, dashed line); and $k^2\ f_\pi\ {}^0H_\pi(k^2)$ (GeV, dot-dashed line). The k^2 dependence is identical to that of the chiral-limit quark mass function, $M(p^2)$, Eq. (40). For other pseudoscalar mesons the momentum dependence of these functions is qualitatively the same, although the normalising magnitude differs

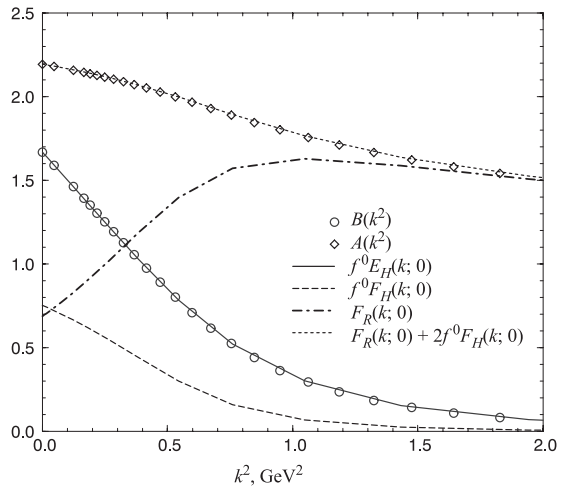

Fig. 13. An illustration of the realisation of the identities Eqs. (19) and (20), which are a necessary consequence of preserving the axial vector Ward — Takahashi identity

the first two identities, Eqs. (19) and (20), is illustrated in Fig. 13. The remaining two identities, Eqs. (21) and (22), are realised in a similar fashion.

5. ADDITIONAL PHENOMENOLOGICAL APPLICATIONS

In the model illustration of Sec. 4 an algebraic *Ansatz* was developed for the dressed-gluon propagator based on the qualitative behaviour of solutions of the gluon DSE. From this basic beginning, I illustrated how one can proceed to calculate hadronic observables. A number of qualitatively significant features emerged, among them DCSB and confinement, all of which are related to the strong momentum dependence of the quark mass function, Eq. (8), in the infrared.

That last observation suggests an alternative phenomenological approach: develop an algebraic *Ansatz* for the dressed-quark propagator. This is not as fundamental as the approach in Sec. 4 because many, apparently distinct features of the dressed-quark propagator are encoded in a few parameters of the *Ansatz* for the dressed-gluon propagator; modelling the dressed-quark propagator directly requires additional parameters to describe correlated effects. However, it has a significant merit: with an algebraic as opposed to a numerical representation of the dressed-quark propagator it is possible to study scattering observables more quickly and easily. The approach can yield quantitatively reliable results provided the *Ansatz* exhibits those essential qualitative features manifest in a direct solution of the quark DSE using a realistic *Ansatz* for the dressed-gluon propagator. Further, in allowing a rapid analysis of a broad range of observable phenomena, it provides a means of exploring the hypothesis that the bulk of hadronic phenomena are simply a manifestation of the nonperturbative, momentum-dependent dressing of the elementary Schwinger functions in QCD.

A simple and widely used model is [15]

$$\bar{\sigma}_S(\xi) = 2\bar{m}\mathcal{F}(2(\xi+\bar{m}^2)) + \mathcal{F}(b_1\,\xi)\mathcal{F}(b_3\,\xi)\,(b_0 + b_2\mathcal{F}(\varepsilon\,\xi))\;, \qquad (56)$$

$$\bar{\sigma}_V(\xi) = \frac{2(\xi+\bar{m}^2) - 1 + e^{-2(\xi+\bar{m}^2)}}{2(\xi+\bar{m}^2)^2}\,, \qquad (57)$$

with $\bar{\sigma}_S(\xi) := \lambda\,\sigma_S(p^2)$, $\bar{\sigma}_V(\xi) := \lambda^2\,\sigma_V(p^2)$, where $p^2 = \lambda^2\,\xi$, λ is a mass-scale, and $\mathcal{F}(y) := [1-\exp(-y)]/y$. This five-parameter form, where $\bar{m}$ is the current-quark mass, combines the effects of confinement * and DCSB with

*The representation of $S(p)$ as an entire function is motivated by the algebraic solutions of Eq. (7) in Refs.16,17.

free-particle behaviour at large, spacelike p^2*. Applying Eq. (28) in this case:

$$-\langle\bar{q}q\rangle^0_\mu \;:=\; \lim_{M^2\to\infty} Z_4(\mu^2,M^2)\,\frac{3}{4\pi^2}\int_0^{M^2} ds\, s\,\sigma^0_S(s)\,, \tag{58}$$

$$= \lambda^3\,\ln\frac{\mu^2}{\Lambda^2_{\rm QCD}}\,\frac{3}{4\pi^2}\,\frac{b_0}{b_1\,b_3}\,, \tag{59}$$

and the pion mass is given by

$$m_\pi^2\, f_\pi^2 = 2\,m\,\langle\bar{q}q\rangle^0_{1\,\rm GeV}\,. \tag{60}$$

In Sec.4.1 we saw that when all the components of Γ_π are retained, Eq. (60) yields an approximation to the pion mass found in a solution of the Bethe — Salpeter equation that is accurate to 2%.

The model has been used for both u/d- and s-quark propagators with the difference between flavours manifest in $b_0^s \neq b_0^{u/d}$, $b_2^s \neq b_2^{u/d}$ and $m_s \neq m_{u/d}$: the first allows for a difference between the K and π in-meson condensates and the second for $M_s^E \neq M_{u/d}^E$, and all three are phenomenological constraints observed in the previous section. As emphasised above, in a solution of the quark DSE using an *Ansatz* for the dressed-gluon propagator, the parameters in Eq. (56) are correlated and one can anticipate this crudely when fitting them.

5.1. Pion Electromagnetic Form Factor. The renormalised impulse approximation to the electromagnetic pion form factor is [15]

$$(p_1+p_2)_\mu\, F_\pi(q^2) := \Lambda_\mu(p_1,p_2) =$$

$$= \frac{2N_c}{N_\pi^2}\int\frac{d^4k}{(2\pi)^4}\,{\rm tr}_D[\bar{\mathcal{G}}_\pi(k;-p_2)S(k_{++})\times$$

$$\times\, i\Gamma^\gamma_\mu(k_{++},k_{+-})\,S(k_{+-})\,\mathcal{G}_\pi(k-q/2;p_1)\,S(k_{--})], \tag{61}$$

$k_{\alpha\beta} := k+\alpha p_1/2+\beta q/2$ and $p_2 := p_1+q$, illustrated in Fig. 14. Here $\mathcal{G}_\pi(k;P)$ is the pion Bethe — Salpeter amplitude normalised such that $E(0;0) = B(0)$ in the chiral limit, in which case the consistent canonical normalisation of the

*At large-p^2: $\sigma_V(p^2) \sim 1/p^2$ and $\sigma_S(p^2) \sim m/p^2$. Therefore the parametrisation does not incorporate the additional $\ln p^2$-suppression characteristic of QCD: it corresponds to $\gamma_m \to 1$ in Eq. (40). It is a useful but not necessary simplification, which introduces model artefacts that are easily identified and accounted for. $\varepsilon = 0.01$ is introduced only to decouple the large- and intermediate-p^2 domains.

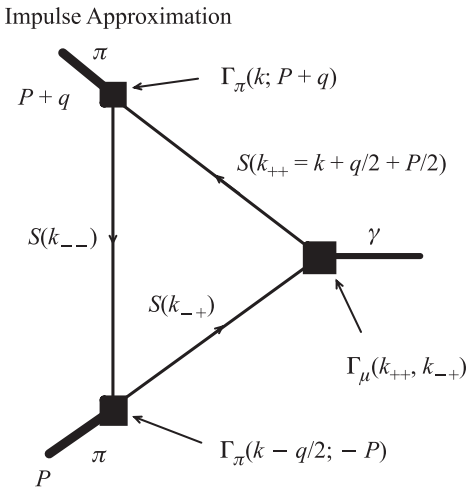

Fig. 14. Impulse approximation to $F_\pi(q^2)$: S labels the dressed-quark propagator; Γ_π, the pion Bethe — Salpeter amplitudes; and Γ_μ, the dressed-quark-photon vertex

Bethe — Salpeter amplitude is

$$2\delta^{ij} N_\pi^2 P_\mu = \int_q^\Lambda \left\{ \mathrm{tr}\left[\bar{\mathcal{G}}_\pi^i(q;-P) \frac{\partial S(q_+)}{\partial P_\mu} \mathcal{G}_\pi^j(q;P) S(q_-) \right] + \right. \tag{62}$$

$$\left. + \mathrm{tr}\left[\bar{\mathcal{G}}_\pi^i(q;-P) S(q_+) \mathcal{G}_\pi^j(q;P) \frac{\partial S(q_-)}{\partial P_\mu} \right] \right\},$$

where $\bar{\mathcal{G}}_\pi(q;-P)^t := C^{-1}\,\mathcal{G}_\pi(-q;-P)\,C$ with $C = \gamma_2\gamma_4$, the charge conjugation matrix, and X^t denotes the matrix transpose of X.

Given S and Eqs. (19)-(22), what form does the Bethe — Salpeter amplitude take?

In Sec. 4.2 we saw that the zeroth Chebyshev moments of the pion Bethe — Salpeter amplitude provided results for m_π and f_π that were indistinguishable from those obtained with the full solution. Also $H_\pi \simeq 0$ and hence it was quantitatively unimportant in the calculation of m_π and f_π. These results are not specific to that particular model; in the latter case because the right-hand side of Eq. (22) is zero and hence in general there is no "seed" term for H_π. We also saw that at large-k^2, independent of assumptions about the form of K, one has

$$E_\pi^0(k^2;P^2) \propto -\langle\bar{q}q\rangle_{k^2}^0 \frac{\alpha(k^2)}{k^2}, \tag{63}$$

and that the same is true of $F_\pi^0(k^2;P^2)$, $k^2\,G_\pi^0(k^2;P^2)$, and $k^2\,H_\pi^0(k^2;P^2)$. This makes manifest the "hard-gluon" contribution to $F_\pi(q^2)$ in Eq. (61). In addition,

in an asymptotically free theory, one has [7]

$$k^2\, G_\pi^0(k^2;P^2) = 2F_\pi^0(k^2;P^2)\,,\; k^2 \gtrsim M_{\rm UV}^2\,, \tag{64}$$

with $M_{\rm UV} := 10\,\Lambda_{\rm QCD}$.

These observations, combined with Eqs. (19)–(22), motivate a model for $\mathcal{G}_\pi$:

$$E_\pi(k;P) = B_0(k^2) \tag{65}$$

with $F_\pi(k;P) = E_\pi(k;P)/(110\,f_\pi)$, $G_\pi(k;P) = 2F_\pi(k;p)/[k^2 + M_{\rm UV}^2]$, and $H_\pi(k;P) \equiv 0$. The relative magnitude of these functions at large k^2 is chosen to reproduce the numerical results in Fig. 12.

The final element in Eq. (61) is $\Gamma_\mu^\gamma(p_1,p_2)$, the renormalised, dressed-quark-photon vertex, and it is because this vertex must satisfy the vector Ward — Takahashi identity:

$$(p_1-p_2)_\mu\, i\Gamma_\mu^\gamma(p_1,p_2) = S^{-1}(p_1) - S^{-1}(p_2)\,, \tag{66}$$

that $(p_1-p_2)_\mu\,\Lambda_\mu(p_1,p_2) = 0$ and no renormalisation constants appear explicitly in Eq. (61). $\Gamma_\mu^\gamma(p_1,p_2)$ has been much studied [5] and, although its exact form remains unknown, its robust qualitative features have been elucidated so that a phenomenologically efficacious *Ansatz* has emerged [18]

$$\begin{aligned} i\Gamma_\mu^\gamma(p,q) &:= i\Sigma_A(p^2,q^2)\,\gamma_\mu + \\ &+ (p+q)_\mu\,\left[\frac{1}{2}i\gamma\cdot(p+q)\,\Delta_A(p^2,q^2) + \Delta_B(p^2,q^2)\right], \end{aligned} \tag{67}$$

$$\Sigma_f(p^2,q^2) := \tfrac{1}{2}\left[f(p^2)+f(q^2)\right],\; \Delta_f(p^2,q^2) := \frac{f(p^2)-f(q^2)}{p^2-q^2}\,, \tag{68}$$

where $f = A, B$. A feature of Eq. (67) is that the vertex is completely determined by the renormalised dressed-quark propagator. In Landau gauge the quantitative effect of modifications, such as that canvassed in Ref.19, is small and can be compensated for by small changes in the parameters that characterise a given model study [20].

The model parameters were determined [15] by optimising a least-squares fit to f_π, r_π and $\langle\bar{q}q\rangle^0_{1\,\rm GeV}$, and a selection of pion form factor data on the domain $q^2 \in [0,4]\,{\rm GeV}^2$. The procedure does not yield a unique parameter set with, for example, the two sets:

	λ(GeV)	$\bar{m}$	b_0	b_1	b_2	b_3
A	0.473	0.0127	0.329	1.51	0.429	0.430,
B	0.484	0.0125	0.314	1.63	0.445	0.405,

(69)

Table 3. Comparison between the calculated values of low-energy pion observables and experiment or, in the case of $(-\langle\bar{q}q\rangle^0_{1\,\mathrm{GeV}})^{1/3}$ and $m_{u/d}$, the values estimated using other theoretical tools. Each set in Eq. (69) yields the same calculated values. $\Lambda_{\mathrm{QCD}} = 0.234$ **GeV**

	Calculated	Experiment
f_π	0.092 GeV	0.092
$(-\langle\bar{q}q\rangle^0_{1\,\mathrm{GeV}})^{1/3}$	0.236	0.236 $\pm$ 0.008 [13]
$m_{u/d}$	0.006	0.008 $\pm$ 0.004 [21]
m_π	0.1387	0.1385
r_π	0.55 fm	0.663 $\pm$ 0.006 [22]
$r_\pi f_\pi$	0.25 (dimensionless)	0.310 $\pm$ 0.003

providing equally good fits, as illustrated in Table 3. There is a domain of parameter sets that satisfy the fitting criterion and they are distinguished only by the calculated magnitude of the pion form factor at large-q^2. The two sets in Eq. (37) delimit reasonable boundaries and illustrate the model dependence in the result. In the chiral limit: $f_\pi^0 = 0.090\,\mathrm{GeV}$.

The quark propagator obtained with these parameter values is pointwise little different to that obtained in Ref.23. One gauge of this is the value of the Euclidean constituent quark mass. Here $M^E_{u/d} = 0.32\,\mathrm{GeV}$, whereas $M^E_{u/d} = 0.30\,\mathrm{GeV}$ in Ref.23. It is also qualitatively similar to the numerical solution described in Sec. 4.1 [7], where $M^E_{u/d} = 0.56\,\mathrm{GeV}$. Indeed, the results are not sensitive to details of the fitting function: fitting with different confining, algebraic forms yields $S(p)$ that is pointwise little changed, and the same results for observables. The earlier parametrisation [23] has been applied more widely, as reviewed in Ref.24, and Table 4 summarises the results.

In the calculations $f_\pi r_\pi$ is 20% too small. This discrepancy cannot be reduced in impulse approximation because the nonanalytic contributions to the dressed-quark-photon vertex associated with π-π rescattering and the tail of the ρ-meson resonance are ignored [29]. It can only be eliminated if these contributions are included. This identifies a constraint on realistic, impulse approximation calculations: they should not reproduce the experimental value of $f_\pi r_\pi$ to better than $\sim 20\%$, otherwise the model employed has unphysical degrees-of-freedom.

The pion form factor calculated [15] using Eqs. (56) and (57) with (69) is compared with available data in Figs. 15 and 16. It is also compared with the result obtained in Ref.23, wherein the calculation is identical *except* that the pseudovector components of the pion were neglected. Figure 15 shows a small, systematic discrepancy between the calculations and the data at low q^2, which is

Table 4. Summary of results obtained using the parametrisation of $S(p)$ introduced in Ref.23, which differs little from that specified by Eqs. (56) and (57). a_J^I are π-π scattering lengths, whose experimental values are discussed in Ref.28, and $F^{3\pi}(4m_\pi^2)$ is the value of the $\gamma\pi \to \pi\pi$ transition form factor at the softest point kinematically accessible. The citations for the calculated results specify the article in which the annotated study is described. The "experimental" values of the current-quark masses and the quark condensate are estimates made using other theoretical tools: see Table 3

	Calculated	"Experiment"
f_π	0.0924 GeV	0.0924 $\pm$ 0.001
f_K	0.113	0.113 $\pm$ 0.001
m_π	0.139	0.138
m_K	0.494	0.494
$m^{\rm ave}_{1\,{\rm GeV}^2}$	0.0045	0.008
$m^{s}_{1\,{\rm GeV}^2}$	0.113	0.1 $\sim$ 0.3
$-\langle\bar{q}q\rangle^{\frac{1}{3}}_{1\,{\rm GeV}^2}$	0.247	0.236 $\pm$ 0.008
$r_{\pi^\pm}$	0.55 fm	0.663 $\pm$ 0.006
$r_{K^\pm}$	0.49 [25]	0.583 $\pm$ 0.041
$r^2_{K^0}$	-0.020 fm^2	-0.054 $\pm$ 0.026
$g_{\pi^0\gamma\gamma}$	0.50 [23] (dimensionless)	0.504 $\pm$ 0.019
$F^{3\pi}(4m_\pi^2)$	1.04 [26]	1 (Anomaly)
a^0_0	0.19 [27]	0.26 $\pm$ 0.05
a^2_0	-0.054	-0.028 $\pm$ 0.012
$2a^0_0 - 5a^2_0$	0.65	0.66 $\pm$ 0.12
a^1_1	0.038	0.038 $\pm$ 0.002
a^0_2	0.0017	0.0017 $\pm$ 0.0003
a^2_2	-0.00029	
f_K/f_π	1.22	1.22 $\pm$ 0.01
$r_{K^\pm}/r_{\pi^\pm}$	0.87	0.88 $\pm$ 0.06

due to the underestimate of r_π in impulse approximation*. The results obtained with or without the pseudovector components of the pion Bethe — Salpeter amplitude are quantitatively the same, which indicates that the pseudoscalar component, E_π, is dominant in this domain.

*Just as in the present calculation, $f_\pi r_\pi = 0.25$ in Ref.23. However, the mass-scale is fixed so that $f_\pi = 0.084$, which is why this result appears to agree better with the data at small-q^2: r_π is larger.

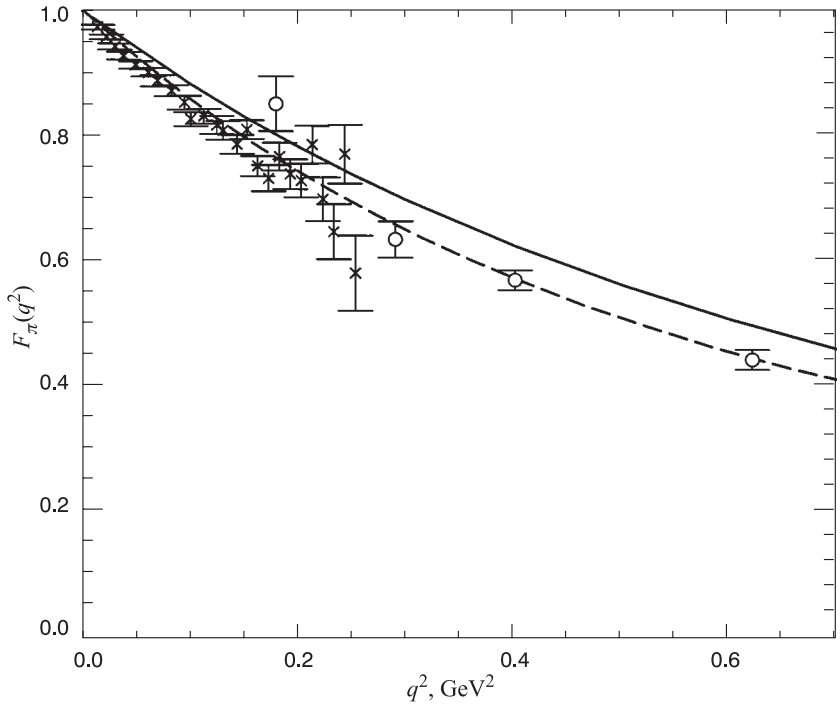

Fig. 15. Calculated pion form factor compared with data at small q^2. The data are from Refs.22 (crosses) and 30 (circles). The solid line is the result obtained when the pseudovector components of the pion Bethe — Salpeter amplitude are included; the dashed-line, when they are neglected [23]. On the scale of this figure, both parameter sets in Eq. (69) yield the same calculated result

The increasing uncertainty in the experimental data at intermediate q^2 is apparent in Fig. 16, as is the difference between the results calculated with or without the pseudovector components of the pion Bethe — Salpeter amplitude. These components provide the dominant contribution to $F_\pi(q^2)$ at large pion energy because of the multiplicative factors: $\gamma \cdot P$ and $\gamma \cdot k \, k \cdot P$, which contribute an additional power of q^2 in the numerator of those terms involving F^2, FG, and G^2 relative to those proportional to E. Using the method of Ref.23 and the model-independent asymptotic behaviour indicated by Eq. (63) one finds

$$F_\pi(q^2) \propto \frac{\alpha(q^2)}{q^2} \, \frac{(-\langle \bar{q} q \rangle^0_{q^2})^2}{f_\pi^4} \, ; \tag{70}$$

i.e., $q^2 F_\pi(q^2) \approx$ const., up to calculable $\ln q^2$-corrections. If the pseudovector components of Γ_π are neglected, the additional numerator factor of q^2 is missing and one obtains [23] $q^4 F_\pi(q^2) \approx$ const.

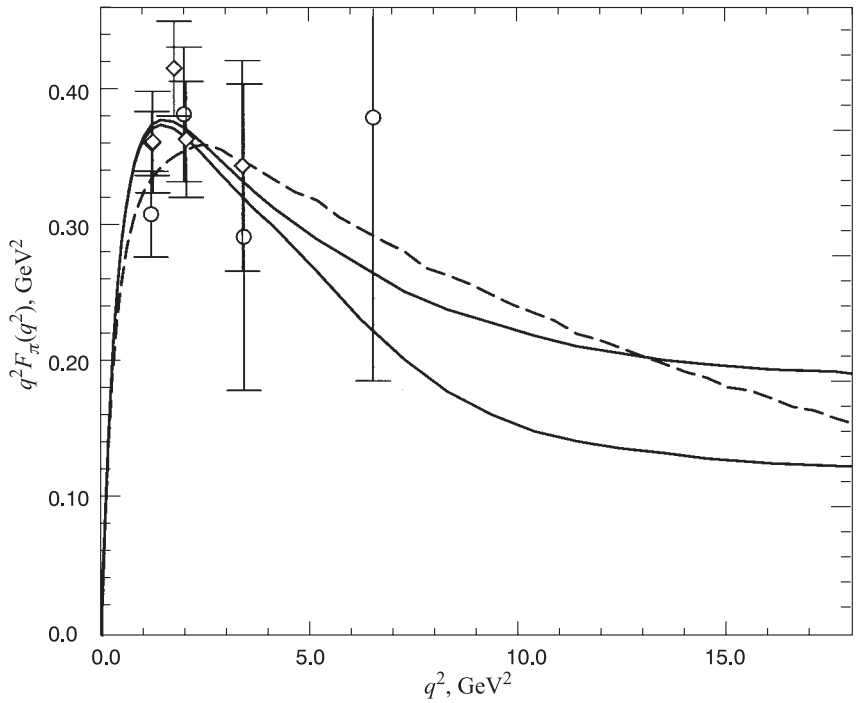

Fig. 16. Calculated pion form factor compared with the largest q^2 data available: diamonds — Ref.30; and circles — Ref.31. The solid lines are the results obtained when the pseudovector components of the pion Bethe — Salpeter amplitude are included (lower line — set A in Eq. (69); upper line — set B), the dashed-line when they are neglected [23]

With this model the behaviour identified in Eq. (70) becomes apparent at $q^2 \gtrsim 2\,M_{UV}^2$. This is the domain on which the asymptotic behaviour indicated by Eq. (63) is manifest. The calculated results, obtained with the two sets of parameters in Eq. (37), illustrate the model dependent uncertainty:

$$q^2 F_\pi(q^2)\big|_{q^2\sim 10-15\,\mathrm{GeV}^2} \sim 0.12 - 0.19\,\mathrm{GeV}^2\,. \tag{71}$$

It arises primarily because the model allows for a change in one parameter to be compensated by a change in another. In this example: $b_2^{\mathsf{B}} > b_2^{\mathsf{A}}$ but $b_0^{\mathsf{B}} + b_2^{\mathsf{B}} = b_0^{\mathsf{A}} + b_2^{\mathsf{A}}$; and $b_1^{\mathsf{A}}\, b_3^{\mathsf{A}} = b_1^{\mathsf{B}}\, b_3^{\mathsf{B}}$, which allows an equally good fit to low-energy properties but alters the intermediate-q^2 behaviour of $F_\pi(q^2)$. As emphasised, in a solution of Eq. (7) these coefficients of the $1/p^4$ and $1/p^6$ terms are correlated and such compensations cannot occur.

As a comparison, evaluating the leading-order perturbative-QCD result with the asymptotic quark distribution amplitude: $\phi_{\rm as}(x) := \sqrt{3}\, f_\pi\, x(1-x)$, yields

$$q^2 F_\pi(q^2) = 16\,\pi f_\pi^2\,\alpha(q^2) \approx 0.15\,{\rm GeV}^2\,, \tag{72}$$

assuming a value of $\alpha(q^2 \sim 10\,{\rm GeV}^2) \approx 0.3$. However, the perturbative analysis neglects the anomalous dimension accompanying condensate formation; e.g., Eqs. (19)-(22) are not satisfied in Ref.32.

5.2. Electroproduction of Vector Mesons. There is an extensive body of literature describing Pomeron phenomenology, all derived from the observation that the total cross section in high-energy scattering: p-p, $\bar{p}$-p, $\pi^{\pm}$-p, γ-p, etc., is forward-peaked and rises slowly with $\sqrt{s}$. This is illustrated [21] in Fig. 17 and can be described [10] by a Pomeron-exchange model of the quark-nucleon interaction with the following features:

1. The quark-Pomeron coupling is $\bar{q}^f(p_2)\Gamma^f_\mu q^f(p_1)$, where $\Gamma_\mu := \beta_f\,\gamma_\mu$ with β_f a flavour-dependent coupling constant. It is the only flavour-dependence in the interaction.

2. The Pomeron "propagator" is characterised by a Regge trajectory:

$$G(s,t) := (\alpha_1 s)^{\alpha_0+\alpha_1 t} \tag{73}$$

with $\alpha_0 > 0$, which ensures the increase with s, and the Pomeron-nucleon coupling is $3\beta_u F_1(t)$, where $F_1(t)$ is the Dirac form factor of the proton.

3. The interaction is used in impulse approximation so that, for example, the $\pi N \to \pi N$ interaction is completely described by

$$\langle P; p_2 m_s' | T_{\pi N\to\pi N} | q; p_1 m_s\rangle :=$$

$$:=\ \Lambda_\mu(q,P)\, 3\beta_{u/d}\, F_1(t)\, G(s,t)\, \bar{u}_{m_s'}(p_2)\gamma_\mu u_{m_s}(p_1)\,, \tag{74}$$

where $u_{m_s}(p_1)$ is a nucleon spinor and $\Lambda_\mu(q,P) := 2\Lambda^u_\mu(q,P) + 2\Lambda^{\bar{d}}_\mu(q,P)$ with

$$\Lambda^f_\mu(q,P) :=$$

$$:=\ N_c\,{\rm tr}_D \int \frac{d^4k}{(2\pi)^4} S_u(k_{-+})\Gamma_\pi(k_{0-})S_d(k_{--})\bar{\Gamma}_\pi(k)S_u(k_{++})\beta_f i\gamma_\mu \tag{75}$$

describing the interaction of the Pomeron with the f-quark in the pion. The parameters: β_f, α_0, α_1, in this model were fixed [10] by requiring a good description of πN and KN scattering, and this is achieved with

$$\beta_{u/d} = 2.35\,{\rm GeV}^{-2},\quad \beta_s = 1.50\,{\rm GeV}^{-2},\quad \alpha_0 = 0.10,\quad \alpha_1 = 0.33\,{\rm GeV}^{-2}\,. \tag{76}$$

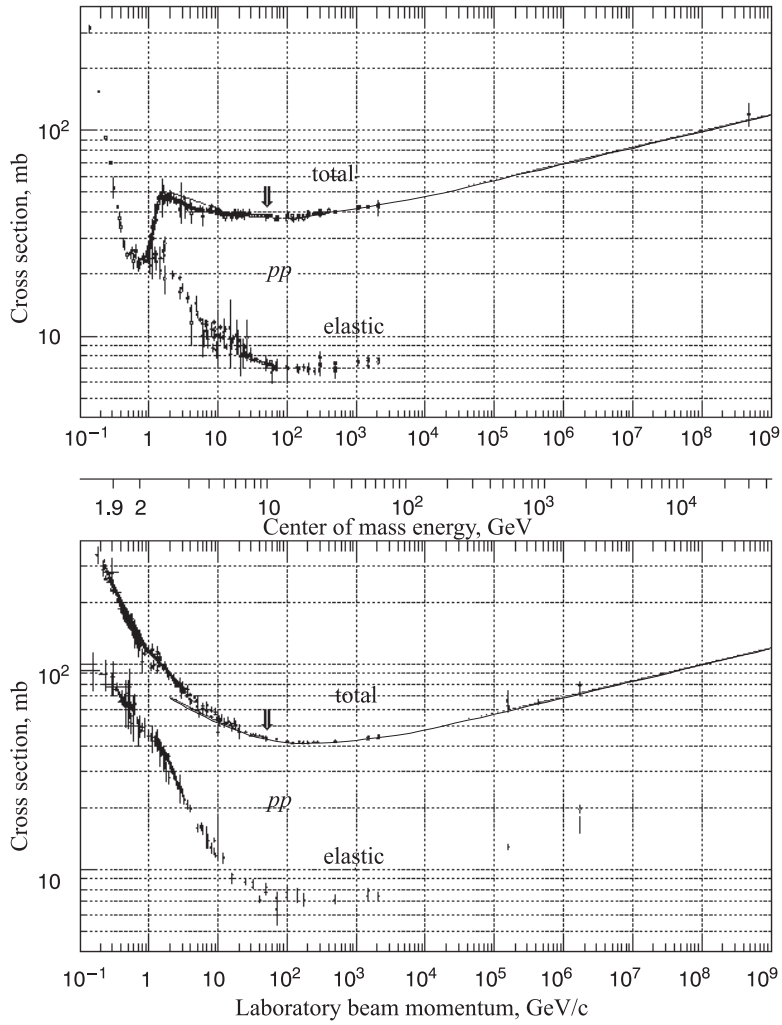

Fig. 17. Total and elastic cross sections for p-p and $\bar{p}$-p scattering. The slow increase of the total cross section with $\sqrt{s}$ at high energy is obvious.

In the diffractive regime the process $e^- p \to e^{-\prime} p' V$, where $V = \rho,\ \phi,\ \psi$, is also expected to proceed via soft-Pomeron exchange and the model introduced above can be applied directly. The matrix element is

$$\langle p_2 m_2; k\lambda_\rho | J_\mu | p_1 m_1 \rangle =$$

$$= 2\beta_f t_{\mu\nu\lambda}(q,k)\, \varepsilon_\lambda^{\lambda_\rho}(k)\, G_{\mathcal{P}}(\bar{w}^2, t)\, 3\beta_u F_1(t)\, \bar{u}(p_2)\gamma_\nu u(p_1)\,, \qquad (77)$$

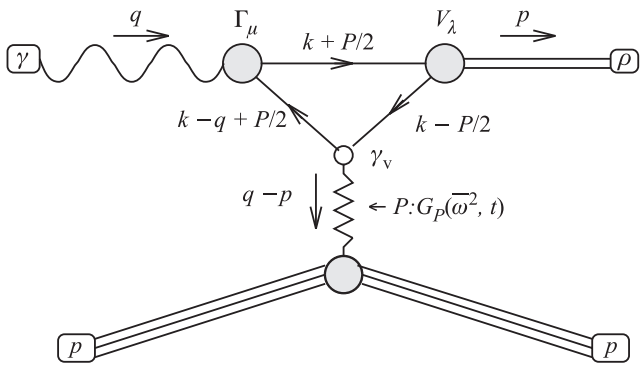

Fig. 18. ρ-meson electroproduction matrix element. $\bar{\omega}^2 := -(q - P/2 + p_1)^2$, where p_1 is the momentum of the struck nucleon

depicted in Fig. 18, where the $\gamma\mathcal{P} \to \rho$ transition form factor is

$$t_{\mu\nu\lambda}(q,P) = 3e_0 \int \frac{d^4k}{(2\pi)^4}\, \mathrm{tr}\left\{ S(k+\tfrac{1}{2}P) \times \right.$$

$$\left. \times\, \Gamma^\gamma_\mu(k+\tfrac{1}{2}P, k-q+\tfrac{1}{2}P)\, S(k-q+\tfrac{1}{2}P)\, \gamma_\nu\, S(k-\tfrac{1}{2}P)\, V_\lambda(k;-P) \right\}. \quad (78)$$

The unknown quantity in Eq. (78) is the vector meson Bethe — Salpeter amplitude, $V_\nu(k;-P)$. In the absence of a solution of the associated Bethe — Salpeter equation, an oft used and phenomenologically efficacious procedure [24] is to parametrise the amplitude in a manner similar to that employed for the pion in Sec. 5.1:

$$V_\nu(k;P) = \left(\gamma_\nu + \frac{P_\nu \gamma\cdot P}{m_V^2} \right) \frac{1}{N_V} \left\{ \mathrm{e}^{-k^2/a_V^2} + \frac{c_V}{1+k^2/b_V^2} \right\}, \quad (79)$$

where N_V is fixed via the canonical normalisation condition: clearly, $P\cdot V(k;P) = 0$. The parameters are

	$a\,(\mathrm{GeV})$	$b\,(\mathrm{GeV})$	c
ρ	0.40	0.008	125.0
ϕ	0.45	0.6	0.3
ψ	1.10	0.0	0.0

(80)

which were fixed [10] by requiring the fit to the dimensionless coupling constants in Eq. (81).

	$g_{\rho\to e^+e^-}$	$g_{\rho\to\pi^+\pi^-}$	$g_{\phi\to e^+e^-}$	$g_{\phi\to K\bar{K}}$	$g_{\psi\to e^+e^-}$
Theory	4.6	6.8	12.7	3.9	11.5
Experiment	5.0	6.1	12.9	4.6	11.5

(81)

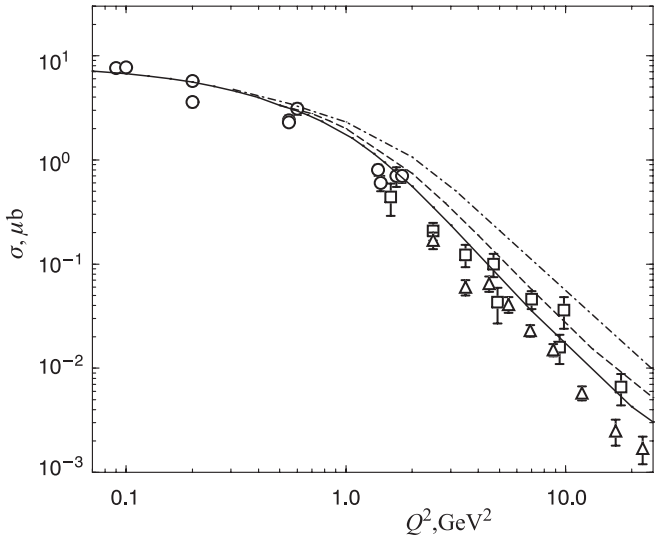

Fig. 19. ρ-meson electroproduction cross section at $W = 15\,\mathrm{GeV}$: solid line — calculated result; long-dashed line — result if $\bar{m}_{u/d} \to 10\,\bar{m}_{u/d}$; dash-dot line — result if $\bar{m}_{u/d} \to$ $\to 25\,\bar{m}_{u/d} \simeq \bar{m}_s$. The data are: circles — Ref.33; squares — Ref.34; triangles — Ref.35

The experimental values of the decay constants were calculated from the widths in Ref.21, and the fit is acceptable given the simplicity of the *Ansatz* for V_ν, which includes only one of the eight scalar functions necessary to completely specify a vector meson bound state. At this point there are no free parameters in the calculation of the electroproduction cross sections.

Figure 19 depicts the Q^2-dependence of the ρ-meson electroproduction cross section and the magnitude is a prediction. There is complete agreement on the entire range of accessible Q^2, with the large Q^2 behaviour [10]: $1/Q^4$, which becomes evident at $Q^2 \simeq 1\text{-}2\,\mathrm{GeV}^2$. Below that point the nonperturbative character of the dressed-quark propagator dominates the evolution of the cross section. It is important to observe the prediction that, the larger the current-quark mass of the constituents, the larger the value of Q^2 at which the asymptotic behaviour is manifest.

The calculated ϕ-meson electroproduction cross section is depicted in Fig. 20. It is in excellent agreement with Refs.36 and 37, which used a nucleon target, as opposed to Ref.35, which averaged over variety of nuclear targets. As could be anticipated from Fig. 19, the onset of the asymptotic $1/Q^4$ behaviour is pushed to larger-Q^2 for the ϕ-meson because the current-quark mass of the constituents, the s-quark, is larger. In calculating the ψ-meson electroproduction cross section

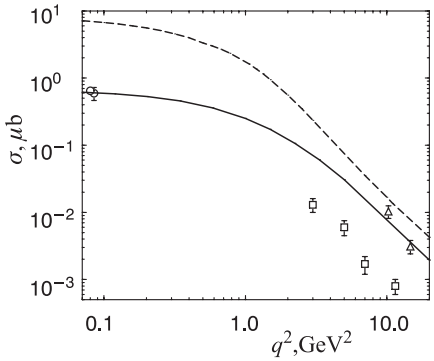

Fig. 20. ϕ-meson electroproduction cross section at $W = 70\,\mathrm{GeV}$: solid line; the dashed line is the ρ-meson result for comparison. The data are: triangles — Ref.35; circles — Ref.36; squares — Ref.37

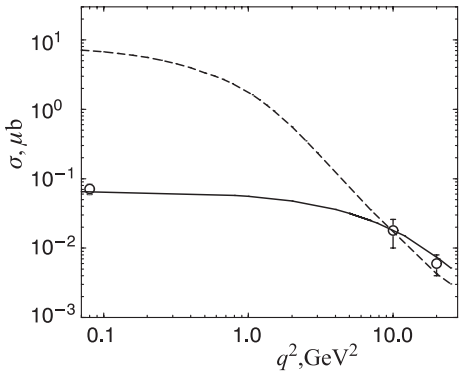

Fig. 21. ψ-meson electroproduction cross section at $W = 100\,\mathrm{GeV}$: solid line; the dashed line is the ρ-meson result at $W = 15\,\mathrm{GeV}$ for comparison. The data are from Refs.38,39

a very simple form was used for the c-quark propagator:

$$S_c(k) := \frac{1}{m_c^2}\,(-i\gamma\cdot k + m_c)\,\mathcal{F}(1 + k^2/m_c^2) \tag{82}$$

with $m_c = 1.2\,\mathrm{GeV}$ ($\sim m_c^{1\,\mathrm{GeV}}$ in Eq. (10)). This and the simple form of the ψ-meson Bethe — Salpeter amplitude anticipate the successful application of DSEs to heavy-meson observables [9]. The calculated cross section is depicted in Fig. 21. The striking prediction, confirmed by recent data, is that although two-orders of magnitude smaller than the ρ-meson cross section at the photoproduction point, the ψ-meson cross section is equal to that of the $W = 100\,\mathrm{GeV}$, ρ-meson cross section at $Q^2 = 15\,\mathrm{GeV}^2$. This is because the large c-quark mass shifts the onset of the asymptotic $1/Q^4$-behaviour to larger-Q^2.

6. FINITE TEMPERATURE AND CHEMICAL POTENTIAL

As we have seen, at zero temperature and chemical potential the low-energy and small-q^2 behaviour of QCD is characterised by confinement and DCSB. The internal scale that marks the boundary between small and large energy in QCD is $M_\chi \sim \Lambda_{\rm QCD}$. As the energy and/or momentum transfer increases, QCD is characterised by asymptotic freedom; i.e., the coupling evolves

$$\alpha_{\rm S}(Q^2, T = 0 = \mu) \stackrel{Q^2\to\infty}{\longrightarrow} 0 \tag{83}$$

and quarks and gluons behave as weakly interacting, massless particles in high-energy and/or large-Q^2 processes.

The study of QCD at finite temperature and baryon number density proceeds via the introduction of the intensive variables: temperature, T; and quark chemical potential, μ. These are additional mass-scales, with which the coupling can *run* and hence, for $T \gg \Lambda_{\rm QCD}$ and/or $\mu \gg \Lambda_{\rm QCD}$, $\alpha_{\rm S}(Q^2 = 0, T, \mu) \sim 0$. It follows that at finite temperature and/or baryon number density there is a phase of QCD in which quarks and gluons are weakly interacting, *irrespective* of the momentum transfer [40]; i.e., a quark-gluon plasma. Such a phase of matter existed approximately one microsecond after the big-bang. In this phase confinement and DCSB are absent and the nature of the strong interaction spectrum is qualitatively different. The contemporary expectation for the position of the phase boundary in the (μ, T)-plane is illustrated in Fig. 22.

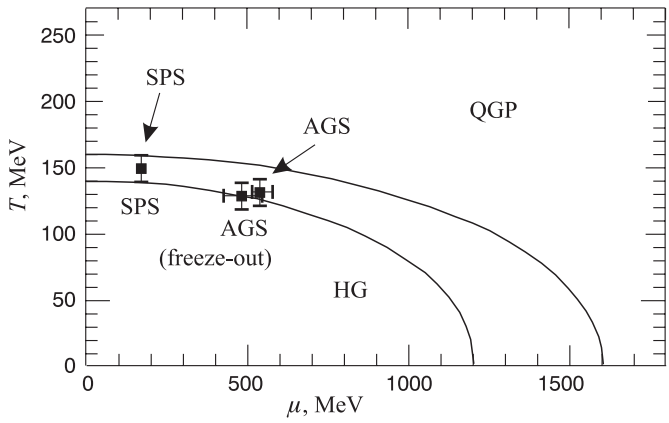

Fig. 22. The anticipated quark-gluon phase boundary in the (μ_N, T)-plane. "HG" — hadron gas, "QGP" — quark-gluon plasma. The nucleon chemical potential: $\mu_N := 3\mu$; i.e., three-times the quark chemical potential. "SPS" and "AGS" mark the points in the plane that is the estimate of these facilities explore.

The path followed in the transition to the plasma is important because it determines some observational consequences of the plasma's existence. For example [41], the time-scale for the expansion of the early universe: $\sim 10^{-5}\,\mathrm{s}$, is large compared with the natural time-scale in QCD: $1/\Lambda_{\mathrm{QCD}} \sim 1\,\mathrm{fm}/c \sim 10^{-23}\,\mathrm{s}$, hence thermal equilibrium is maintained throughout the QCD transition. Therefore, if the transition is second-order, the ratio $B :=$ baryon-number/entropy, remains unchanged from that value attained at an earlier stage in the universe's evolution. However, a first-order transition would be accompanied by a large increase in entropy density and therefore a reduction in B after the transition. Hence the order of the QCD transition constrains the mechanism for baryon number generation in models describing the formation of the universe, since with a second-order transition this mechanism is only required to produce the presently observed value of B and need not allow for dilution. In the absence of quarks, QCD has a first-order deconfinement transition, and with three or four massless quarks a first-order chiral symmetry restoration transition is expected [41]. A current, primary question is: what happens in the realistic case of two light quark flavours?

Nonperturbative methods are necessary to study the phase transition, which is characterised by qualitative changes in order parameters such as the quark condensate. One widely used approach is the numerical simulation of finite temperature lattice-QCD, with the first simulations in the early eighties and extensive efforts since then [42]. Here I focus on the application of DSEs. This is a new usage and much remains to be learnt: these are exploratory studies. One goal is to develop DSE models of QCD at finite-T and μ (QCD_{μ}^{T}) that can be used to check the results of numerical simulations, and be constrained by them. These models can then be employed to extrapolate into that domain presently inaccessible to lattice studies, such as finite chemical potential and the effects of T and μ on bound state properties, the latter of which are expected to provide the signatures of quark-gluon plasma formation in relativistic heavy ion collisions.

Before discussing details it is interesting to provide a human scale for the temperatures and densities involved. The natural scale in QCD is $\Lambda_{\mathrm{QCD}} \sim$ 200 MeV and temperatures of this order of magnitude will be necessary to create the plasma. $\Lambda_{\mathrm{QCD}} \sim 10^{10}\times$ room-temperature! It represents a temperature on the astrophysical and cosmological scale. Nuclear matter density $\rho_0 \approx 3 \times 10^{14}$ g/cm^3 = 0.16 N/fm^3 and this is more than $10^{13}\times$ the density of solid lead! The density at the core of a neutron star is expected to be approximately $4\,\rho_0$ [43] and it is densities on this order that are anticipated to be required for plasma formation.

The expectation of the existence of a new phase of matter, the quark-gluon plasma, has led to the construction of a Relativistic Heavy Ion Collider (RHIC) at Brookhaven National Laboratory. Construction is to be completed in 1999. It will use counter-circulating, colliding 100 A GeV ^{197}Au beams to generate a total

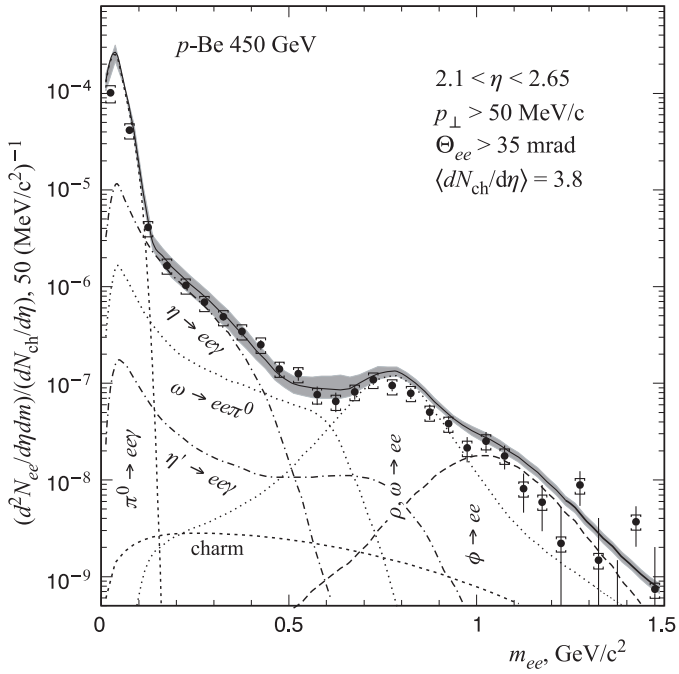

Fig. 23. Mass spectra for inclusive e^+-e^- pairs in 450 GeV p-Be collisions showing the data and various contributions from hadron decays. The shaded region indicates the systematic error on the summed contributions [45]

centre-of-mass energy of ~ 40 TeV, in an effort to produce an equilibrated quark-gluon plasma. It is anticipated to approach the quark-gluon plasma via a low baryon density route. Contemporary, fixed target experiments at the Brookhaven-AGS and CERN-SpS explore a high baryon density environment at much lower centre-of-mass energies. These experiments are crucial in developing the expertise necessary for operating detectors under RHIC conditions but they are not expected to "discover" the plasma. The CERN-SpS experiments have nevertheless produced some interesting results.

One example is the "NA45-CERES" experiment [44], which studies e^+-e^- pair production in heavy ion collisions. $e^\pm$ pairs leave the interaction region without interacting strongly and hence they are a probe of the early stages of the interaction. In Fig. 23 I illustrate the dilepton spectrum obtained in high-energy p-Be collisions. It is well described by known hadron decays. The same is true of p—Au collisions. However, this is not the case in S-Au collisions, as illustrated in Fig. 24. There the known hadron decays describe the data only for $m_{ee} < 300$ MeV, which is the region dominated by π^0 Dalitz decays. At higher energies the shape of the spectrum is different and shows a strong enhancement

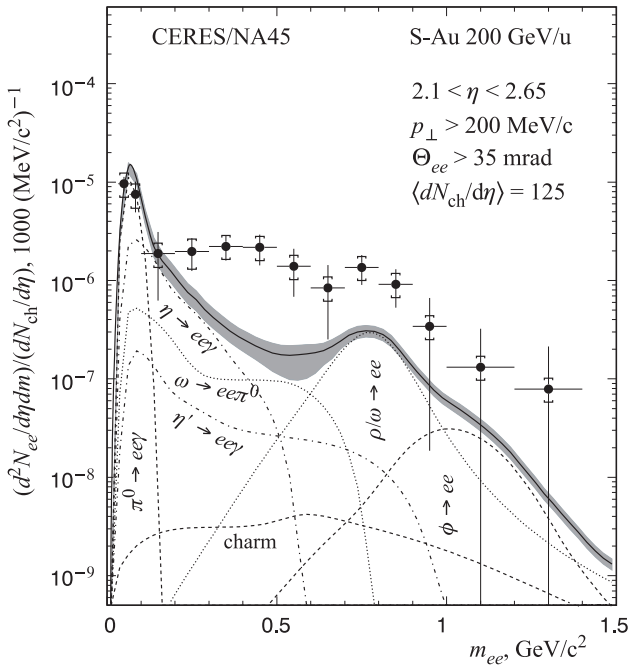

Fig. 24. Mass spectra for inclusive e^+-e^- pairs in 200 GeV S-Au collisions showing the data and various contributions from hadron decays. The shaded region indicates the systematic error on the summed contributions [45]

in the dilepton yield. Integrating over the region $0.2 < m_{ee} < 1.5$ GeV the enhancement factor is

$$5.0 \pm 0.7\,\text{stat.} \pm 2.0\,\text{syst.} \tag{84}$$

The enhancement persists in Pb—Au collisions [44]. What explanation can be offered?

One model calculation [46] shows that this enhancement can be explained by a medium-induced reduction of the ρ-meson's mass; another [47], that it follows from an increase in the ρ-meson's width. A decrease in the ρ-meson's mass is consistent with the QCD sum rules analysis of Ref.48 but inconsistent with that of Ref.49, which employs a more complex phenomenological model for the in-medium spectral density used in matching the two sides of the sum rule. In Ref.49 there is no shift in the ρ-meson mass but a significant increase in its width. The consistency between Refs.47 and 49 is not surprising since, in contrast to Ref.48, they both rely heavily on effective Lagrangians with elementary hadron degrees-of-freedom. These are possibilities that can be explored using DSEs, which focusing on dressed-quark and -gluon degrees of freedom is an approach most akin to Ref.48. A first attempt [50], summarised in Sec. 7.6, predicts a

15% suppression of m_ρ at nuclear matter density but employs a model that is inadequate to address Γ_ρ.

6.1. Notes on Field Theory. Equilibrium statistical field theory can be understood by analogy with equilibrium statistical mechanics. For a particle moving in a potential V the density matrix is given by the path integral

$$\rho(x, x'; T := 1/\beta) :=$$

$$\int_{x(0)=x}^{x(\beta)=x'} \mathcal{D}x(\tau)\, \exp\left\{ -\int_0^\beta d\tau \left[\underline{\frac{1}{2} m\dot{x}(\tau)^2 - V(x(\tau))} \right] \right\}, \qquad (85)$$

where the underlined term is just the Lagrangian. All of the thermodynamic information about this system can be obtained from the partition function

$$Z(T) := \int_V dx\, \rho(x, x, T)\,; \qquad (86)$$

for example, the pressure $P = T \ln Z(T)/V$ and the baryon density $\rho^B = (1/3)\partial P/\partial\mu$.

The equilibrium thermodynamics of a quantum field theory is also completely specified by a partition function, or generating functional. In the particular case of a self-interacting scalar field this is given by the functional integral:

$$\mathcal{Z}[T] \;\; := \;\; \int \Pi_{\tilde{x},\tau\in[0,\beta]}\, D\phi(\tilde{x},\tau)\, \exp\left(-\int_0^\beta d\tau \int d^3x\, \mathcal{L}^E(x;\phi) \right), \qquad (87)$$

where $\mathcal{L}^E(x;\phi)$ is the Euclidean Lagrangian density describing the interaction of $\phi(\tilde{x},\tau)$, whose boundary conditions are periodic:

$$\phi(\tilde{x}, \tau = 0) = \phi(\tilde{x}, \tau = \beta)\,. \qquad (88)$$

The boundary conditions for fermions are antiperiodic:

$$\psi(\tilde{x}, \tau = 0) = -\psi(\tilde{x}, \tau = \beta)\,. \qquad (89)$$

This difference in boundary conditions is the reason for the difference between the Matsubara frequencies of fermions and bosons and hence why fermions acquire a screening mass at finite temperature.

It is immediately obvious that the $O(4)$ invariance of the Euclidean theory is lost: at finite temperature (and/or chemical potential) the theory exhibits only an $O(3)$ symmetry corresponding to spatial rotations and translations. This is why the formalism, necessarily used in lattice simulations, is only applicable to equilibrium systems — there is no generator of translations in time. One also notes from Eq. (87) that as $T \to \infty$ one dimension disappears completely and

hence the corresponding $(d-1)$-dimensional theory is a candidate to describe the infinite-temperature limit of a d-dimensional theory.

The finite temperature, free fermion Lagrangian density is

$$\mathcal{L}^E_{\rm Free}(\bar\psi,\psi) = \bar\psi(\vec{x},\tau)\,\left(\vec\gamma\cdot\vec\partial + \gamma_4\,\partial_\tau + m\right)\,\psi(\vec{x},\tau)\,. \tag{90}$$

Introducing a Fourier decomposition:

$$\psi(\vec{x},\tau) = T\sum_{n=-\infty}^{\infty}\int\frac{d^3p}{(2\pi)^3}\,\psi(\vec{p},\omega_n)\mathrm{e}^{i\vec{p}\cdot\vec{x}+i\omega_n\tau}\,, \tag{91}$$

antiperiodicity entails that the fermion Matsubara frequencies are

$$\omega_n = (2n+1)\,\pi\,T\,,\ n\in\mathbb{Z} \tag{92}$$

and the free fermion action is

$$S^E_\beta[\bar\psi,\psi]_{\rm Free} = T\sum_{n=-\infty}^{\infty}\int\frac{d^3p}{(2\pi)^3}\,\bar\psi(\vec{p},\omega_n)\,\left(i\vec\gamma\cdot\vec{p}+i\gamma_4\omega_n+m\right)\,\psi(\vec{p},\omega_n)\,. \tag{93}$$

From this one identifies the finite temperature, free fermion propagator

$$S(p) = \frac{1}{i\vec\gamma\cdot\vec{p}+i\gamma_4\,\omega_n+m}\,. \tag{94}$$

Analogous arguments, using the periodic boundary conditions, lead to an identification of the free boson propagator

$$D(p,\Omega_n) = \frac{1}{|\vec{p}|^2+\Omega_n^2+m^2}\,, \tag{95}$$

where $\Omega_n = 2\,\pi\,n\,T$. Having obtained the free particle propagators one can proceed to define a perturbation theory. As an example, in massless ϕ^4 theory the one-loop correction to the ϕ propagator is

$$\propto T\sum_{n=-\infty}^{\infty}\int\frac{d^3p}{(2\pi)^3}\,\frac{1}{\Omega_n^2+|\vec{p}|^2}\,. \tag{96}$$

The sum can be evaluated:

$$T\sum_{n=-\infty}^{\infty}\frac{1}{\Omega_n^2+|\vec{p}|^2} = \frac{1}{|\vec{p}|}\,\frac{1}{\exp(|\vec{p}|/T)-1} + T-\text{independent piece}\,, \tag{97}$$

to yield the Bose-Einstein factor. This is a source of problems: for large temperatures

$$\frac{1}{\exp(|\vec{p}|/T)-1} = \frac{T}{|\vec{p}|} \tag{98}$$

and one can thereby encounter additional infrared divergences.

These are particularly serious in QCD. To illustrate this [51] consider an $(\ell+1)$-gluon-loop diagram and focus on the $n=0$ mode, which obviously yields the dominant infrared behaviour. The estimate is made easier if one neglects the tensor structure and notes that: from the vertices there is a factor of $g^{2\ell}\,p^{2\ell}$; the loop-sum-integral gives $(T\int_{p^2\in[0,T]}d^3p)^{\ell+1}$; and the propagators, $(p^2+m^2)^{-3\ell}$, where m is a possible, dynamically generated mass-scale. A little thought and calculation shows that the net order of a given diagram in perturbation theory is

$$\begin{array}{ccc} \ell=1,2 & \ell=3 & \ell\geq 4 \\ g^{2\ell}\,T^4 & g^6\,T^4\,\ln(T/m) & g^6\,T^4\,[g^2T/m]^{\ell-3}. \end{array} \tag{99}$$

Clearly, if $m=0$ the diagrams are infrared divergent for $\ell>2$. The divergences may cancel when all diagrams of a given order are summed but that is difficult to verify. Suppose instead that the mass-scale $m\sim g\,T$, as does the Debye mass in QED, then no problem arises: at each order above $\ell=3$ the diagrams are suppressed by powers of the coupling and a self-consistent calculation of the mass-scale is straightforward. This underlies the successful application of the method of "hard thermal loops" [52]. However, suppose that $m\sim g^2T$, which is the next possibility. In this case every diagram above $\ell=2$ contributes with the same strength: g^6, which presents a serious impediment to the application of perturbation theory!

The introduction of a quark chemical potential modifies Eq. (93):

$$S^E_\beta[\bar\psi,\psi]_{\rm Free}:=$$
$$:=\;T\sum_{n=-\infty}^{\infty}\int\frac{d^3p}{(2\pi)^3}\,\bar\psi(\vec p,\omega_n)\;(i\vec\gamma\cdot\vec p+i\gamma_4\,\omega_n-\gamma_4\mu+m)\;\psi(\vec p,\omega_n) \tag{100}$$

so that even the free Dirac operator is not hermitian and hence the QCD action is necessarily complex. As such it does not specify a probability measure, which precludes the straightforward application of Monte-Carlo methods in the evaluation of the partition function. However, the application of DSEs remains straightforward. The propagators and vertices are complex, so twice as many functions are required to represent them but otherwise there are no complications. Thus they provide a nonperturbative means of exploring this domain, which is presently inaccessible in lattice simulations.

6.2. Some Lattice Results. Since the early eighties, as one branch of the extensive application of lattice methods in many areas of QCD, Monte-Carlo simulations have been used to estimate the finite temperature QCD partition function [53]. These studies have contributed considerably to the current understanding of the nature of the quark-gluon plasma. Due to the persistent limitation of computational power many analyses have focused on the pure gauge sector, which exhibits a first-order deconfinement transition at a critical temperature of

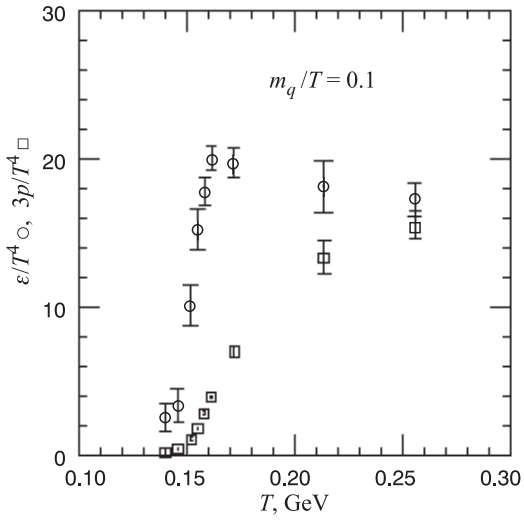

Fig. 25. Energy density and pressure for 2-light-flavour QCD on lattices with four temporal lattice sites, from Ref.58

$T_c^{N_f=0} \approx 270\,\mathrm{MeV}$ [54]. In studying the chiral transition this commonly used quenched approximation is inadequate because the details depend sensitively on the number of active (light) flavours. It is therefore necessary to include the fermion determinant.

That is even more important when $\mu \neq 0$ because the Dirac operator is not hermitian and thus the fermion determinant acquires an explicit imaginary part, in addition to those terms associated with axial anomalies. The QCD action being complex entails that the study of finite density is significantly more difficult than that of finite temperature. Simulations that ignore the fermion determinant at $\mu \neq 0$ encounter a forbidden region, which begins at $\mu = m_\pi/2$ [55], and since $m_\pi \to 0$ in the chiral limit this is a serious limitation, preventing a reliable study of chiral symmetry restoration. The phase of the fermion determinant is essential in eliminating this artefact [56].

QCD with dynamical quarks is a contemporary focus and for two flavours of light quarks the theory appears [57] to exhibit a second-order transition at a critical temperature $T_c^{N_f=2} \approx 150\,\mathrm{MeV}$. This is illustrated in Fig. 25, which shows a rapid change in the energy density in a small region around $150\,\mathrm{MeV}$. For three or more light quark flavours the continuum theory is expected to have a first order chiral symmetry restoration transition.

The quark condensate is an order parameter for chiral symmetry breaking, with its nonzero value at $T = 0$ responsible for the pion mass being proportional to the square-root of the light current-quark masses. Its behaviour near the

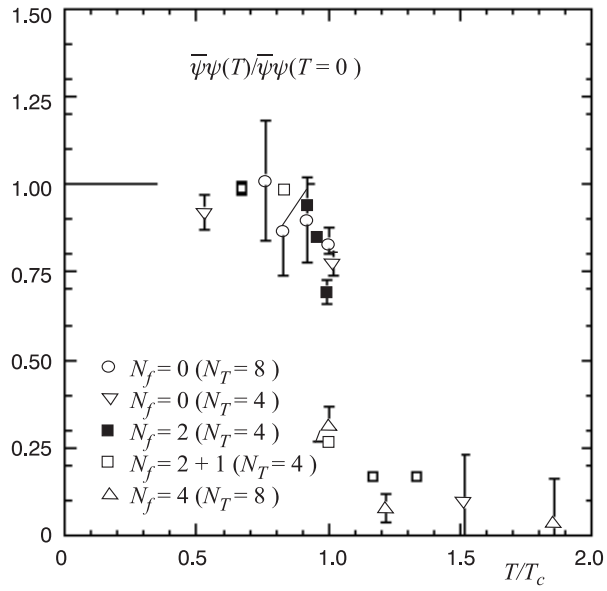

Fig. 26. Chiral condensate calculated [57] using staggered fermions and normalised to its zero temperature value. Only the $N_f = 0$ results are extrapolated to zero quark mass

critical temperature is depicted in Fig. 26, and the rapid, qualitative change with increasing T is easily apparent. Very important is that, independent of the number of light-quark flavours, the condensate is *unchanged* for $T < 0.9\,T_c$. It suggests that hadron properties are insensitive to T until very near the phase boundary.

The simulations with dynamical fermions are still preliminary, and many uncertainties remain. For example, a review [59] of recent results obtained with larger lattices and lighter quarks reports a significant lattice-volume-dependence for the critical exponents of the two light-flavour chiral symmetry restoration transition: the transition may even be first order! This might be an artefact of introducing lighter dynamical quarks, which drive the simulations to stronger coupling. The order of the transition with three and four flavours also remains unclear. With these uncertainties it is apparent that the lattice study of the phase transition will require further, even more computer-intensive simulations.

7. DSEs AT FINITE T AND μ

The contemporary application of DSEs at finite temperature and chemical potential is a straightforward extension of the $T = 0 = \mu$ studies. The direct approach is to develop a finite-T extension of the *Ansatz* for the dressed-gluon propagator. The quark DSE can then be solved and, having the dressed-quark and -gluon propagators, the response of bound states to increases in T and μ

can be studied. As a nonperturbative approach that allows the simultaneous study of DCSB and confinement, the DSEs have a significant overlap with lattice simulations: each quantity that can be estimated using lattice simulations can also be calculated using the DSEs. This means they can be used to check the lattice simulations, and importantly, that lattice simulations can be used to constrain their model-dependent aspects. Once agreement is obtained on the common domain, the DSEs can be used to explore phenomena presently inaccessible to lattice simulations.

7.1. Quark DSE. The renormalised dressed-quark propagator at finite-(T,μ) has the general form

$$S(\vec{p},\tilde{\omega}_k) = \frac{1}{i\vec{\gamma}\cdot\vec{p}\,A(\vec{p},\tilde{\omega}_k) + i\gamma_4\,\tilde{\omega}_k C(\vec{p},\tilde{\omega}_k) + B(\vec{p},\tilde{\omega}_k)} \tag{101}$$

$$\equiv -i\vec{\gamma}\cdot\vec{p}\,\sigma_A(\vec{p},\tilde{\omega}_k) - i\gamma_4\,\tilde{\omega}_k\sigma_C(\vec{p},\tilde{\omega}_k) + \sigma_B(\vec{p},\tilde{\omega}_k)\,, \tag{102}$$

where $\tilde{\omega}_k := \omega_k + i\mu$. The complex scalar functions: $A(\vec{p},\tilde{\omega}_k)$, $B(\vec{p},\tilde{\omega}_k)$ and $C(\vec{p},\tilde{\omega}_k)$ satisfy:

$$\mathcal{F}(\vec{p},\tilde{\omega}_k)^* = \mathcal{F}(\vec{p},\tilde{\omega}_{-k-1})\,, \tag{103}$$

$\mathcal{F} = A, B, C$, and although not explicitly indicated they are functions only of $|\vec{p}|^2$ and $\tilde{\omega}_k^2$.

The DSE for the renormalised dressed-quark propagator is

$$S^{-1}(\vec{p},\tilde{\omega}_k) = Z_2^A\, i\vec{\gamma}\cdot\vec{p} + Z_2\,(i\gamma_4\,\tilde{\omega}_k + m_{\rm bm}) + \Sigma'(\vec{p},\tilde{\omega}_k)\,, \tag{104}$$

where Z_2^A and Z_2 are renormalisation constants, $m_{\rm bm}$ is the bare mass, and the regularised self energy is

$$\Sigma'(\vec{p},\tilde{\omega}_k) = i\vec{\gamma}\cdot\vec{p}\,\Sigma'_A(\vec{p},\tilde{\omega}_k) + i\gamma_4\,\tilde{\omega}_k\,\Sigma'_C(\vec{p},\tilde{\omega}_k) + \Sigma'_B(\vec{p},\tilde{\omega}_k)\,, \tag{105}$$

with

$$\Sigma'_{\mathcal{F}}(\vec{p},\tilde{\omega}_k) =$$

$$= \int_{l,q}^{\bar{\Lambda}} \frac{4}{3}\,g^2\,D_{\mu\nu}(\vec{p}-\vec{q},\tilde{\omega}_k-\tilde{\omega}_l)\frac{1}{4}{\rm tr}\,[\mathcal{P}_{\mathcal{F}}\gamma_\mu S(\vec{q},\tilde{\omega}_l)\Gamma_\nu(\vec{q},\tilde{\omega}_l;\vec{p},\tilde{\omega}_k)]\,, \tag{106}$$

where $\mathcal{P}_A := -(Z_1^A/p^2)i\gamma\cdot p$, $\mathcal{P}_B := Z_1$, $\mathcal{P}_C := -(Z_1/\tilde{\omega}_k)i\gamma_4$, Z_1^A and Z_1 are vertex renormalisation constants, and $\int_{l,q}^{\bar{\Lambda}} := T\sum_{l=-\infty}^{\infty}\int^{\bar{\Lambda}}\frac{d^3q}{(2\pi)^3}$. This last is a mnemonic to represent a translationally invariant regularisation of the integral with $\bar{\Lambda}$ the regularisation mass scale.

In Eq. (106) the Landau-gauge, finite-(T,μ) dressed-gluon propagator has the form

$$g^2 D_{\mu\nu}(\vec{p},\Omega) = P^L_{\mu\nu}(\vec{p},\Omega)\,\Delta_F(\vec{p},\Omega) + P^T_{\mu\nu}(\vec{p})\,\Delta_G(p,\Omega), \tag{107}$$

where

$$P^T_{\mu\nu}(\vec{p}) \;:=\; \begin{cases} 0; & \mu \text{ and/or } \nu = 4, \\ \delta_{ij} - \dfrac{p_i p_j}{p^2}; & \mu,\nu = 1,2,3 \end{cases}, \tag{108}$$

$$P^L_{\mu\nu}(\vec{p},\Omega) \;:=\; \delta_{\mu\nu} - \frac{p_\mu p_\nu}{\sum_{\alpha=1}^4 p_\alpha p_\alpha} - P^T_{\mu\nu}(p);\ \mu,\nu = 1,\ldots,4\,. \tag{109}$$

A "Debye-mass" for the gluon appears as a T-dependent contribution to Δ_F.

In renormalising we require that

$$S^{-1}(\vec{p},\tilde{\omega}_0)\big|^{\mu=0}_{\vec{p}^2+\tilde{\omega}_0^2=\zeta^2} = i\vec{\gamma}\cdot\vec{p} + i\gamma_4\,\omega_0 + m_R^\zeta\,, \tag{110}$$

where ζ is the renormalisation point and m_R^ζ is the renormalised current-quark mass. This entails that the renormalisation constants are:

$$Z_2^A(\zeta^2,\bar{\Lambda}^2) \;=\; 1 - \Sigma'_A(\vec{p},\tilde{\omega}_0)\big|^{\mu=0}_{|\vec{p}|^2+\tilde{\omega}_0^2=\zeta^2}\,, \tag{111}$$

$$Z_2(\zeta^2,\bar{\Lambda}^2) \;=\; 1 - \Sigma'_C(\vec{p},\tilde{\omega}_0)\big|^{\mu=0}_{|\vec{p}|^2+\tilde{\omega}_0^2=\zeta^2}\,, \tag{112}$$

$$m_R^\zeta \;=\; Z_2 m_{\rm bm} + \Sigma'_B(\vec{p},\tilde{\omega}_0)\big|^{\mu=0}_{|\vec{p}|^2+\tilde{\omega}_0^2=\zeta^2}\,, \tag{113}$$

and yields the renormalised self energies:

$$\mathcal{F}(\vec{p},\tilde{\omega}_k) = \xi_{\mathcal{F}} + \Sigma'_{\mathcal{F}}(\vec{p},\tilde{\omega}_k) - \Sigma'_{\mathcal{F}}(\vec{p},\tilde{\omega}_0)\big|^{\mu=0}_{|\vec{p}|^2+\tilde{\omega}_0^2=\zeta^2}\,, \tag{114}$$

where $\mathcal{F} = A,\ B,\ C$; $\xi_A = 1 = \xi_C$ and $\xi_B = m_R^\zeta$.

In studying confinement one cannot assume that the analytic structure of a dressed propagator is the same as that of the free particle propagator: it must be determined dynamically. Indeed, one knows that the $\tilde{p}_k := (\vec{p},\tilde{\omega}_k)$-dependence of A and C is qualitatively important since it can conspire with that of B to eliminate free-particle poles in the dressed-quark propagator [17]. In this case the propagator does not have a Lehmann representation so that, in general, the Matsubara sum cannot be evaluated analytically. More importantly, it either complicates or precludes a real-time formulation of the finite temperature theory, which makes the study of nonequilibrium thermodynamics a very challenging problem. In addition, as we will see, this $\tilde{p}_k$-dependence of A and C can be a crucial factor in determining the behaviour of bulk thermodynamic quantities such as the pressure and entropy; being responsible for these quantities reaching their respective Stefan – -Boltzmann limits only for very large values of T and μ. It is therefore important in any DSE study to retain $A(\tilde{p}_k)$ and $C(\tilde{p}_k)$, and their dependence on $\tilde{p}_k$.

7.2. Phase Transitions and Order Parameters. Phase transitions are characterised by the behaviour of an order parameter, $\langle X \rangle$, the expectation value of an operator. In the ordered phase of a system: $\langle X \rangle \neq 0$, whereas in the disordered phase $\langle X \rangle = 0$. A phase transition is first-order if $\langle X \rangle \to 0$ discontinuously, whereas it is second-order if $\langle X \rangle \to 0$ continuously. For a second-order transition, the length-scale associated with correlations in the system diverges as $\langle X \rangle \to 0$ and one can define a set of critical exponents that characterise the behaviour of certain macroscopic properties at the transition point. For example, in a system that is ferromagnetic for temperatures less than some critical value, T_c, the magnetisation, M, is an order parameter and in the absence of an external magnetic field $M \propto (T_c - T)^\beta$ for $T \sim T_c^-$, where β is the critical exponent. At $T = T_c$ the behaviour of the magnetisation in the presence of an external field, $h \to 0^+$, defines another critical exponent, δ: $M \propto h^{(1/\delta)}$. In a system that can be described by mean field theory these critical exponents are

$$\beta^{\rm MF} = 0.5\,, \qquad \delta^{\rm MF} = 3.0\,. \tag{115}$$

The problem is that it can be difficult to identify the order parameter relevant to the discussion of a phase transition.

One order parameter for the chiral symmetry restoration transition is well known — it is the quark condensate, defined via the renormalised dressed-quark propagator [7]:

$$-\langle \bar{q} q \rangle_\zeta := N_c \lim_{\bar\Lambda\to\infty} Z_4(\zeta,\bar\Lambda) \int_{l,q}^{\bar\Lambda} \frac{B_0(\tilde{p}_k)}{|\vec{p}|^2 A_0(\tilde{p}_k)^2 + \tilde{\omega}_l^2 C_0(\tilde{p}_k)^2 + B_0(\tilde{p}_k)^2}\,, \tag{116}$$

for each massless quark flavour, where the subscript "0" denotes that the scalar functions: A_0, B_0, C_0, are obtained as solutions of Eq. (104) in the chiral limit. The functions have an implicit ζ-dependence. An equivalent order parameter is

$$\mathcal{X} := \mathsf{Re}\, B_0(\vec{p}=0,\tilde{\omega}_0)\,, \tag{117}$$

which was used in Refs.60–62. Thus the zeroth Matsubara mode determines the character of the chiral phase transition, a conjecture explored in Ref.63.

What is an order parameter for deconfinement?

In Sec.2.3 I observed that the analytic properties of Schwinger functions play an important role in confinement. For illustrative simplicity, set $\mu = 0$, the generalisation to $\mu \neq 0$ is not difficult, and consider

$$\Delta_{B_0}(x,\tau=0) := T \sum_{n=-\infty}^{\infty} \frac{1}{4\pi x}\,\frac{2}{\pi} \int_0^\infty dp\, p\, \sin(px)\, \sigma_{B_0}(p,\omega_n) \tag{118}$$

$$:= \frac{T}{2\pi x} \sum_{n=0}^{\infty} \Delta_{B_0}^n(x)\,. \tag{119}$$

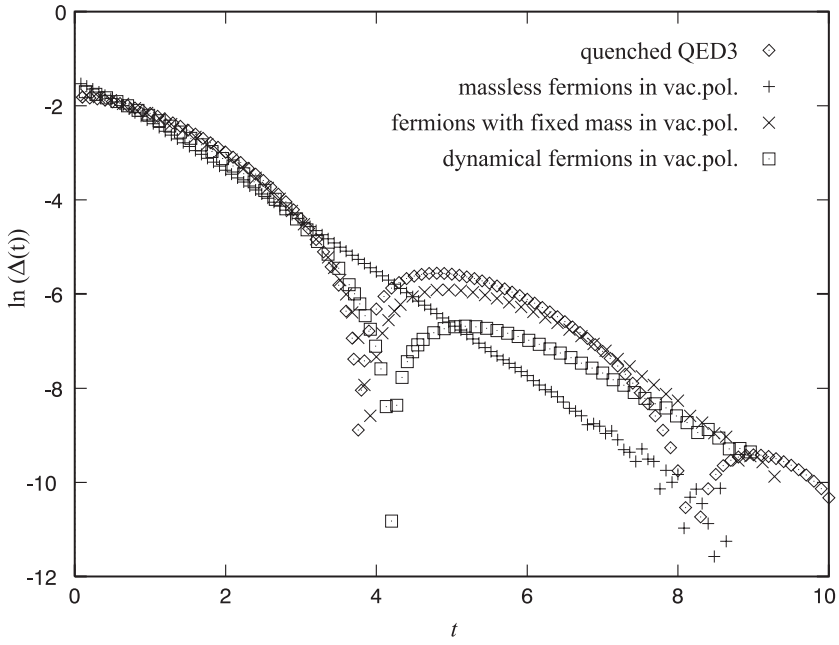

Fig. 27. $-E(t) := \ln \Delta(t)$ in QED$_3$. Here the analogue of the mass-function is $E'(t)$ and the difference between the unconfined theory: "+", and the confining theories is unmistakable

For a free fermion of mass M, $\sigma_{B_0}(p, \omega_n) = M/(\omega_n^2 + p^2 + M^2)$ and

$$\Delta_B^n(x) = M\, \mathrm{e}^{-x\sqrt{\omega_n^2 + M^2}} \ : \tag{120}$$

the $n = 0$ term dominates the sum. In this case the "mass-function"

$$M(x;T) \ := \ \frac{d}{dx}\left(-\ln\left|\Delta_{B_0}^0(x)\right|\right) = \sqrt{\pi^2 T^2 + M^2}\,. \tag{121}$$

The most important observation is that for a free particle $M(x,T)$ has a fixed, real value, which identifies the mass-pole in the propagator. It also exhibits the fermion "screening mass" $= \pi T$, which becomes important for $T \sim M/\pi$. In the context of dynamical mass generation: $M \sim M^E$. Since $M_{u/d}^E \approx 450\,\mathrm{MeV}$ one anticipates that finite-T effects will become important at $T \sim 150\,\mathrm{MeV}$ (or finite μ effects at $\mu \sim 450\,\mathrm{MeV}$). For a boson of mass M_b, $M(x;T) = M_b$: there is no screening mass.

How does $\Delta^0(x)$ behave if the dressed-propagator does not have a Lehmann representation? An example [64] is

$$\mathcal{D}(p,\Omega) = \frac{p^2+\Omega_n^2+M^2}{(p^2+\Omega_n^2+M^2)^2+4\,b^4}\,, \tag{122}$$

which has complex conjugate poles. In this case

$$\Delta^0_{\mathcal{D}}(x) = \mathrm{e}^{-Mx}\,\cos[bx]\,; \tag{123}$$

i.e., the Schwinger function oscillates and the mass-function has singularities, which is an unambiguous signal for the absence of a Lehmann representation and hence confinement!

An order parameter for confinement is now obvious [65]. Denote the position of the first zero in $\Delta^0_{B_0}(x)$ by $r_0^{z_1}$, which is inversely proportional to the distance of the poles from the real axis. Define $\kappa_0 := 1/r_0^{z_1}$, then $\kappa_0 \propto b$ and deconfinement is observed if, for some $T = T_c$, $\kappa_0(T_c) = 0$: at this point thermal fluctuations have overwhelmed the confinement scale-parameter and the poles have migrated to the real-axis. This criterion generalises easily to the case of $\mu \neq 0$ and to situations in which the dressed-propagator has an essential singularity rather than complex conjugate poles. It is also valid for both light and heavy quarks.

An analogue of this criterion, with

$$\Delta(t) := \frac{1}{2\pi}\int_{-\infty}^{\infty} dp_4\,\mathrm{e}^{ip_4 t}\,\sigma_S(\vec{p}=0,p_4)\,, \tag{124}$$

has been used to very good effect in an analysis [66] of QED$_3$ at $T = 0$. QED$_3$ is confining in quenched approximation but not when massless fermions are allowed to influence the propagation of the photon. In that case complete charge screening is possible. Confinement is recovered in the theory if the fermion in the photon vacuum polarisation loop is massive. This application is summarised in Fig.27.

7.3. Illustration at $(T \neq 0, \mu = 0)$**.** As a first example I summarise a study [60] that uses a one-parameter, model dressed-gluon propagator. This parameter, m_t, is a mass-scale that marks the boundary between the perturbative and nonperturbative domains, and its value, $m_t = 0.69$ GeV, was fixed in $T = 0$ studies [67]. The extension of the model to finite-T involves no additional parameters and is defined with: $\Delta_F(p,\Omega) := \mathcal{D}(p,\Omega;m_D)$ and $\Delta_G(p,\Omega) := := \mathcal{D}(p,\Omega;0)$;

$$\mathcal{D}(p,\Omega;m) := \frac{16}{9}\pi^2\left[\frac{2\pi}{T}m_t^2\delta_{0\,n}\delta^3(p) + \frac{1-\mathrm{e}^{\left[-\left(\mathrm{p}^2+\Omega^2+\mathrm{m}^2\right)/(4\mathrm{m}_\mathrm{t}^2)\right]}}{p^2+\Omega^2+m^2}\right]\,, \tag{125}$$

where $m_{\rm D}^2 = (8/3)\,\pi^2 T^2$ is the perturbatively evaluated "Debye-mass"*. The quark DSE was solved using the rainbow approximation

$$\Gamma_\mu(q,\omega_l;p,\omega_k) = \gamma_\mu\,. \tag{126}$$

I have discussed this truncation in Secs. 2.4 and 4, and here only note that in $T=0$ studies it has proven to be reliable in Landau gauge; i.e., at this level an efficacious phenomenology with a more sophisticated vertex *Ansatz* only requires a small quantitative modification of the parameters that characterise the small-k^2 behaviour of the dressed-gluon propagator [65]. Using this truncation, mutually consistent constraints are $Z_1^A = Z_2^A$ and $Z_1 = Z_2$.

The quark DSE was solved numerically with $m_R^\zeta = 1.1\,{\rm MeV}$, $\zeta = 9.47\,{\rm GeV}$. The $T=0$ fitting of m_t and m_R ensured a best χ^2-fit to a range of pion observables, yielding

$$\begin{array}{cccc} f_\pi = 92.4 & m_\pi = 139.5 & r_\pi N_\pi = 0.24 & g_{\pi^0\gamma\gamma} = 0.45 \\ (92.4 \pm 0.3) & (138.3 \pm 0.5) & (0.31 \pm 0.004) & (0.50 \pm 0.02) \\ a_0^0 = 0.16 & a_0^2 = -0.041 & a_1^1 = 0.028 & a_2^0 = 0.0022 \\ (0.21 \pm 0.02) & (-0.040 \pm 0.003) & (0.038 \pm 0.002) & (0.0017 \pm 0.0003) \end{array} \tag{127}$$

with the experimental values listed in parentheses**. The finite-T study reproduces these results to within 6% at $T = 5\,{\rm MeV}$, using the finite-T generalisations of the formulae in Ref.67:

$$m_\pi^2\, N_\pi^2 = \langle m_R^\zeta\,(\bar q q)_\zeta\rangle_\pi\,; \tag{128}$$

$$cd..\langle m_R^\zeta\,(\bar q q)_\zeta\rangle_\pi \;\; := \;\; 8N_c \int_{k,p}^{\bar\Lambda} B_0\,\left(\sigma_{B_0} - B_0\,\left[\omega_k^2\sigma_C^2 + p^2\sigma_A^2 + \sigma_B^2\right]\right)\,,$$

which vanishes linearly with m_R^ζ; the canonical normalisation constant is

$$\begin{aligned} N_\pi^2 = 2N_c \int_{k,p}^{\bar\Lambda} B_0^2\,\Big\{ & \sigma_A^2 - 2\left[\omega_k^2\sigma_C\sigma_C' + p^2\sigma_A\sigma_A' \,+\, \sigma_B\sigma_B'\right] \\ & -\frac{4}{3}\,p^2\,\left(\left[\omega_k^2\left(\sigma_C\sigma_C'' - (\sigma_C')^2\right) \,+\, p^2\left(\sigma_A\sigma_A'' - (\sigma_A')^2\right) + \sigma_B\sigma_B'' - (\sigma_B')^2\right]\right)\Big\}\,, \end{aligned} \tag{129}$$

*The influence of the Debye-mass on finite-T observables is qualitatively unimportant, even in the vicinity of the chiral symmetry restoration transition. The ratio of the coefficients in the two terms in Eq. (125) is such that the long-range effects associated with $\delta_{0\,k}\delta^3(p)$ are completely cancelled at short-distances; i.e., for $|\vec x|^2\, m_t^2 \ll 1$.

**In Sec. 5.1 I discussed why $r_\pi N_\pi \approx 0.25$ in impulse approximation. The π-π scattering lengths fitted in Ref.67 were taken from Ref.68.

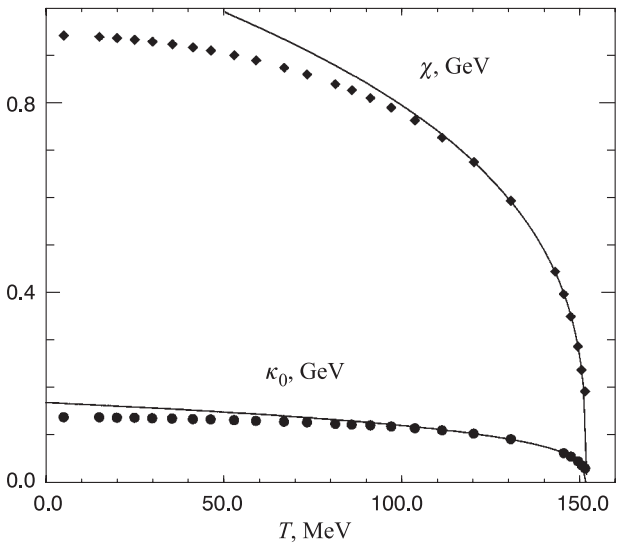

Fig. 28. The order parameters for chiral symmetry restoration ($\mathcal{X}(T)$, diamonds) and deconfinement ($\kappa_0(T)$, circles) both vanish at $T_c = 150$ MeV. The parameters for the fitted curves are presented in Table 5

with $\sigma'_B \equiv \partial\sigma_B(p^2,\omega_k)/\partial p^2$, etc.; and the pion decay constant is obtained from

$$f_\pi\, N_\pi \;=\; 4N_c \int_p^\Lambda B_0 \left\{\sigma_A\sigma_B + \frac{2}{3}|\vec{p}|^2\,(\sigma'_A\sigma_B - \sigma_A\sigma'_B)\right\} . \qquad (130)$$

Equations (128)—(130) were derived under the assumption that $\Gamma_\pi = i\gamma_5 B_0$. Some of the limitations of this assumption were discussed in Secs. 4.2 and 5.1, and they are considered further in Ref.7. It is quantitatively unreliable near the transition temperature, however, the qualitative behaviour of N_π and f_π is the same, see Table 5. Only after these studies were completed was it understood that N_π provides the best approximation to the leptonic decay constant when $\Gamma_\pi = i\gamma_5 B_0$ is assumed.

The calculated T-dependence of the chiral symmetry and deconfinement order parameters is depicted in Fig. 28. The curves in the figure, fitted on $T \in [120, 150]$ MeV, are of the form $\alpha\,(1 - T/T_c)^\beta$ with $T_c \approx 150$ MeV and α, β given in Table 5. The transitions are coincident and second-order with $\beta_{\mathcal{X}} = \beta_{\kappa_0}$, within errors: $\sim 10\%$. This estimate of $\beta_{\mathcal{X}}$ is not a mean field value and it agrees with a lattice estimate [69]: $\beta^{\rm lat} = 0.30 \pm 0.08$. It has been argued [41] that two-light-flavour QCD is in the universality class of the $N = 4$ Heisenberg magnet, for which $\beta^{\rm H} = 0.38 \pm 0.01$ and both the DSE and lattice results are broadly

Table 5. Parameters characterising the behaviour of the listed quantities, fitted to $\alpha\,(1 - T/T_c)^{\beta}$, near $T_c = 150$ MeV

	α	β
$\mathcal{X}$	1.1 GeV	0.33
κ_0	0.16 GeV	0.30
N_π^2	$(0.18\ \mathrm{GeV})^2$	1.1
$f_\pi N_\pi$	$(0.15\ \mathrm{GeV})^2$	0.93
$\langle m_R(\bar{q}q)\rangle$	$(0.15\,\mathrm{GeV})^4$	0.92
m_π	0.12 GeV	-0.11
f_π	0.12 GeV	0.36

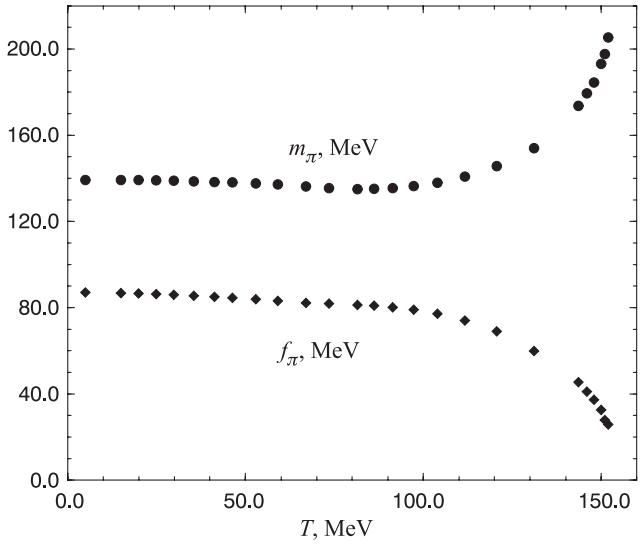

Fig. 29. Temperature dependence of the pion mass ($m_\pi(T)$, circles) and pion weak-decay constant ($f_\pi(T)$, diamonds)

consistent with this value. However, neither of these estimates of β survives more exhaustive study [59,70], and the most recent analyses [70,71] suggest that in DSE models whose long-range part is described by the regularised singularity in Eq. (125) the chiral symmetry restoration transition at finite-T is described by a mean-field value of β.

The behaviour of pion observables calculated from Eqs.(128)—(130) is depicted in Fig.29. f_π and m_π are weakly sensitive to T for $T < 0.7\,T_c^{\mathcal{X}}$, and this is also seen in lattice simulations; e.g., the quark condensate in Fig. 26 and f_π in Fig. 30. However, as T approaches $T_c^{\mathcal{X}}$, the mass eigenvalue in the

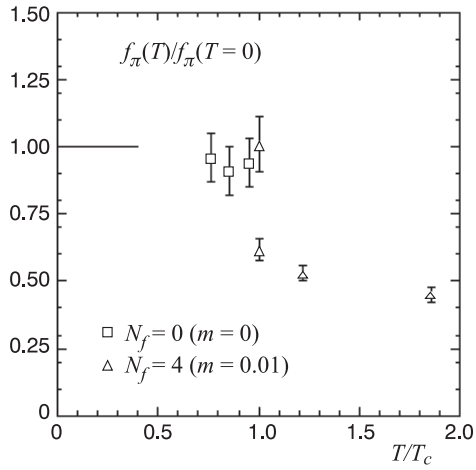

Fig. 30. Temperature dependence of the pion weak-decay constant on a $32^3 \times 8$ lattice [57]

pion Bethe — Salpeter equation moves to increasingly larger values, as thermal fluctuations overwhelm attraction in the channel, until at $T = T_c^{\mathcal{X}}$ there is no solution and $f_\pi \to 0$. This means that the pion-pole contribution to the four-point, quark-antiquark correlation function disappears; i.e., there is no quark-antiquark pseudoscalar bound state for $T > T_c^{\mathcal{X}}$. That may have important consequences for a wide range of physical observables [72], if borne out by improved studies; e.g., such T-dependence for f_π and m_π would lead to a 20% reduction in the $\pi \to \mu\nu_\mu$ decay widths at $T \approx 0.9\, T_c^{\mathcal{X}}$.

7.4. Complementary study at $(T = 0, \mu \neq 0)$**.** The finite-μ behaviour of the same model [67] has also been explored [62]. The dressed-gluon propagator has the simple form [67]

$$g^2 D_{\mu\nu}(k) = \left(\delta_{\mu\nu} - \frac{k_\mu k_\nu}{k^2}\right) \frac{\mathcal{G}(k^2)}{k^2}\,, \tag{131}$$

$$\frac{\mathcal{G}(k^2)}{k^2} = \frac{16}{9}\pi^2 \left[4\pi^2 m_t^2 \delta^4(k) + \frac{1 - \mathrm{e}^{-[k^2/(4m_t^2)]}}{k^2}\right], \tag{132}$$

and the rainbow approximation is used again. Neither the dressed propagator nor vertex have explicit μ-dependence, which can arise through quark vacuum polarisation insertions. As such they may be inadequate at large values of μ, particularly near any critical chemical potential. However, in the absence of finite-μ studies of these quantities, the exploration of such models is useful, and one can assess the results obtained in the light of existing experiments and related theoretical studies.

The renormalised dressed-quark propagator is

$$S(p_{[\mu]}) := -i\vec{\gamma}\cdot\vec{p}\,\sigma_A(p_{[\mu]}) - i\gamma_4\,\omega_{[\mu]}\,\sigma_C(p_{[\mu]}) + \sigma_B(p_{[\mu]})\,, \qquad (133)$$

where $p_{[\mu]} := (\vec{p}, \omega_{[\mu]})$, with $\omega_{[\mu]} := p_4 + i\mu$. The quark DSE and the renormalisation conditions are similar to those discussed in the previous section, and the equation has two qualitatively distinct solutions: a chirally symmetric Wigner–Weyl mode, characterised by $B_0 \equiv 0$; and a confining Nambu–Goldstone mode, characterised by $B_0 \not\equiv 0$.

To explore the possibility of a phase transition one calculates the relative stability of the different phases, which is measured by the difference in pressure between them. The pressure is obtained directly from the partition function, $\mathcal{Z}$: it is the sum of all vacuum-to-vacuum transition amplitudes. In "stationary phase" approximation, the partition function is given by the tree-level auxiliary-field effective action [73] and the pressure is:

$$P[S] := \frac{T}{V}\ln\mathcal{Z} = \frac{T}{V}\left\{\mathrm{TrLn}\left[\frac{1}{T}S^{-1}\right] - \frac{1}{2}\mathrm{Tr}\left[\Sigma S\right]\right\}. \qquad (134)$$

It is a functional of $S(p_{[\mu]})$. In the absence of interactions $\Sigma \equiv 0$ and Eq. (134) yields the free fermion partition function. [Additive gluon contributions cancel in the pressure difference and are neglected.] The contribution of hadrons and hadron-like correlations to the partition function are neglected in Eq. (134). At the level of approximation consistent with Eq. (134) these terms are an additive contribution that can be estimated using the *hadronisation* techniques of Ref.74. After a proper normalisation of the partition function; i.e., subtraction of the vacuum contribution, they are the only contributions to the partition function in the confinement domain. They are easy to calculate and are considered no further here as they are not a significant influence on the position of the phase boundary.

The pressure difference is

$$\frac{1}{2N_f N_c}\,\mathcal{B}(\mu) := \int_p^\Lambda \left\{\ln\left[\frac{|\,\vec{p}\,|^2 A_0^2 + \omega_{[\mu]}^2 C_0^2 + B_0^2}{|\,\vec{p}\,|^2 \hat{A}_0^2 + \omega_{[\mu]}^2 \hat{C}_0^2}\right] + \right.$$

$$\left. + |\,\vec{p}\,|^2\,(\sigma_{A_0} - \hat{\sigma}_{A_0}) + \omega_{[\mu]}^2\,(\sigma_{C_0} - \hat{\sigma}_{C_0})\right\}, \qquad (135)$$

which defines a μ-dependent "bag constant" [75]. In Eq. (135), $\hat{A}$ and $\hat{C}$ represent the solution of Eq.(104) obtained when $B_0 \equiv 0$; i.e., when DCSB is absent. This solution exists for all μ. $\mathcal{B}(\mu)$ is plotted in Fig. 31. It is positive when the Nambu–Goldstone phase is dynamically favoured; i.e., has the highest pressure, and becomes negative when the Wigner pressure becomes larger. The critical chemical potential is the zero of $\mathcal{B}(\mu)$; i.e., $\mu_c = 375\,\mathrm{MeV}$. This abrupt switch from the Nambu–Goldstone to the Wigner–Weyl phase signals a first order transition.

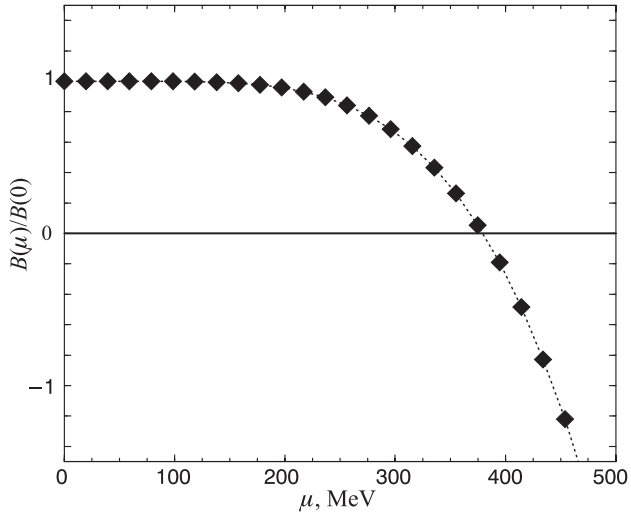

Fig. 31. $\mathcal{B}(\mu)$ from (135); $\mathcal{B}(\mu) > 0$ marks the domain of confinement and dynamical chiral symmetry breaking. The zero of $\mathcal{B}(\mu)$ is $\mu_c = 375\,\mathrm{MeV}$. $\mathcal{B}(0) = (0.104\,\mathrm{GeV})^4$, which can be compared with the value $\sim (0.145\,\mathrm{GeV})^4$ commonly used in bag-like models of hadrons [74]

The order parameter for chiral symmetry restoration is that given in Eq. (117), while the confinement order parameter at $(T = 0, \mu \neq 0)$ is derived from

$$\Delta_S(\tau) := \frac{1}{2\pi} \int_{-\infty}^{\infty} dp_4\, \mathrm{e}^{ip_4\tau}\, \sigma_{B_0}(\vec{p} = 0, \omega_{[\mu]})\,, \tag{136}$$

an analogue of Eq. (118). For a free, massive fermion $\sigma_B(\vec{p} = 0, \omega_{[\mu]}) = M/(\omega^2_{[\mu]} + M^2)$. This function has poles at $p_4^2 = -(M \pm \mu)^2$, which are associated with the μ-induced offset of the particle and antiparticle zero-point energies, and

$$\Delta_S(\tau) = \frac{1}{2}\, \mathrm{e}^{-(M-\mu)\,\tau}\, \theta(M - \mu)\,, \tag{137}$$

which is positive-definite and monotonically decreasing. In contrast, as observed above, for a Schwinger function with complex-conjugate p^2-poles, $\Delta_S(\tau)$ has zeros at $\tau > 0$.

The μ-dependence of the order parameters for chiral symmetry restoration and deconfinement is depicted in Fig. 32. The chiral order parameter *increases* with increasing chemical potential up to μ_c, with $\mathcal{X}(\mu_c)/\mathcal{X}(0) \approx 1.2$, whereas $\kappa(\mu)$ is insensitive to increasing μ. At μ_c they both drop immediately and discontinuously to zero, as expected of a first-order phase transition. The increase of the chiral order parameter with μ is a necessary consequence of the momentum dependence

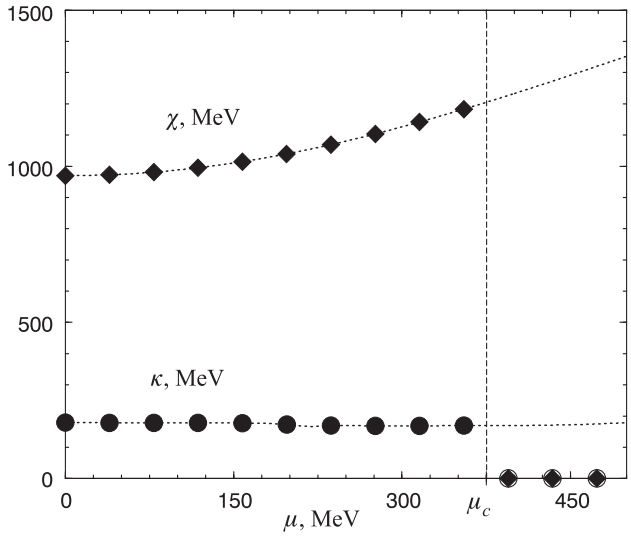

Fig. 32. The order parameters for chiral symmetry restoration [$\mathcal{X}$, diamonds] and deconfinement [κ, circles]. $\mu_c = 375\,\mathrm{MeV}$.

of the scalar piece of the quark self energy, $B(p_{[\mu]})$, as is easily seen in Ref. 61 and in Secs. 7.5 and 7.6. The vacuum quark condensate behaves in qualitatively the same manner as $\mathcal{X}$.

The behaviour of m_π and f_π is illustrated in Fig. 33. One observes that although the chiral order parameter *increases* with μ, m_π *decreases* slowly as μ increases. This slow fall continues until $\mu \approx 0.7\,\mu_c$, when $m_\pi(\mu)/m_\pi(0) \approx 0.94$. At this point m_π begins to increase although, for $\mu < \mu_c$, $m_\pi(\mu)$ does not exceed $m_\pi(0)$. This precludes pion condensation, in qualitative agreement with Ref.76. The behaviour of m_π results from mutually compensating increases in $\langle m_R^\zeta(\bar{q}q)_\zeta\rangle_\pi$ and N_π^2. This is a manifestation of the manner in which dynamical chiral symmetry breaking protects pseudoscalar meson masses against rapid changes with μ. The pion leptonic decay constant is insensitive to the chemical potential until $\mu \approx 0.7\,\mu_c$, when it increases sharply so that $f_\pi(\mu_c^-)/f_\pi(\mu=0) \approx$ ≈ 1.25. The relative insensitivity of m_π and f_π to changes in μ, until very near μ_c, mirrors the behaviour of these observables at finite-T [60]. For example, it leads only to a 14% increase in the $\pi \to \mu\nu$ decay width at $\mu \approx 0.9\,\mu_c$. The universal scaling conjecture of Ref.77 is inconsistent with the anticorrelation we observe between the μ-dependence of f_π and m_π.

Comparing the μ-dependence of f_π and m_π with their T-dependence, one observes an anticorrelation; e.g., at $\mu = 0$, f_π falls continuously to zero as T is increased towards $T_c \approx 150\,\mathrm{MeV}$ [60]. This too is a necessary consequence of the

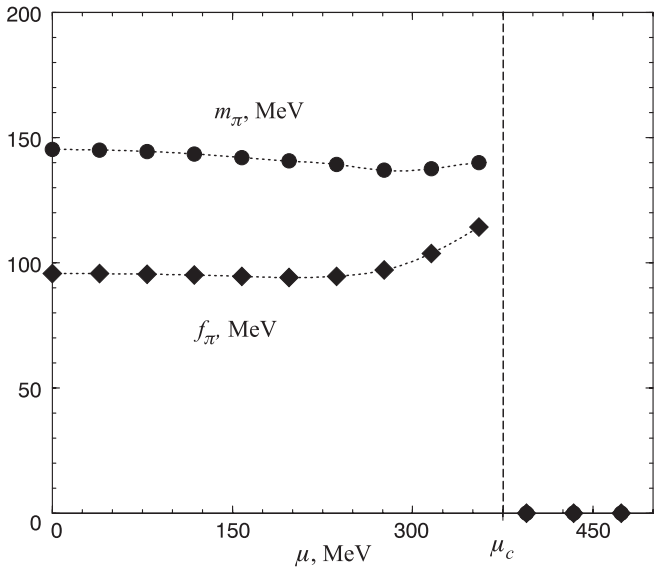

Fig. 33. Chemical potential dependence of the pion mass [m_π, circles] and pion leptonic decay constant [f_π, diamonds]

momentum-dependence of the quark self-energy. In calculating these observables the natural dimension is mass-squared, and their behaviour at finite T and μ is determined by $\mathsf{Re}(\omega^2_{[\mu]}) \sim [\pi^2 T^2 - \mu^2]$, where the T-dependence arises from the introduction of the fermion Matsubara frequency: $p_4 \to (2n+1)\pi T$. Hence when such a quantity decreases with T it will increase with μ, and vice-versa. This is elucidated in Secs. 7.5 and 7.6, and in Ref.50.

The confined-quark vacuum consists of quark-antiquark pairs correlated in a scalar condensate. Increasing μ increases the scalar density: $(-\langle\bar{q}q\rangle)$. This result is an expected consequence of confinement, which entails that each additional quark must be locally paired with an antiquark thereby increasing the density of condensate pairs as μ is increased. For this reason, as long as $\mu < \mu_c$, there is no excess of particles over antiparticles in the vacuum and hence the baryon number density remains zero [61]; i.e., $\rho_B^{u+d} = 0\,,\ \forall \mu < \mu_c$. This is just the statement that quark-antiquark pairs confined in the condensate do not contribute to the baryon number density.

The quark pressure, $P^{u+d}[\mu]$, can be calculated [61], see Sec. 7.5, and one finds that after deconfinement it increases rapidly, as the condensate "breaks-up", and an excess of quarks over antiquarks develops. The baryon-number density,

$\rho_B^{u+d} = (1/3)\partial P^{u+d}/\partial\mu$, also increases rapidly, with

$$\rho_B^{u+d}(\mu \approx 2\mu_c) \simeq 3\,\rho_0\,, \tag{138}$$

where $\rho_0 = 0.16\,\mathrm{fm}^{-3}$ is the equilibrium density of nuclear matter. For comparison, the central core density expected in a $1.4\,M_\odot$ neutron star is 3.6-4.1 ρ_0 [43]. Finally, at $\mu \sim 5\mu_c$, the quark pressure saturates the ultrarelativistic limit: $P^{u+d} = \mu^4/(2\pi^2)$, and there is a simple relation between baryon-density and chemical-potential:

$$\rho_B^{u_F+d_F}(\mu) = \frac{1}{3}\,\frac{2\mu^3}{\pi^2}\,,\ \forall\mu \gtrsim 5\mu_c\,, \tag{139}$$

so that $\rho_B^{u_F+d_F}(5\mu_c) \sim 350\,\rho_0$. Thus the quark pressure in the deconfined domain overwhelms any finite, additive contribution of hadrons to the equation of state, which anticipating this was neglected in Ref.62. This discussion suggests that a quark-gluon plasma may be present in the core of dense neutron stars.

7.5. Simultaneous study of $(T \neq 0, \mu \neq 0)$**.** This is the most difficult problem and the most complete study [61] to date employs a simple *Ansatz* for the dressed-gluon propagator:

$$g^2 D_{\mu\nu}(\vec{p},\Omega_k) = \left(\delta_{\mu\nu} - \frac{p_\mu p_\nu}{|\vec{p}|^2 + \Omega_k^2}\right) 2\pi^3\,\frac{\eta^2}{T}\,\delta_{k0}\,\delta^3(\vec{p})\,, \tag{140}$$

which exhibits the infrared enhancement suggested by Ref.6. As an infrared-dominant model that does not represent well the behaviour of $D_{\mu\nu}(\vec{p},\Omega_k)$ away from $|\vec{p}|^2 + \Omega_k^2 \approx 0$, some model-dependent artefacts arise. However, there is significant merit in its simplicity and, since the artefacts are easily identified, the model remains useful as a means of elucidating many of the qualitative features of more sophisticated *Ansätze*.

With this model, using the rainbow approximation, the QCD$_\mu^T$ gap equation, or DSE for the dressed-quark propagator, is [3]

$$S^{-1}(\vec{p},\omega_k) = S_0^{-1}(\vec{p},\tilde{\omega}_k) + \tfrac{1}{4}\eta^2\gamma_\nu S(\vec{p},\tilde{\omega}_k)\gamma_\nu\,. \tag{141}$$

A simplicity inherent in Eq. (140) is now apparent: it allows the reduction of an integral equation to an algebraic equation, in whose solution many of the qualitative features of more sophisticated models are manifest, as will become clear. In terms of the scalar functions introduced in Eq. (101), Eq. (141) reads

$$\eta^2 m^2 = B^4 + mB^3 + \left(4\tilde{p}_k^2 - \eta^2 - m^2\right)B^2 - m\,\left(2\,\eta^2 + m^2 + 4\,\tilde{p}_k^2\right)B\,, \tag{142}$$

$$A(\tilde{p}_k) = C(\tilde{p}_k) = \frac{2B(\tilde{p}_k)}{m + B(\tilde{p}_k)}\,. \tag{143}$$

Of particular interest is the chiral limit, $m = 0$. In this case Eq. (142) reduces to a quadratic equation for $B(\tilde{p}_k)$, which has two qualitatively distinct solutions. The "Nambu–Goldstone" solution, for which

$$B(\tilde{p}_k) \;=\; \begin{cases} \sqrt{\eta^2 - 4\tilde{p}_k^2}\,, & \mathsf{Re}(\tilde{p}_k^2) < \frac{\eta^2}{4} \\ 0\,, & \text{otherwise} \end{cases} \tag{144}$$

$$C(\tilde{p}_k) \;=\; \begin{cases} 2\,, & \mathsf{Re}(\tilde{p}_k^2) < \frac{\eta^2}{4} \\ \frac{1}{2}\left(1 + \sqrt{1 + \frac{2\eta^2}{\tilde{p}_k^2}}\right), & \text{otherwise}\,, \end{cases} \tag{145}$$

describes a phase of this model in which: 1) chiral symmetry is dynamically broken, because one has a nonzero quark mass-function, $B(\tilde{p}_k)$, in the absence of a current-quark mass; and 2) the dressed-quarks are confined, because the propagator described by these functions does not have a Lehmann representation. The alternative "Wigner" solution, for which

$$\hat{B}(\tilde{p}_k) \equiv 0, \quad \hat{C}(\tilde{p}_k) = \frac{1}{2}\left(1 + \sqrt{1 + \frac{2\eta^2}{\tilde{p}_k^2}}\right), \tag{146}$$

describes a phase of the model in which chiral symmetry is not broken and the dressed-quarks are not confined.

With these two "phases", characterised by qualitatively different, momentum-dependent modifications of the quark propagator, this model can be used to explore chiral symmetry restoration and deconfinement, and elucidate aspects of the method in such studies.

In this model the relative stability of the different phases is measured by a (T, μ)-dependent "bag constant" [75],

$$\mathcal{B}(T,\mu) \;:=\; P[S_{\rm NG}] - P[S_{\rm W}]\,, \tag{147}$$

where $S_{\rm NG}$ means Eq. (101) obtained from Eq. (144) and $S_{\rm W}$, Eq. (101) obtained from Eq. (146). As above, $\mathcal{B}(T,\mu) > 0$ indicates the stability of the confined (Nambu–Goldstone) phase and hence the phase boundary is specified by that curve in the (T,μ)-plane for which

$$\mathcal{B}(T,\mu) \;\equiv\; 0\,. \tag{148}$$

In the chiral limit

$$\mathcal{B}(T,\mu) =$$

$$= \eta^4\, 2N_c N_f \frac{\bar{T}}{\pi^2} \sum_{l=0}^{l_{\rm max}} \int_0^{\bar{\Lambda}_l} dy\, y^2 \left\{ \mathsf{Re}\left(2\bar{p}_l^2\right) - \mathsf{Re}\left(\frac{1}{C(\bar{p}_l)}\right) - \ln\left|\bar{p}_l^2 C(\bar{p}_l)^2\right| \right\}, \tag{149}$$

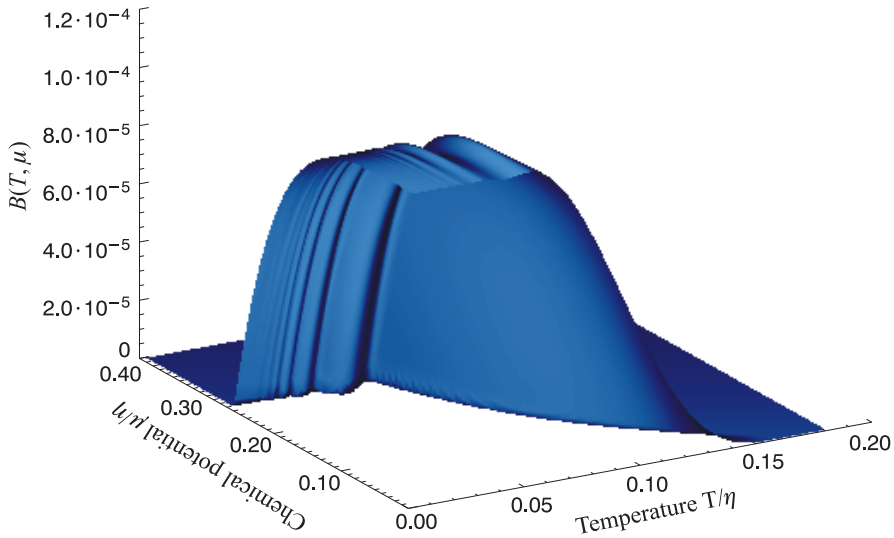

Fig. 34. $\mathcal{B}(T,\mu)$ from Eq. (149); $\mathcal{B}(T,\mu) > 0$ marks the confinement domain. The scale is set by $\mathcal{B}(0,0) = (0.102\,\eta)^4 = (0.109\,\mathrm{GeV})^4$; $\eta = 1.06\,\mathrm{GeV}$ [12]

with: $\bar{T} = T/\eta$, $\bar{\mu} = \mu/\eta$; l_{max} is the largest value of l for which $\bar{\omega}^2_{l_{\max}} \leq \frac{1}{4} + \bar{\mu}^2$ and this also specifies $\omega_{l_{max}}$, $\bar{\Lambda}^2 = \bar{\omega}^2_{l_{\max}} - \bar{\omega}^2_l$, $\bar{p}_l = (\vec{y}, \bar{\omega}_l + i\bar{\mu})$. $\mathcal{B}(T,\mu)$ is depicted in Fig. 34 and the critical line in Fig. 35. The deconfinement and chiral symmetry restoration transitions are coincident.

For $\mu = 0$ the transition is second order and the critical temperature is $T_c^0 = 0.159\,\eta$, which using the value of $\eta = 1.06\,\mathrm{GeV}$ obtained by fitting the π and ρ masses [12] corresponds to $T_c^0 = 0.170\,\mathrm{GeV}$. This is only 12% larger than the value obtained in Sec. 7.3, [60], and the order of the transition is the same. However, in the present case the critical exponent is $\beta = 0.5$. For any $\mu \neq 0$ the transition is first-order, as revealed by close scrutiny of Fig. 34. For $T = 0$ the critical chemical potential is $\mu_c^0 = 0.3\,\mathrm{GeV}$, which is $\approx 30\%$ smaller than the result in Sec. 7.4 [62]. One notes from Fig. 35 that $\mu_c(T)$ is insensitive to T until $T \approx 0.3\,T_c^0$. The discontinuity in the order parameters vanishes as $\mu \to 0$.

In the deconfinement domain, illustrated clearly in Fig. 35, the quarks contribute an amount

$$P[S_{\mathrm{W}}] = \eta^4\, 2N_c N_f \frac{\bar{T}}{\pi^2} \sum_{l=0}^{\infty} \int_0^{\infty} dy\, y^2 \left\{ \ln \left| \beta^2 \tilde{p}_l^2 \hat{C}(\bar{p}_l)^2 \right| - 1 + \mathsf{Re} \left(\frac{1}{\hat{C}(\bar{p}_l)} \right) \right\} \tag{150}$$

to the pressure, which must be renormalised to zero on the phase boundary. Just as for free fermions, this expression is formally divergent and one must isolate and

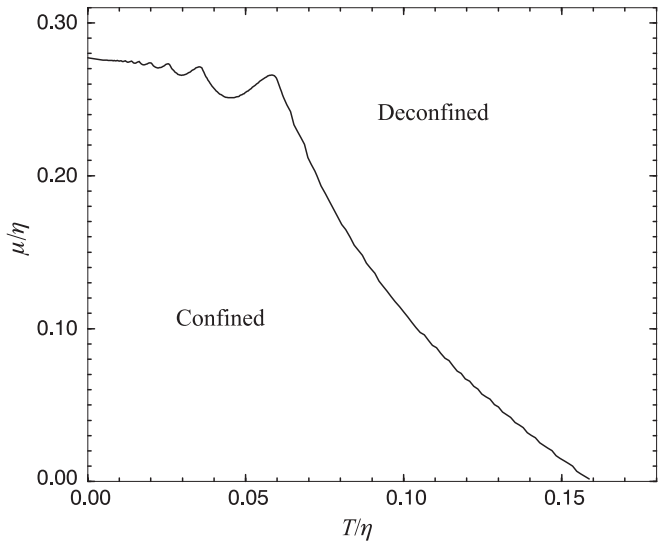

Fig. 35. The phase boundary in the $(\bar{T}, \bar{\mu})$-plane obtained from (148) and (149). The "structure" in this curve, apparent for small-T, is an artefact of the inadequate representation of the quark-quark interaction in the ultraviolet by Eq. (140)

define the active, temperature-dependent contribution. This is difficult because, in general, $\hat{C}(\bar{p}_l)$ is only known numerically and hence it is not possible to evaluate $P[S_{\rm W}]$ analytically. A method for the numerical evaluation of Eq. (150) was developed in Ref.61.

Consider the derivative of the integrand in Eq. (150):

$$\sum_{l=0}^{\infty} \frac{d}{d\bar{T}} \left\{ \ln \left| \beta^2 \bar{p}_l^2 \hat{C}(\bar{p}_l)^2 \right| - 1 + \mathsf{Re} \left(\frac{1}{\hat{C}(\bar{p}_l)} \right) \right\} =$$

$$= \sum_{l=0}^{\infty} \left\{ -\frac{1}{\bar{T}} \left[\frac{(y-\bar{\mu})^2}{(y-\bar{\mu})^2 + \bar{\omega}_l^2} + \frac{(y+\bar{\mu})^2}{(y+\bar{\mu})^2 + \bar{\omega}_l^2} \right] + \mathsf{Re} \left(\frac{2\hat{C}(\bar{p}_l) - 1}{\hat{C}(\bar{p}_l)^2} \frac{d\hat{C}(\bar{p}_l)}{d\bar{T}} \right) \right\} . \tag{151}$$

In the absence of interactions $C(\bar{p}_l) \equiv 1$, the second term is zero and

$$-\frac{2}{\bar{T}} \sum_{l=0}^{\infty} \left[\frac{(y-\bar{\mu})^2}{(y-\bar{\mu})^2 + \bar{\omega}_l^2} + \frac{(y+\bar{\mu})^2}{(y+\bar{\mu})^2 + \bar{\omega}_l^2} \right] = \frac{d}{d\bar{T}} \left\{ \frac{e(y)}{\bar{T}} + \mathcal{I}(e(y)) \right\} , \tag{152}$$

where in this case $e(y) = y$ and

$$\mathcal{I}(\zeta) = \ln \left[1 + \exp \left(-\frac{\zeta - \bar{\mu}}{\bar{T}} \right) \right] + \ln \left[1 + \exp \left(-\frac{\zeta + \bar{\mu}}{\bar{T}} \right) \right] . \tag{153}$$

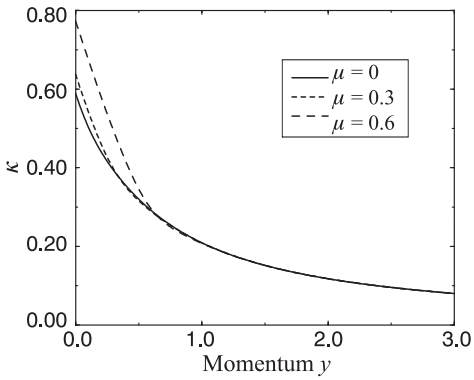

Fig. 36. $\kappa(y,\bar{\mu})$, which describes the nonperturbative modification of the free particle dispersion law, for $\bar{\mu} = 0, 0.3, 0.6$. By assumption, it is independent of T

Appropriately inserting Eq. (152) for the parenthesised term in Eq. (150), and neglecting T-independent terms one obtains,

$$P[S_0] = \eta^4 N_c N_f \frac{\bar{T}}{\pi^2} \int_0^\infty dy\, y^2\, \mathcal{I}(y) \tag{154}$$

$$= \eta^4 N_c N_f \frac{1}{12\pi^2} \left(\bar{\mu}^4 + 2\pi^2 \bar{\mu}^2 \bar{T}^2 + \frac{7}{15}\pi^4 \bar{T}^4 \right) , \tag{155}$$

which is the massless free particle pressure.

To proceed in the general case, the assumption is made [61] that the nontrivial momentum dependence of $\hat{C}(\bar{p}_l)$, which is manifest in all DSE-models of QCD$^T_\mu$, acts primarily to modify the usual massless, free particle dispersion law. One evaluates the sum on the right-hand side of (151) numerically and uses the form on the right-hand side of Eq. (152) to fit a modified, T-independent dispersion law, $\underline{e}(y,\bar{\mu}) = y + \kappa(y,\bar{\mu})$, to the numerical results. The existence of a $\kappa(y,\bar{\mu})$ that provides a good χ^2-fit on the deconfinement domain is understood as an *a posteriori* justification of the assumption. In Ref.61 the relative error between the fit and the numerical results is $< 10\%$ on the entire T-domain.

The calculated form of $\kappa(y,\bar{\mu})$ is depicted in Fig. 36; it only depends weakly on $\bar{\mu}$. The form indicates a persistence of nonperturbative effects into the domain of deconfinement, evident in the nontrivial momentum dependence of $\hat{C}(\bar{p}_l)$ and its slow evolution to the asymptotic value $\hat{C}(\bar{p}_l) = 1$. The effect of this is to generate a mass-scale in the massless dispersion law: $\kappa(0,0) \simeq 0.6 \sim 2\bar{\mu}_c^0$. This mass-scale is unrelated to the chiral-symmetry order parameter, $\mathcal{X}$ in Eq. (117), and is a qualitatively new feature of the study. For $\bar{\mu} > 5\bar{\mu}_c^0$ the explicit mass-scale introduced by the chemical potential overwhelms the dynamically generated scale.

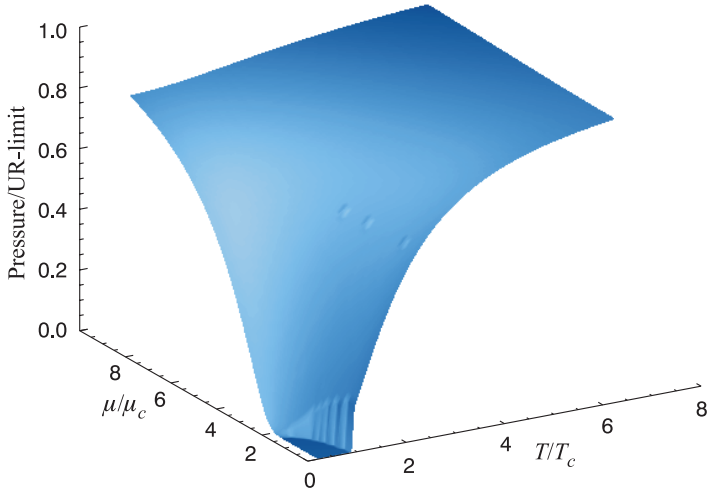

Fig. 37. The quark pressure, $P_q(\bar{T},\bar{\mu})$, normalised to the free, massless (or Ultra-Relativistic) result, Eq. (155)

Using this result, Eq. (150) becomes

$$P[S_{\rm W}] \;=\; \eta^4\, N_c N_f \frac{\bar{T}}{\pi^2} \int_0^\infty dy\, y^2\, \mathcal{I}(\underline{e}(y,\bar{\mu}))\,, \tag{156}$$

and the quark pressure in this DSE-model of QCD$^T_\mu$ is

$$P_q(T,\mu) = \theta(\mathcal{D})\,\{P[S_{\rm W}] - P[S_{\rm W}]|_{\partial\mathcal{D}}\}\,, \tag{157}$$

where $\mathcal{D}$ is the domain marked "Deconfined" in Fig. 35, $\theta(\mathcal{D})$ is a step function, equal to one for $(T,\mu) \in \mathcal{D}$, and $P[S_{\rm W}]|_{\partial\mathcal{D}}$ indicates the evaluation of this expression on the boundary of $\mathcal{D}$, as defined by the intersection of a straight-line from the origin in the (T,μ)-plane to the argument-value. It is plotted in Fig. 37, which illustrates clearly that in this model the free particle (Stefan–Boltzmann) limit is reached at large values of $\bar{T}$ and $\bar{\mu}$. The approach to this limit is slow, however. For example, at $\bar{T} \sim 0.3 \sim 2\bar{T}^0_c$, or $\bar{\mu} \sim 1.0 \sim 3\bar{\mu}^0_c$, Eq. (157) is only 50% of the free particle pressure, Eq. (155). A qualitatively similar result is observed in numerical simulations of lattice-QCD actions at finite-T [42]. This feature results from the slow approach to zero with y of $\kappa(y,\bar{\mu})$, illustrated in Fig. 36, and emphasises the persistence of the momentum dependent modifications of the quark propagator.

With the definition and calculation of the pressure, $P_q(T,\mu)$, all the remaining bulk thermodynamic quantities that characterise the model can be calculated. As

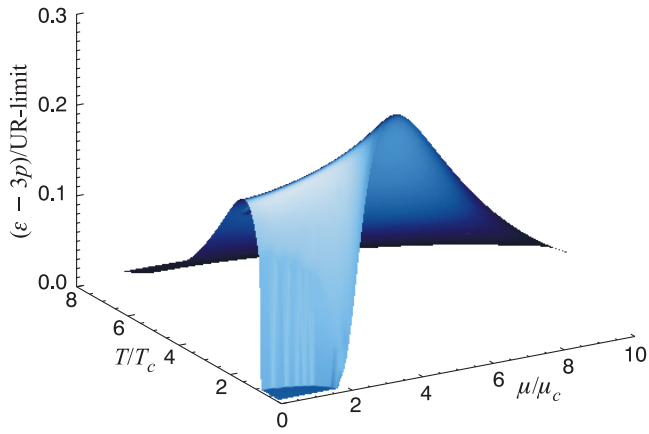

Fig. 38. The "interaction measure", $\Delta(T,\mu)$, normalised to the free, massless result for the pressure, Eq. (155)

an example the "interaction measure": $\Delta := \epsilon - 3P$, where ϵ is the energy density, is plotted in Fig. 38. It is zero for an ideal gas, hence the name: Δ measures the interaction-induced deviation from ideal gas behaviour. This figure provides a very clear indication of the persistence of nonperturbative effects into the deconfinement domain, with a $\mu = 0$ maximum of $\Delta \approx 0.2\, P[S_0]$ at $T \approx 2T_c$ and a $T = 0$ maximum of $\Delta \approx 0.3\, P[S_0]$ at $\mu \approx 3\mu_c$. Both Figs. 37 and 38 indicate that there is a "mirroring" of finite-T behaviour in the μ-dependence of the bulk thermodynamic quantities.

7.6. π and ρ properties. The model discussed in the last section has been used [50] to study the (T,μ)-dependence of π and ρ properties, and to elucidate other features of the models described above that employ a more sophisticated *Ansatz* for the dressed-gluon propagator. In these applications its simplicity is particularly helpful.

To begin, consider the vacuum quark condensate, which in this model is

$$-\langle\bar{q}q\rangle = \eta^3\, \frac{8N_c}{\pi^2}\bar{T} \sum_{l=0}^{l_{\max}} \int_0^{\bar{\Lambda}_l} dy\, y^2\, \mathsf{Re}\left(\sqrt{\frac{1}{4} - y^2 - \tilde{\omega}_l^2}\right) : \qquad (158)$$

for $T = 0 = \mu$, $(-\langle\bar{q}q\rangle) = \eta^3/(80\,\pi^2) = (0.11\,\eta)^3$. In Fig. 39 one observes that $(-\langle\bar{q}q\rangle)$ decreases with T but *increases* with increasing μ, up to a critical value of $\mu_c(T)$ when it drops discontinuously to zero. These results are in qualitative and semiquantitative agreement with the $(T = 0, \mu \neq 0)$ and $(T \neq 0, \mu = 0)$ studies described in Secs. 7.3 and 7.4. The increase with μ is also qualitatively identical to that observed in a random matrix theory with the global symmetries of the QCD partition function [78]. $(-\langle\bar{q}q\rangle)$ must increase with μ in the confinement

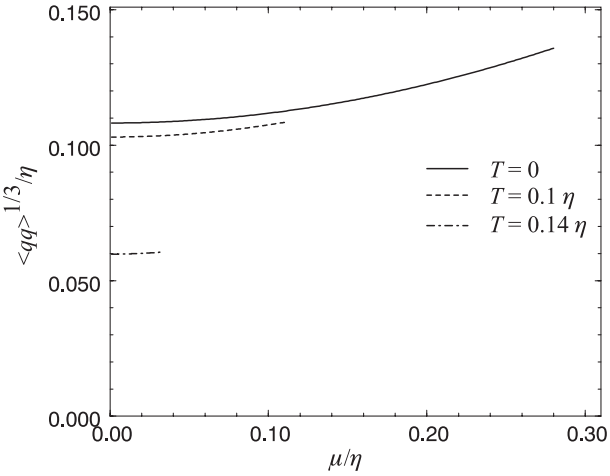

Fig. 39. The quark condensate, Eq. (158), as a function of μ for a range of values of T. In all existing studies, in which the quark mass function has a realistic momentum dependence, it increases with μ and decreases with T. At the critical chemical potential, $\mu_c(T)$, $(-\langle\bar{q}q\rangle)$ drops discontinuously to zero, as expected of a first-order transition. For $\mu = 0$ it falls continuously to zero, exhibiting a second-order transition at $T_c(\mu = 0) = 0.16\,\eta$.

domain because confinement entails that each additional quark must be locally-paired with an antiquark, thereby increasing the density of condensate pairs. This vacuum rearrangement is manifest in the behaviour of the necessarily-momentum-dependent scalar part of the quark self energy, $B(\tilde{p}_k)$. In this model Eqs. (128)-(130) yield very simple expressions in the chiral limit; for example*,

$$f_\pi^2 \;=\; \eta^2 \frac{16 N_c}{\pi^2} \bar{T} \sum_{l=0}^{l_{\max}} \frac{\bar{\Lambda}_l^3}{3} \left(1 + 4\,\bar{\mu}^2 - 4\,\bar{\omega}_l^2 - \frac{8}{5}\,\bar{\Lambda}_l^2\right) . \qquad (159)$$

Characteristic in Eq. (159) is the combination $\mu^2 - \omega_l^2$, which entails that, whatever change f_π undergoes as T is increased, the *opposite* occurs as μ is increased. Without calculation, Eq. (159) indicates that f_π will *decrease* with T and *increase* with μ. This provides a simple elucidation of the results described above. Figure 40 illustrates this behaviour for $m \neq 0$. The (T, μ)-dependence of m_π, from Eq. (128), is also depicted in Fig. 40. It is *insensitive* to changes in μ and only increases slowly with T, until T is very near the critical temperature. As in Sec. 7.4, this insensitivity is the result of mutually cancelling increases in $\langle m\,\bar{q}q\rangle_\pi$

*This is the expression for N_π^2 from Eq. (129), which provides a better approximation to the pion leptonic decay constant than Eq. (130) when one assumes $\Gamma_\pi(p; P) = i\gamma_5\, B_0(p^2)$.

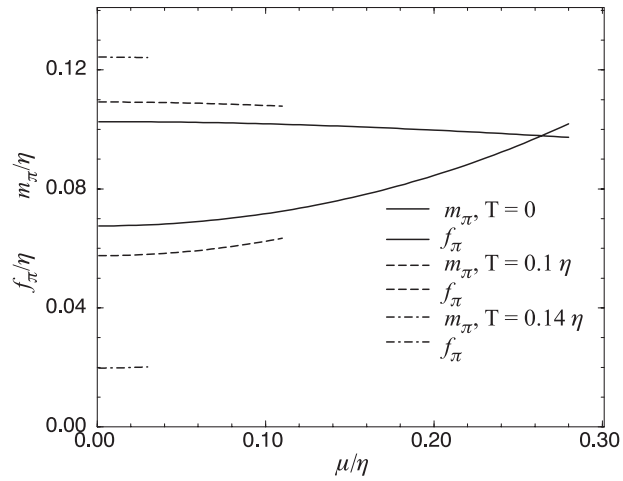

Fig. 40. The pion mass, Eq. (128), and weak decay constant, Eq. (129), as a function of μ for a range of values of T. m_π falls slowly and uniformly with μ [$m_\pi(T = 0, \mu_c) = 0.95\, m_\pi(T = 0, \mu = 0)$] but increases with T. Such a decrease is imperceptible if the ordinate has the range in Fig. 41. f_π increases with μ and decreases with T [$f_\pi(T = 0, \mu_c) = 1.51\, f_\pi(T = 0, \mu = 0)$]

and f_π, and is a feature of studies that preserve the momentum-dependence of the confined, dressed-quark degrees of freedom in bound states.

With $\eta = 1.37\,\mathrm{GeV}$ and $m = 30\,\mathrm{MeV}$, one obtains $f_\pi = 92\,\mathrm{MeV}$ and $m_\pi = 140\,\mathrm{MeV}$ at $T = 0 = \mu$. That large values of η and m are required is a quantitative consequence of the inadequacy of Eq. (140) in the ultraviolet: the large-p^2 behaviour of the scalar part of the dressed-quark self energy is incorrect. This defect is remedied easily [7] without qualitative changes to the results presented here [71].

ρ-meson properties are more difficult to study: one must solve the vector-meson Bethe — Salpeter equation directly. As described above, the ladder truncation of the kernel in the inhomogeneous axial-vector vertex equation and the rainbow truncation of the quark DSE form an AV-WTI identity preserving pair [3]. It follows that the ladder BSE is accurate for flavour-nonsinglet pseudoscalar and vector bound states of equal-mass quarks because of a cancellation in these channels between diagrams of higher order in the systematic expansion illustrated in Fig. 7.

A ladder BSE using the $T = 0$ limit of Eq. (140) was introduced in Ref.12. It has one notable pathology: the bound state mass is determined only upon the additional specification that the constituents have zero relative momentum. That specification leads to a conflict with Eqs. (19)-(22), which follow from the AV-

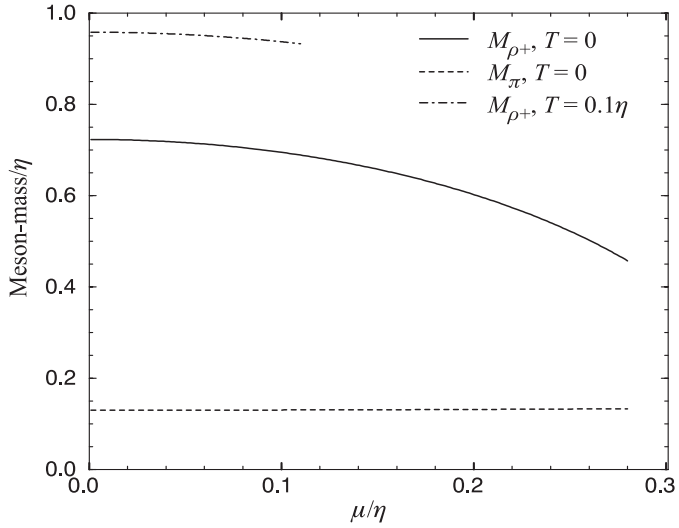

Fig. 41. $M_{\rho+}$ and m_π as a function of $\bar{\mu}$ for $\bar{T} = 0, 0.1$. On the scale of this figure, m_π is insensitive to this variation of T. The current-quark mass is $m = 0.011\,\eta$, which for $\eta = 1.06\,\mathrm{GeV}$ yields $M_{\rho+} = 770\,\mathrm{MeV}$ and $m_\pi = 140\,\mathrm{MeV}$ at $T = 0 = \mu$

WTI, and is an artefact of implementing the delta-function limit discontinuously; i.e., these identities are manifest for any finite-width representation of the delta-function, as this width is reduced continuously to zero. In other respects this ladder BSE provides a useful qualitative and semi-quantitative tool for analysing features of the pseudoscalar and vector meson masses. For example, Goldstone's theorem is manifest, in that the π is massless in the chiral limit, and also m_π^2 rises linearly with the current-quark mass. Further, there is a naturally large splitting between m_π and m_ρ, which decreases slowly with the current-quark mass.

To illustrate this and determine the response of m_ρ to increasing T and μ, the BSE of Ref.12 was generalised [50] to finite-(T,μ) as

$$\Gamma_M(\tilde{p}_k;\check{P}_\ell) = -\frac{\eta^2}{4}\,\mathsf{Re}\left\{\gamma_\mu\, S(\tilde{p}_i+\tfrac{1}{2}\check{P}_\ell)\,\Gamma_M(\tilde{p}_i;\check{P}_\ell)\,S(\tilde{p}_i-\tfrac{1}{2}\check{P}_\ell)\,\gamma_\mu\right\}\,, \quad (160)$$

where $\check{P}_\ell := (\vec{P},\Omega_\ell)$. The bound state mass is obtained by considering $\check{P}_{\ell=0}$ and, in ladder truncation, the ρ- and ω-mesons are degenerate.

The π equation admits the solution

$$\Gamma_\pi(P_0) = \gamma_5\left(i\theta_1 + \vec{\gamma}\cdot\vec{P}\,\theta_2\right) \quad (161)$$

and yields the mass plotted in Fig. 41. The mass behaves in qualitatively the same manner as m_π in Fig. 40, from Eq. (128), as required if Eq. (160) is to provide a reliable guide. In particular, it vanishes in the chiral limit.

For the ρ-meson there are two components: one longitudinal and one transverse to $\vec{P}$. The solution of the BSE has the form

$$\Gamma_\rho = \left\{ \begin{array}{l} \gamma_4\, \theta_{\rho+} \\ \left(\vec{\gamma} - \frac{1}{|\vec{p}|^2}\, \vec{P}\vec{\gamma}\cdot\vec{P}\right)\, \theta_{\rho-} \end{array} \right. , \tag{162}$$

where $\theta_{\rho+}$ labels the longitudinal and $\theta_{\rho-}$ the transverse solution. The eigenvalue equation obtained from Eq. (160) for the bound state mass, $M_{\rho\pm}$, is

$$\frac{\eta^2}{2}\, \mathsf{Re}\left\{\sigma_S(\omega_{0+}^2 - \tfrac{1}{4}M_{\rho\pm}^2)^2 - \left[\pm\,\omega_{0+}^2 - \tfrac{1}{4}M_{\rho\pm}^2\right]\sigma_V(\omega_{0+}^2 - \tfrac{1}{4}M_{\rho\pm}^2)^2\right\} = 1\,. \tag{163}$$

The equation for the transverse component is obtained with $[-\omega_{0+}^2 - \frac{1}{4}M_{\rho-}^2]$ in (163). Using the chiral-limit solutions, Eq. (144), one obtains immediately that

$$M_{\rho-}^2 = \frac{1}{2}\,\eta^2,\ \textit{independent}\ \text{of}\ T\ \text{and}\ \mu. \tag{164}$$

This is the $T = 0 = \mu$ result of Ref.12. Even for nonzero current-quark mass, $M_{\rho-}$ changes by less than 1% as T and μ are increased from zero toward their critical values. Its insensitivity is consistent with the absence of a constant mass-shift in the transverse polarisation tensor for a gauge-boson.

For the longitudinal component one obtains in the chiral limit:

$$M_{\rho+}^2 = \tfrac{1}{2}\eta^2 - 4(\mu^2 - \pi^2 T^2)\,. \tag{165}$$

The characteristic combination $[\mu^2 - \pi^2 T^2]$ again indicates the anticorrelation between the response of $M_{\rho+}$ to T and its response to μ, and, like a gauge-boson Debye mass, that $M_{\rho+}^2$ rises linearly with T^2 for $\mu = 0$. The $m \neq 0$ solution of Eq. (163) for the longitudinal component is plotted in Fig. 41. As signalled by Eq. (165), $M_{\rho+}$ *increases* with increasing T and *decreases* as μ increases*.

I stated that contributions from skeleton diagrams not included in the ladder truncation of the vector meson BSE do not alter the calculated mass significantly because of cancellations between these higher order terms [3]. This is illustrated explicitly in two calculations: Ref.79, which shows that the $\rho \to \pi\pi \to \rho$ contribution to the real part of the ρ self energy; i.e., the π-π induced mass-shift, is only -3%; and Ref.80, which shows, for example, that the contribution to the ω-meson mass of the $\omega \to 3\pi$-loop is negligible. Therefore, ignoring such

*There is a 25% difference between the value of η required to obtain the $T = 0 = \mu$ values of m_π and f_π, from Eq. (128) and Eq. (129), and that required to give $M_{\rho\pm} = 0.77\,\text{GeV}$. This is a measure of the quantitative accuracy of this algebraic model.

contributions does not introduce uncertainty into estimates of the vector meson mass based on Eq. (160).

Equation (163) can also be applied to the ϕ-meson. The transverse component is insensitive to T and μ, and the behaviour of the longitudinal mass, $M_{\phi+}$, is qualitatively the same as that of the ρ-meson: it increases with T and decreases with μ. Using $\eta = 1.06\,\mathrm{GeV}$, the model yields $M_{\phi\pm} = 1.02\,\mathrm{GeV}$ for $m_s = 180\,\mathrm{MeV}$ at $T = 0 = \mu$.

In a 2-flavour, free-quark gas at $T = 0$ the baryon number density is $\rho_B = 2\mu^3/(3\pi^2)$, by which gauge nuclear matter density, $\rho_0 = 0.16\,\mathrm{fm}^{-3}$, corresponds to $\mu = \mu_0 := 260\,\mathrm{MeV} = 0.245\,\eta$. At this chemical potential the algebraic model yields

$$M_{\rho+}(\mu_0) \approx 0.75 M_{\rho+}(\mu = 0)\,, \tag{166}$$

$$M_{\phi+}(\mu_0) \approx 0.85 M_{\phi+}(\mu = 0)\,. \tag{167}$$

The study summarised in Sec. 7.4 [62], indicates that a better representation of the ultraviolet behaviour of the dressed-gluon propagator expands the horizontal scale in Fig. 41, with the critical chemical potential increased by 25%. This suggests that a more realistic estimate is obtained by evaluating the mass at $\mu_0' = 0.20\,\eta$, which yields

$$M_{\rho+}(\mu_0') \approx 0.85 M_{\rho+}(\mu = 0)\,, \tag{168}$$

$$M_{\phi+}(\mu_0') \approx 0.90 M_{\phi+}(\mu = 0)\,; \tag{169}$$

a small, quantitative modification. The difference between Eqs. (166) and (168), and that between Eqs. (167) and (169), is a measure of the theoretical uncertainty in the estimates in each case. This reduction in the vector meson masses is quantitatively consistent with that calculated in Ref.48 and conjectured in Ref.81. At the critical chemical potential for $T = 0$, $M_{\rho+} \approx 0.65\, M_{\rho+}(\mu = 0)$ and $M_{\phi+} \approx 0.80\, M_{\phi+}(\mu = 0)$.

This simple model of QCD_μ^T preserves the momentum-dependence of gluon and quark dressing, which is an important qualitative feature of more sophisticated studies. Its simplicity means that many of the consequences of that dressing can be demonstrated algebraically. For example, it elucidates the origin of an anticorrelation, found for a range of quantities, between their response to increasing T and that to increasing μ.

Both $(-\langle\bar{q}q\rangle)$ and f_π decrease with T and increase with μ, and this ensures that m_π is insensitive to increasing μ and/or T until very near the edge of the domain of confinement and DCSB. The mass of the transverse component of the vector meson is insensitive to T and μ while the mass of the longitudinal component increases with increasing T but decreases with increasing μ. This behaviour is opposite to that observed for $(-\langle\bar{q}q\rangle)$ and f_π, and hence the scaling

law conjectured in Ref.81 is inconsistent with this calculation, as it is with others of this type.

This study has two primary limitations. First, the width of the vector mesons cannot be calculated because the solution of Eq. (160) does not provide a realistic Bethe — Salpeter amplitude. Second, the calculation of meson-photon observables at $T = 0 = \mu$ only became possible with the determination [5] of the form of the dressed-quark-photon vertex. Its generalisation to nonzero-(T, μ) is a necessary precursor to the study of these processes.

8. CLOSING REMARKS

These lecture notes illustrate the contemporary application of Dyson — Schwinger equations to the analysis of observable strong interaction phenomena, highlighting the positive aspects and successes. Many recent, interesting studies have been neglected; a calculation of the electric dipole moment of the ρ-meson [82] and an exploration of η-η' mixing [83] among them. However, a simple enquiry of "http://xxx.lanl.gov/find/hep-ph" with the keywords: "Dyson — Schwinger" or "Schwinger — Dyson", will provide a guide to other current research.

In all phenomenological applications, modelling is involved, in particular, of the behaviour of the dressed Schwinger functions in the infrared. [The ultraviolet behaviour is fixed because of the connection with perturbation theory.] This is tied to the need to make truncations in order to define a tractable problem. Questions will always be asked regarding the fidelity of the modelling. The answers can only come slowly as, for example, more is learnt about the constraints that Ward Identities and Slavnov — Taylor identities in the theory can provide. That approach has been particularly fruitful in QED [5], and already in the development of a systematic truncation procedure for the kernel of the quark DSE and meson BSE [3, 4]. In the meantime, and as is common, phenomenological applications provide a key to understanding which elements of the approach need improvement: one must push and prod to find the weak links.

Acknowledgments. I am grateful to the faculty and staff at JINR-Dubna for their hospitality during this workshop, and especially to L. Kalinovskaya and Yu. Kalinovsky for their particular care. This work was supported by the US Department of Energy, Nuclear Physics Division, under contract no.W-31-109-ENG-38, the National Science Foundation under grant no. INT-9603385, and Deutscher Akademischer Austauschdienst.

REFERENCES

1. **Roberts C.D., Williams A.G.** — Prog. Part. Nucl. Phys., 1994, v.33, p.477: hep-ph/9403224.
2. **Roberts C.D.** — "Dyson — Schwinger Equations in QCD", in *Light-Front Quantization and Non-Perturbative QCD*, edited by Vary J.P. and Wolz F. (International Institute of Theoretical and Applied Physics, Ames, 1997), pp.212-239: http://www.iitap.iastate.edu/reports/lfw/contens.html.
3. **Bender A., Roberts C.D., Smekal L.V.** — Phys. Lett. B, 1996, v.380, p.7: nucl-th/9602012.
4. **Roberts C.D.** In: *Quark Confinement and the Hadron Spectrum II,* edited by Brambilla N. and Prosperi G.M. (World Scientific, Singapore, 1997), pp.224-230: nucl-th/9609039
5. **Bashir A., Kizilersu A., Pennington M.R.** — Phys. Rev. D, 1998, v.57, p.1242; and references therein: hep-ph/9707421.
6. **Brown N., Pennington M.R.** — Phys. Rev. D, 1989, v.39, p.2723.
7. **Maris P., Roberts C.D.** — Phys. Rev. C, 1997, v.56, p.3369: nucl-th/9708029.
8. **Maris P., Roberts C.D.** — "Differences between Heavy- and Light-Quarks", in *Rostock 1997, Progress in Heavy Quark Physics*, edited by Beyer M., Mannel T. and Schröder H.: nucl-th/9710062.
9. **Ivanov M.A., Kalinovsky Yu., Maris P., Roberts C.D.** — Phys. Rev. C, 1998, v.57, p.1991: nucl-th/9711023.
10. **Pichowsky M.A., H.Lee T.-S.** — Phys. Rev. D, 1997, v.56, p.1644: nucl-th/9612049;
Pichowsky M.A. — "Nonperturbative Quark Dynamics in Diffractive Processes", PhD Thesis, University of Pittsburgh.
11. **Maris P., Roberts C.D.** — "QCD Bound States and Their Response to Extremes of Temperature and Density", to appear in the proceedings of the *Workshop on Nonperturbative Methods in Field Theory*, University of Adelaide, Adelaide, South Australia, Feb. 1998: nucl-th/9806nnn.
12. **Munczek H.J., Nemirovsky A.M.** — Phys. Rev. D, 1983, v.28, p.181.
13. **Leinweber D.B.** — Ann. Phys., 1997 v.254, p.328: nucl-th/9510051.
14. **Miransky V.** — Mod. Phys. Lett. A, 1990, v.5, p.1979.
15. **Maris P., Roberts C.D.** — "Pseudovector Components of the Pion, $\pi^0 \to \gamma\gamma$, and $F_\pi(q^2)$: nucl-th/9804062.
16. **Munczek H.** — Phys. Lett. B, 1986, v.175, p.215.
17. **Burden C.J., Roberts C.D., Williams A.G.** — Phys. Lett. B, 1992, v.285, p.347.
18. **Ball J.S., Chiu T.-W.** — Phys. Rev. D, 1980, v.22, p.2542.
19. **Curtis D.C., Pennington M.R.** — Phys. Rev. D, 1992, v.46, p.2663.
20. **Hawes F.T., Roberts C.D., Williams A.G.** — Phys. Rev. D, 1994, v.49, p.4683.
21. **Particle Data Group (Barnett R.M. et al.)** — Phys. Rev. D, 1996, v.54, p.1: http://pdg.lbl.gov/.
22. **Amendolia S.R.** et al. — Nucl. Phys. B, 1986, v.277, p.168.
23. **Roberts C.D.** — Nucl. Phys. A, 1996, v.605, p.475: hep-ph/9408233
24. **Tandy P. C.** — Prog. Part. Nucl. Phys., 1997, v.39, p.117: nucl-th/9705018.
25. **Burden C.J., Roberts C.D., Thomson C.D.** — Phys. Lett. B, 1996, v.371, p163: nucl-th/9511012.
26. **Alkofer R., Roberts C.D.** — Phys. Lett. B, 1996, v.369, p.101: hep-ph/9510284.
27. **Roberts C.D., Cahill R.T., Sevior M.E., Iannela N.** — Phys. Rev. D, 1994, v.49, p.125: hep-ph/9304315.

28. **Počanić D.** — Summary of π-π Scattering Experiments, in *Chiral Dynamics: Theory and Experiment*, edited by Bernstein A. M. and Holstain B. R., Lecture Notes in Physics, v.452, (Springer, Berlin, 1995), 95: hep-ph/9412339.
29. **Kalinovsky Yu., Mitchell K.L., Roberts C.D.** — Phys. Lett. B, 1997, v.399, p.22: nucl-th/9610047.
30. **Bebek C.J. et al.** — Phys. Rev. D, 1976, v.13, p.25.
31. **Bebek C.J. et al.** — Phys. Rev. D, 1978, v.17, p.1693.
32. **Farrar G.R., Jackson D.R.** — Phys. Rev. Lett., 1979, v.43, p.246.
33. **Shambroom W.D. et al.** — Phys. Rev. D, 1982, v.26, p.1.
34. **Aubert J.J. et al.** — Phys. Lett. B, 1985, v.161, p.203.
35. **Arneodo M. et al.** — Nucl. Phys. B, 1994, v.429 p.503.
36. **Derrick M. et al.** — Phys. Lett. B, 1996, v.377, p.259: hep-ex/9601009.
37. **Derrick M. et al.** — Phys. Lett. B, 1996, v.380, p.220: hep-ex/9604008.
38. **Derrick M. et al.** — Phys. Lett. B, 1995, v.350, p.120: hep-ex/9503015.
39. **Aid S. et al.** — Nucl. Phys. B, 1996, v.468, p.3: hep-ex/9602007.
40. **Collins J.C., Perry M.J.** — Phys. Rev. Lett., 1975, v.34, p.1353.
41. **Rajagopal K.** — The Chiral Phase Transition in QCD: Critical Phenomena and Long-Wavelength Pion Oscillations, in *Quark-Gluon plasma,* edited by Hwa R.C. (World Scientific, New York, 1995), 484: hep-ph/9504310.
42. **Engels J. et al.** — Phys. Lett. B, 1997, v.396, p.210: hep-lat/9612018; and references therein.
43. **Wiringa R. B., Fiks V., Fabrocini A.** — Phys. Rev. C, 1988, v.38, p.1010.
44. **Drees A.** — Dilepton Enhancement at the CERN SpS, in Proceedings of the *XXVth International Workshop on Gross Properties of Nuclei and Nuclear Excitations*, Hirschegg 1997, edited by Feldmeier H., Knoll J., Nörenberg W. and Wambach J. (GSI-Darmstadt, 1997), 178.
45. This figure can be found at: http:/ceres6.physi.uni-heidelberg.de/ceres/referenceData/Index.html.
46. **Li G.G., Ko C.M., Brown G.E.** — Phys. Rev. Lett., 1995, v.75. p.4007: nucl-th/9504025.
47. **Rapp R., Chanfray G., Wambach J.** — Nucl. Phys. A, 1997, v.617, p.472: hep-ph/9702210.
48. **Jin X., Leinweber D.B.** — Phys. Rev. C, 1995, v.52, p.3344: nucl-th/9510064.
49. **Klingl F., Kaiser N., Weise W.** — Nucl. Phys. A, 1997, v.624, p.527: hep-ph/9704398.
50. **Maris P., Roberts C.D., Schmidt S.** — Phys. Rev. C, 1998, v.57, p.R2821: nucl-th/9801059.
51. **Kapusta J.I.** — "Finite-Temperature Field Teory" (Cambridge University Press, Cambridge UK, 1989).
52. **Pisarski R. D.** — Phys. Rev. Lett., 1989, v.63, p.1129; **Braaten E., Pisarski R.D.** — Nucl. Phys. B, 1990, v.337, p.569; *ibid* B, 1990, v.339, p.310; Phys. Rev. Lett., 1990, v.64, p.1338; **Frenkel J., Taylor J.C.** — Nucl. Phys. B, 1990, v.334, p.199.
53. **De Tar C.** — "Quark Gluon Plasma in Numerical Simulations of Lattice QCD", in *Quark-Gluon Plasma*, ed. Hwa R. C. (World Scientific, New York, 1995), 1: hep-ph/9504325.
54. **Ukawa A.** — Nucl. Phys. B, 1990, v.17 (Proc. Suppl.), p.118; and references therein.
55. **Lombardo M.-P., Kogut J.B., Sinclair D.K.** — Phys. Rev. D, 1996, v.54, p.2303: hep-lat/9511026.
56. **Halasz M.A., Jackson A.D., Verbaarschot J.J.M.** — Phys. Rev. D, 1997, v.56, p.5140: hep-lat/9703006.

57. **Karsch F.** — Nucl. Phys. A, 1995, v.590, p.367c: hep-lat/9503010.

58. **Blum T. et al.** — Phys. Rev. D, 1995, v.51, p.5153: hep-lat/9410014.

59. **Laermann E.** — "Thermodynamics Using Wilson and Staggered Quarks": hep-lat/9802030.

60. **Bender A., Blaschke D., Kalinovsky Yu., Roberts C.D.** — Phys. Rev. Lett., 1996, v.77, p.3724: nucl-th/9606006.

61. **Blaschke D., Roberts C.D., Schmidt S.** — "Thermodynamic Properties of a Simple, Confining Model", Phys. Lett. B, in press: nucl-th/9706070.

62. **Bender A. et al.** — "Deconfinement at Finite Chemical Potential", Phys. Lett. B, in press: nucl-th/9710069.

63. **Jackson A.D., Verbaarschot J.J.M.** — Phys. Rev. D, 1996, v.53, p.7223: hep-ph/9509324.

64. **Häbel U., Könning R., Reusch H.-G., Stingl M., Wigard S.** — Z. Phys. A, 1990, v.336, p.423; **Häbel U., Könning R., Reusch H.-G., Stingl M., Wigard S.** — Z. Phys. A, 1990, v.336, p.435.

65. **Hawes F.T., Roberts C.D., Williams A.G.** — Phys. Rev. D, 1994, v.49, p.4683: hep-ph/9309263.

66. **Maris P.** — Phys. Rev. D, 1995, v.52, p.6087: hep-ph/9508323.

67. **Frank M.R., Roberts C.D.** — Phys. Rev. C, 1996, v.53, p.390: hep-ph/9508225.

68. **Sevior M.E.** — Nucl. Phys. A, 1992, v.543, p.275c.

69. **Karsch F., Laermann E.** — Phys. Rev. D, 1994, v.50, p.6954: hep-lat/9406008.

70. **Blaschke D., Hoell A., Roberts C.D., Schmidt S.** — "Analysis of Chiral and Thermal Susceptibilities": nucl-th/9803030.

71. **Maris P.,** private communication.

72. **Blaschke D. et al.** — Nucl. Phys. A, 1995, v.592, p.561.

73. **Haymaker R.W.** — Riv. Nuovo Cim., 1991, v.14, series 3, no.8.

74. **Cahill R.T.** — Aust. J. Phys., 1989, v.42, p.171.

75. **Cahill R.T., Roberts C.D.** — Phys. Rev. D, 1985, v.32, p.2419.

76. **Yabu H., Myhrer F., Kubodera K.** — Phys. Rev. D, 1994, v.50, p.3549: nucl-th/9402014.

77. **Brown G.** — Nucl. Phys. A, 1988, v.488, p.689c.

78. **Halasz M.A.,** private communication.

79. **Mitchell K.L., Tandy P.C.** — Phys. Rev. C, 1997, v.55, p.1477: nucl-th/9607025.

80. **Hollenberg L.C.L., Roberts C.D., McKellar B.H.J.** — Phys. Rev. C, 1992, v.46, p.2057.

81. **Brown G.E., Rho M.** — Phys. Rev. Lett., 1991, v.66, p.2720.

82. **Hecht M.B., McKelar B.H.J.** — Phys. Rev. C, 1998, v.57, p.2638: hep-ph/9704326.

83. **Klabucar D., Kekez D.** — "η and η' at the Limits of Applicability of a Coupled Schwinger – Dyson and Bethe – Salpeter Approach in the Ladder Approximation": hep-ph/9710206.